3D MEMS Microassembly

by

Chau Do

A thesis
presented to the University of Waterloo
in fulfillment of the
thesis requirement for the degree of
Master of Applied Science
in
Systems Design Engineering

Waterloo, Ontario, Canada, 2008

© Chau Do 2008

I hereby declare that I am the sole author of this thesis. This is a true copy of the thesis, including any required final revisions, as accepted by my examiners.

I understand that my thesis may be made electronically available to the public.

Abstract

Due to the potential uses and advantages of 3D microelectromechanical systems (MEMS), research has been ongoing to advance the field. The intention of my reasearch is to explore different gripper designs and their interaction with corresponding components to establish a 3D microassembly system. In order to meet these goals, two grippers were designed using different mechanisms for grasping. At the same time, corresponding parts capable of being constructed into a 3D microstructure were designed to interact with the grippers. The microcomponents were fabricated using PolyMUMPS, a part of the Multi-User MEMS Processes (MUMPS), and experimentation was conducted with the goal of constructing a 3D microstructure. The results were partially successful in that both grippers were able to pick up coresonponding parts and bring them out of plane in order to make them stand up. However, a final 3D microstructure was unfortunately not achieved due to time constraints. This will be left to future researchers who continue the project.

On the equipment side a microassembly system was fully integrated using cameras for vision and motors with micro-resolution for movement. A computer program was used to control each part of the system. The cameras provided feedback from various views, allowing the operator to observe what was happening to the microcomponents. The grippers were attached to one of the motors and manipulated to pick up the parts. The final overall system proved sufficient for microassembly, but had some areas that could be improved upon.

Acknowledgements

I would like to thank my labmates, especially KM and JL, who supported me by listening to my rants and helping me when I needed it. I would also like to thank CBC, her role as a good friend and drinking buddy made things much easier to handle. Thanks also go out to my supervisor, Dr. John Yeow, for introducing me to the MEMS field and giving me the opportunity to do research in this area.

Finally, I would like to thank my family, especially my brother and aunt and uncle in London, Ontario. They have let me mooch off of them countless times and I would like them to know that free food to a grad student is priceless.

Dedication

I would like to dedicate this to my parents and brother, who without their contributions throughout the years I would not have been able to reach this point in life. Much of my success is owed to their sacrifices.

Contents

List of Tables . . . vii

List of Figures . . . viii

1 Introduction **1**

1.1 Background . . . 1

1.2 Microassembly . . . 5

2 Design Considerations **9**

2.1 Comments . . . 9

2.2 Fabrication Process . . . 9

2.3 Bonding Type . . . 11

2.4 Passive versus Active . . . 12

2.5 Potential Applications . . . 13

3 Design **16**

3.1 Comments . . . 16

3.2 Gripper Design . . . 16

3.3 Bonding Pad . . . 17

3.4 Tethers . . . 18

3.5 Gripper A . . . 20

3.5.1 Functionality . . . 20

3.5.2 Mathematical Analysis . . . 24

3.5.3 Simulation 30
3.6 Gripper B 34
3.6.1 Functionality 34
3.6.2 Mathematical Analysis 42
3.6.3 Simulation 44
3.7 Antenna design 46
3.8 Tether adjustment 52

4 Equipment Setup **54**
4.1 Comments 54
4.2 Required Movements 55
4.3 Stage 56
4.4 Micromanipulator 57
4.4.1 MT-75S Stands 57
4.4.2 MPC 200 Controller 58
4.4.3 MP-285 Micromanipulator 59
4.5 Cameras 63

5 Experiments and Results **65**
5.1 Comments 65
5.2 Gripper Bonding and Removal 65
5.3 Grasping a Part 69
5.4 Reorienting Part 73
5.5 Insertion 74

6 Conclusions **80**
6.1 Design 80
6.1.1 Gripper Design 80

6.1.2 Insertion Interfaces 81

6.2 Equipment Setup 82

6.2.1 Camera Setup 82

6.2.2 Probe Setup 83

Appendix A **85**

A.1 Future Applications 85

A.1.1 Calculations 88

A.1.2 Horn Antenna 89

A.1.3 Ridge Flare 91

References 95

List of Tables

2.1 PolyMUMPS layers and thickness 10

3.1 Buckling calculations 27

3.2 Beam transverse forces 30

3.3 Summary of results for beam analysis 35

3.4 Summary of results for serpentine spring analysis 45

3.5 Tether forces 53

4.1 Summary of ranges for MT-75S stands 57

4.2 Summary of ranges for the MP-285 59

A.1 DRGH Design values 88

A.2 PolyMUMPS layer summary 88

List of Figures

1.1 Bulk machined cantilever 3

1.2 Out-of-plane hinges 4

1.3 Electro-thermal Grippers 7

2.1 Macro Yagi-Uda antenna 15

2.2 Printed Yagi-Uda antenna 15

3.1 Tether Design 19

3.2 Gripper A 21

3.3 Interior arm dimensions 22

3.4 Exterior arm dimensions 22

3.5 Gripper A Interface 23

3.6 Side view of Gripper A and interface 24

3.7 Beam end restrictions 25

3.8 Forces and moments on fixed-guided beam 28

3.9 Exterior arm buckling 31

3.10 Interior arm buckling 32

3.11 Exterior arm bending 32

3.12 Interior arm bending 33

3.13 Displacement of interior arm 33

3.14 Von Misses stress of interior arm 34

3.15 Gripper B 35

3.16 Gripper B sacrificial part 36

3.17 Gripper B removed 37

3.18 Serpentine spring 38

3.19 MEMSPro image of side arm 39

3.20 Different layers of side arm 39

3.21 Gripper B interface 40

3.22 Side view of grasped part 41

3.23 Typical serpentine spring 43

3.24 Serpentine spring and crab leg dimensions 43

3.25 Deformation of the serpenting spring 45

3.26 Von Mises stress from displacment 46

3.27 Driven element 48

3.28 Antenna column 49

3.29 Base part 49

3.30 T-notch 50

3.31 T-notch interface 50

3.32 L-hook 51

3.33 L-hook interface 51

3.34 Reaction force on grippers 52

4.1 Potential microcomponent movement 55

4.2 Setup 56

4.3 MT-75S Stand 58

4.4 MP-285 Micromanipulator 60

4.5 MAE attached to dovetail 61

4.6 Rotation of the dovetail 61

4.7 Probe holder 62

5.1 Overhead view of bonded gripper 66

5.2 Removed gripper 67

5.3 Adhesive leakage through etch holes 68

5.4 Failed bonding attempt 69

5.5 Grasped part for gripper A 70

5.6 Damaged gripper 70

5.7 Side view of anchor 72

5.8 Rotated part 73

5.9 Inserted part for gripper A 74

5.10 L-hook inserted part for gripper B 75

5.11 T-notch inserted part for gripper B 76

5.12 Wide view of inserted parts 76

5.13 Angled camera view for part insertion 77

5.14 Overhead view of inserted parts 78

6.1 Damaged Gripper A 81

6.2 Camera on rotational arm 83

A.1 Double Ridge Guide Horn 86

A.2 Cross section of DRGH 86

A.3 Horn antenna dimensions 90

A.4 Antenna ridge dimensions 92

A.5 Impedance Taper 93

A.6 HFSS horn antenna 93

Chapter 1

Introduction

1.1 Background

Microelectromechanical systems (MEMS) are systems on the micro scale, 1/1000th of a millimeter, but can encompass more than simply electric and mechanical systems. For example, they may include thermal, optical, magnetic and fluidic systems. MEMS can be used in a variety of situations such as sensors and actuators to name a few. Due to the different uses and the numerous environments in which they can be used, MEMS designs must consider more than the physical dimensions of the components but also issues such as how to package the components and integration with the macro world in order to provide power and transmit signals.

Economically, MEMS have been successfully integrated in several areas such as inkjet printer heads and micromirrors for projector displays, resulting in lucrative profits. Additionally, MEMS products have enjoyed successful use in the automotive industry, mainly in the area of sensors such as accelerometers, pressure and flow sensors and gyroscopes. Estimations predict the MEMS market in the automotive industry will grow to $2.2 billion by 2011 [6]. Expansion into areas such as microfluidics and bioMEMS show that there are numerous areas that can benefit from MEMS. Subsequently, it is important to continue research in this area for further development.

The fabrication of MEMS is done using techniques adopted from the microelectronics industry. For this reason most MEMS are fabricated using lithographic techniques on flat silicon surfaces [9]. This includes basic processing steps such as

different types of chemical vapour deposition (CVD) and wet and dry etching techniques. Typically, MEMS fabrication processes fall within two categories: surface micromachining and bulk micromachining.

Specifically, surface micromaching involves deposition of multiple thin layers onto the silicon surface and in between each deposition, etching each layer as necessary to form the desired MEMS structure. Consequently, the layers are built on top of the silicon surface. The layers can consist of sacrificial layers and mechanical layers which make up the components. The sacrificial layers allow for elevation of the mechanical layers and are generally removed at the end of fabrication. Typical materials used for the mechanical and sacrificial layers are polysilicon and silicon oxide respectively. Characteristically, surface micromachining results in good planar properties but is limited vertically, making it difficult to form three-dimensional structures.

Alternatively, bulk micromaching involves etching into the silicon substrate to form the desired MEMS structure. This involves removing significant amounts of the silicon using both wet and dry etching. The chemical reactions have the goal of oxidizing the silicon in order to make it possible to then remove it, leaving behind the desired structure. Bulk micromachining can result in more three-dimensional structures, however the complexity of the structures within an area is limited by the reactions used to make them [10].

Each fabrication process is limited in terms of the materials used and the dimensions that can be achieved (for example the number of layers that can be deposited may be limited). These restrictions limit the potential structures that may be designed and in most cases result in two dimensional designs. One approach that is used to create three-dimensional structures as mentioned previously, is to use sacrificial layers and deposit structural layers on top of the sacrificial layers and subsequently removing the sacrificial layers. Using this method, structures like the micro-coils of [35] can be created. These micro-coils are created in two parts, the bottom conductor lines used to provide electrical connection to each coil and the air bridges which form the micro-coils themselves. The air bridges are constructed by forming a 3D photoresist mold, which provides holes for the posts of the air bridges and a central support section on which the bridge connecting the posts is formed. Metal electroplating is used to form the air bridge itself and fill in the sections of the mold. Finally the mold is removed to leave behind the coils. This

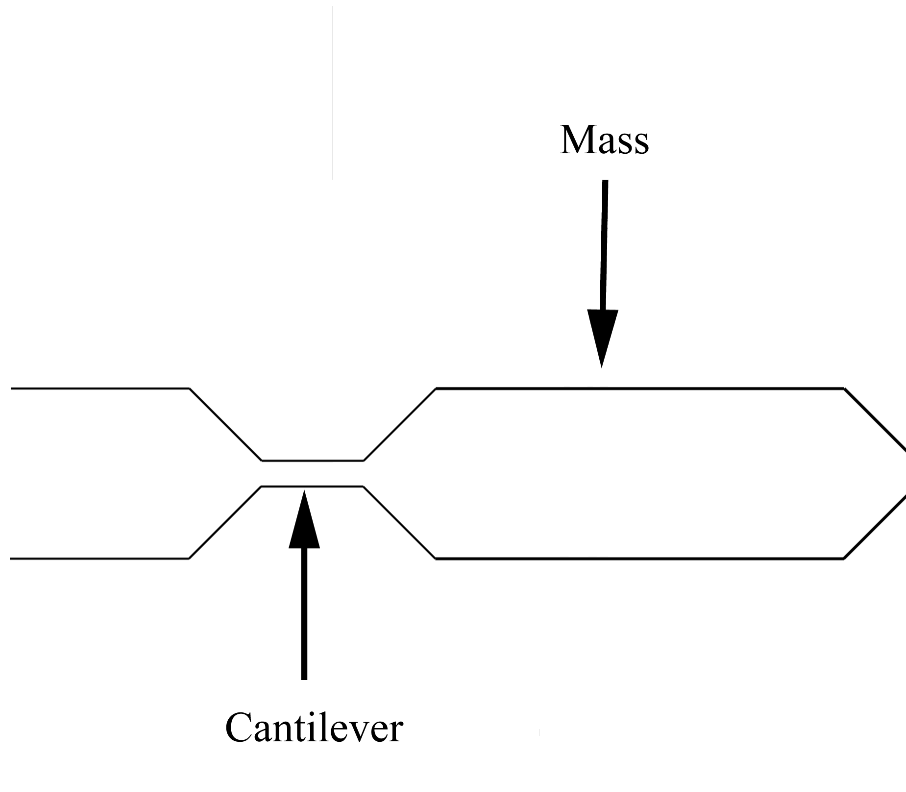

Figure 1.1: A 3D bulk micromachined cantilever is used in an accelerometer.

example demonstrates how a fairly simple 3D structure can be created.

Using bulk micromachining, three-dimensional structures can be created by etching into the substrate as can be seen by the cantilever structure used within an accelerometer in figure 1.1. In [36], a capacitive accelerometer is created by using anisotropic etching to create a mass attached to cantilever arms. Here it can be seen that etching into the silicon is particularly useful in creating the large mass at the end of the cantilever, which bends correspondingly with the force applied to change the capacitance value of the accelerometer.

Other methods such as hinges are used to bring the structures out of plane. An example of this can be seen in figure 1.2. To create hinges, [11] describes using two layers of polysilicon with two sacrificial layers. The second layer of polysilicon is anchored to the substrate, while the first layer is completely removed but restricted by the second layer. Once all the sacrificial layers are taken away, the hinged plate is moved out of plane. One way of bringing the plate out of plane is to use a probe tip to slide underneath the released plate. Another example in the case of magnetic materials, the plate can be brought out-of-plane using a magnetic field [12]. The

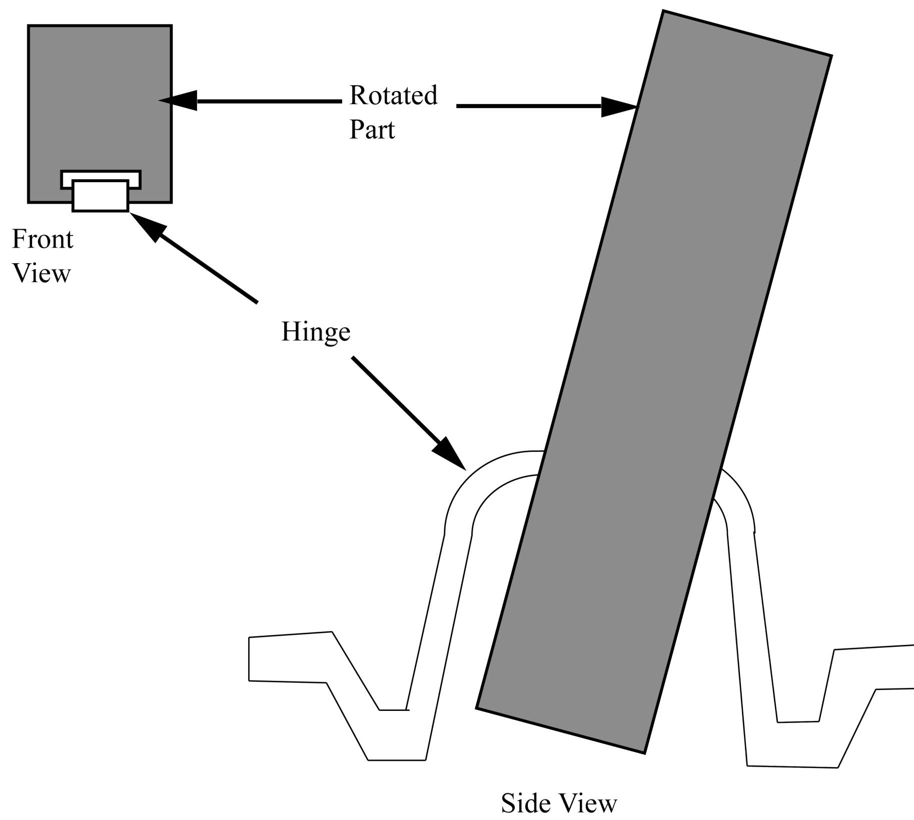

Figure 1.2: Hinges can be fabricated and brought out of plane to create 3D structures.

hinge allows for three-dimensional structures to be created and by interlocking two hinges, their position after being brought out-of-plane can be accurately controlled [11]. Despite this, another step is required to build on top of the raised plates. In other words, the hinge mechanism is limited to bringing structures out-of-plane that are directly connected to the substrate, which limits the potential structures that can be created.

Although the prior examples show possible three-dimensional structures achievable with the current fabrication process, it is clear that they are also limited. In all three examples, the structures must be attached to the substrate in some manner. In addition the materials of the resulting structures are dependent on the fabrication process meaning it is difficult to integrate different materials if they are not compatible within the same fabrication process. These are only a few of the potential setbacks and it is clear that the final structures that can be achieved are subject to the restrictions imposed by the etching and deposition (if applicable) processes of each fabrication process. Microassembly is a potential method that can be used to overcome these disadvantages.

1.2 Microassembly

Microassembly is the process of assembling micro structures by moving parts from their original position into new positions. This may involve manipulating the parts by rotating and translating them. In addition the parts may be integrated with each other to form more complex structures. In this manner, the different designs that can be realized are not limited to the fabrication processes used to make them, which typically result in two dimensional structures [13]. This also allows the integration of parts from different chips with each other. Microassembly can be broken down into two main categories, serial and parallel.

Parallel assembly involves the assembly of multiple parts at a time allowing for a larger throughput as compared to serial microassembly. This typically involves the simultaneous transferring of parts from point A to point B. To achieve this, parallel assembly usually involves short-range attractive forces and random agitation of the parts and is broken down into two types: deterministic and stochastic.

Deterministic parallel assembly involves wafer-to-wafer transfer of the micro

parts. Typically, one wafer provides the parts and the second wafer provides the receiving sites, to which the parts are to be transferred. Consequently, the main concern is in transferring the parts, which involves the proper alignment of the two chips. Stochastic parallel assembly is based on the principle of particles moving towards a state of minimal potential energy. As a result of this, the final binding sites should have the state of minimal potential energy and enough energy should be provided to the parts in order to move them to these sites [14].

Despite the clear advantages of parallel assembly in terms of throughput, it is also clear that the resulting structures are limited in design. The mass transferring of components from one chip to another limits the complexity of the designs that can be accomplished. In addition, it is difficult to build upon the structures after one transfer using the same technique.

As the name suggests, serial assembly is the sequential assembly of parts, typically using pick and place techniques. This involves the use of microtools which are capable of picking up the parts, manipulating them and integrating the parts with either another part or a receiving site in the substrate. The microtools can be fabricated on the same chip as the parts they will pick up or on another chip as long as they are capable of interfacing with the parts. Due to the difficulty in manipulating microcomponents, it is beneficial to plan the orientation of the fabricated micro parts in order to reduce the steps required to assemble a three-dimensional structure [14].

Typically movements of the microtools are controlled by a human operator who will need to interact with equipment on the macro world scale. Macro-world equipment capable of micro scale resolution in terms of movement are interfaced with the microtools. In this manner, the microtools can be used to manipulate the microcomponents through the operator controlling the equipment. Sensor equipment, typically in the form of visual systems are used to provide feedback to the operator. Eventually, the process can become automated, increasing the overall throughput. This can be done by developing software capable of controlling the equipment. The robustness of this automation can be greatly increased with the use of image processing software or other sensory techniques, capable of providing feedback, allowing the system to self-correct if necessary.

In general, a microtool is a microgripper, a part that has one section which is interfaced with the macro world equipment and controlled by it. A second section

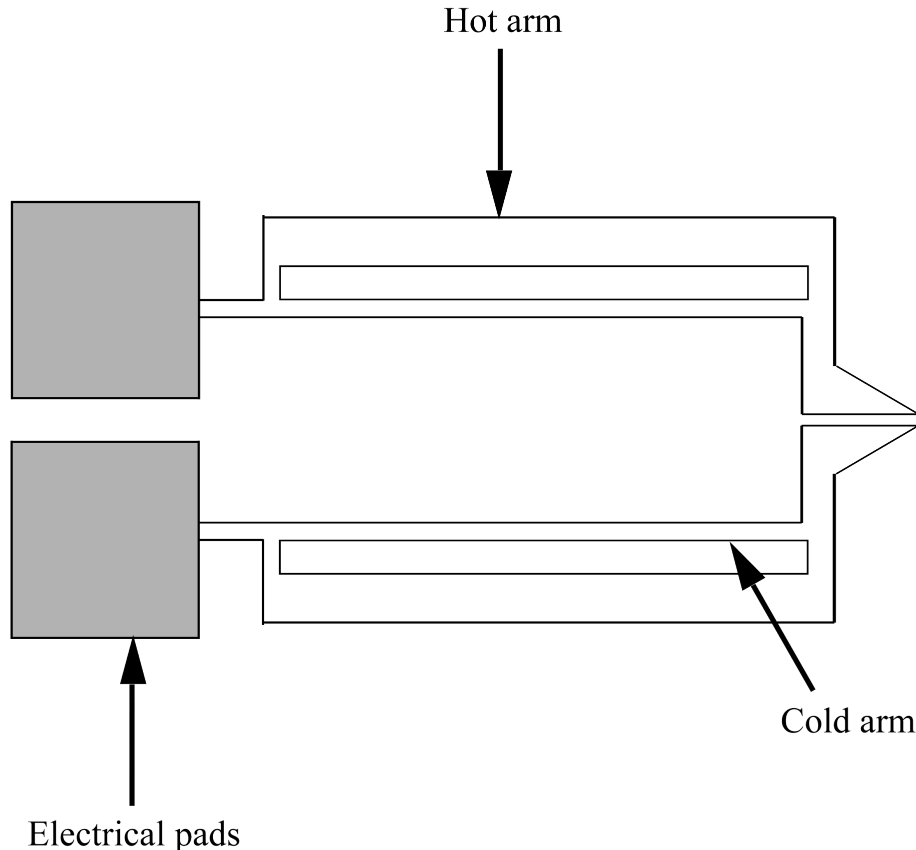

Figure 1.3: A gripper with actuation using the electro-thermal technique.

is used to interface with the parts. The controlled microgripper is then used to interact with the parts that will make up the final structure. Microgrippers can fall into different categories such as passive and active grippers. In general, passive grippers use compliant parts which bend in order to conform to the shape of the micro components. For example this can be done through the use of beams, which bend outwards to accommodate a part and bend back applying a force keeping the part in place.

Active grippers on the other hand, use some form of energy source in order to provide actuation. The typical sources of energy are electro-thermal where an electric current is passed through the structure and as resistive heating occurs, certain portions of the gripper expand allowing for actuation. Classic examples of this technique can be seen in figure 1.3 [15, 18]. A second common type is electro-static where an electric voltage is applied to the structure and capacitive forces attract and repel causing the actuation [17]. These two mechanisms can be

used for tweezers-like structures, which are used to pick up a part. In the case of the electro-thermal tweezers shown in figure 1.3, when the energy is applied to the arms, they heat up and certain areas expand causing the arms to bend outwards. Different designs result in different bending ranges.

More unique mechanisms have been used in order to pick and place objects. For example [19] used micro holes in order to pick up objects. The micro holes are created by using bulk micromachining with isotropic etching. Before touching the object, the end effector is heated up above room temperature. Then the object is touched and the end effector is allowed to cool down and a negative pressure develops inside the micro holes. Due to the positive pressure outside, the part is pushed against the end effector and is subsequently picked up. To release the part, the end effector is heated up again. The heating mechanism used was heat conduction.

Another type of tweezers are the ortho-tweezers disclosed in [20]. The ortho-tweezers are comprised of two probes in the X and Y directions that are orthogonal to each other. By careful positioning of the probes with respect to each other, they are able to rotate and pick up parts. These examples vary in the mechanisms they use and show the diversity in the microtools that can be used to pick up microcomponents.

The main goal of this research is to investigate different gripper designs while at the same time establishing a working assembly and test system for 3D MEMS. This will be achieved by first conducting a literary review. At the time the research began, certain equipment had already been purchased, such as the micromanipulator explained later. Therefore, due to costs constraints, another goal is to incorporte these pre-purchased parts into a working system, buying new equipment as necessary. A seconday goal was to assemble a 3D MEMS system. Due to time constraints, the completion of this was unfortunately not possible.

Chapter 2

Design Considerations

2.1 Comments

Prior to designing the grippers and the corresponding parts for them to interact with, various limiting factors must be taken into consideration. An obvious factor is the type of gripper actuation, which is essentially a choice between passive and active actuation. Another consideration is the method of interaction between the macro and micro world which will have an impact on the shape of the gripper. In addition because the fabrication process is outsourced, the limitations that come with it play a large role in what designs are possible. These and other factors will be described in more detail in the following sections.

2.2 Fabrication Process

The fabrication process used was PolyMUMPS, a surface micromaching process provided through the Canadian Microelectronics Corporation (CMC) Microsystems. PolyMUMPS supplies three structural layers of polysilicon and a final metal layer for conduction. To create different elevations in the parts, sacrificial silicon oxide is applied in between each polysilicon layer. The oxide is then removed at the end of the process to release the structures.

Typical industry standard processes are used to apply, pattern and remove each of the layers. In particular, low pressure chemical vapour deposition (LPCVD) is

Layer	Thickness(μm)
Poly 0	0.5
Oxide 1	2.0
Poly 1	2.0
Oxide 2	0.75
Poly 2	1.5
Metal	0.5

Table 2.1: Thicknesses of different layers of the PolyMUMPS process.

used to apply the layers of silicon, which are then patterned using photolithography. Reactive ion etching (RIE) is then applied afterwards to leave behind the desired layer. The final layer is gold which is applied using liftoff. The polysilicon layers are released at the very end by removing the silicon oxide layers. This is done by submersing the chip into a bath of 49% hydrofluoric (HF) solution [21]. Table 2.1 outlines the layers in the order in which they are applied on the substrate and their corresponding thicknesses.

Due to restrictions in the equipment, it is necessary to provide fabrication rules to the user, dictating things such as how much overlap the different layers can have with each other and the minimum size of a layer. Given these rules and the fixed thickness, significant limitations are placed on the possible designs. Hence these must be taken into consideration during the design process to ensure a feasible product.

In particular, one of the most significant limitations is the number of structural layers. Keeping in mind that to create three-dimensional structures using microassembly, it is necessary to have the components fully released from the substrate. Since Poly 0 is deposited directly on the substrate, it cannot be used as a structural layer for the grippers and in most cases the parts. Subsequently, that leaves only the Poly 1 and Poly 2 layers as structural layers to create the components. Subsequently, the resulting structures of the PolyMUMPS process are essentially planar.

2.3 Bonding Type

After the grippers are fabricated on the chip, they must somehow be picked up and connected to a robotic arm for manipulation. This is an extremely difficult step considering the grippers are on the micro scale whereas the arm is on the macro scale. To interface between the two, a probe with a micron scale tip was used. Such probes have diameters of a few millimeters on one end and are narrowed to a diameter of microns at the other. Hence they are the ideal bridge between the two. This will be explained in more detail under the equipment section.

Taking this into consideration, the gripper design must include an area that will allow for bonding to the probe in addition to a tip that will interact with the parts. This increases the size of the gripper, but is a necessity. The design of this area, from hereon referred to as the bonding pad, is rather straightforward as only a simple rectangular area of large enough size is required to accommodate the probe tip. The most difficult consideration is how large to make the bonding pad. Clearly a larger area will make bonding to the probe tip easier, but this will take up precious fabrication space on the substrate. This information depends on how a connection between the probe tip and bonding pad is created. Both solder and adhesives are feasible options for bonding on the micro-scale and consequently were taken into consideration.

Although solder was successfully used in [24], it introduces numerous difficulties. The obvious one is the need to heat up the solder to inconvenient melting temperatures for bonding to the gripper. Considering the lowest solder temperature is 125°C, there is a need for a controllable heating source, further complicating the setup and introducing a potential source of injury. Another point of concern is the amount of contraction that occurs during the cooling of the solder. It was reported in [24] that the cooling effect of the solder for multi-pad grippers (i.e. grippers with more than one bonding pad for electrical connections) caused damage to the structure due to contraction of the solder, making the grippers unusable. In the end, the difficulty in using solder ruled it out as the solution to the problem.

Alternatively, there are numerous commercially available adhesives. They vary depending on the type of materials to be bonded, the desired cure method and time, and the viscosity and thickness of the adhesive among other things. In the case of the gripper, the final metal layer of gold can be used to create a metal-metal bond.

The cure time should be as short as possible and the texture of the adhesive should be on the thick side for easier application. Another thing to consider is whether or not it needs to be electrically conducting. This is dependent on whether the gripper is passive or active as an active one will require an electrical path. Both conducting and non-conducting adhesives are readily available. Considering the vast selection of products and the ease of application, it was decided that an adhesive bond was the best one.

To go back to bonding pad size, the method used to apply the adhesive determines how much space is required. Commercial adhesive application machines are available and apply a fixed amount of product each time. These however were not accessible for use due to the cost of the equipment and hence a manual application method was considered and found to be feasible.

2.4 Passive versus Active

One of the biggest considerations is what type of actuation method will be used to move sections of the gripper in order to grasp and release parts. This dictates the whole design of the gripper and the setup of the equipment since different actuation methods have different bonding requirements. Typically, gripper actuation falls into the two categories of passive and active, both of which come with their advantages and disadvantages.

As mentioned previously, passive grippers do not require any energy source and usually rely on compliant, bendable sections which are used to "grasp" components. As a result, passive grippers are almost always guaranteed to be able to pick up their components since they typically interact with a corresponding interface specifically designed for them. This however comes at the cost of adding the interface to each part, which can be a significant increase in size, taking up valuable chip space. In addition these interfaces may hinder the use of the part. On the other hand because they do not require any electrical source, they need only 1 bonding pad, making the bonding step much easier.

Active grippers on the other hand can pick up objects of various sizes, but are limited by the amount of actuation that can be achieved. In addition they require an electrical source. This means that at least two bonding pads are required to

form a current path or different points of voltages. Consequently, this complicates the setup, which now requires a voltage source and two or more probes to connect to each boding pad. In addition a review of previously designed active grippers [15, 17] shows that some designs may require a high level of voltage, creating a potentially dangerous work environment.

At the time of designing the grippers, a bonding method and its corresponding equipment setup was not yet established. This made it a large potential source of failure, especially considering a manual application of adhesive approach was to be taken. Taking into consideration the complications of bonding and manipulating a gripper with multiple bonding pads which would be the case for active grippers, it was decided that the passive gripper had greater potential for success in terms of available experimental resources. For these reasons, a passive approach was chosen.

2.5 Potential Applications

The main goal of the project was to establish a working 3D microassembly system. This can be further broken down into smaller goals, such as having a working gripper design and establishing the necessary equipment setup. A lower priority goal was to construct a working 3D MEMS device. Unfortunately, due to time restrictions it was unlikely that the project would progress far enough to this point. Especially considering it is reasonably expected to take approximately two design iterations on the gripper design to have an efficiently working gripper. However, since the gripper must have some parts to work with for the testing phase, it only makes sense to have these parts form a potential device.

As mentioned previously, there are numerous successful MEMS devices on the market. These range from accelerometers to inkjet heads. Initially a study of these devices was conducted in hopes of determining if there were any advantages in constructing them using 3D microassembly. When it was clear that none existed, the focus shifted to antennas. Currently the majority of MEMS antennas are 2D due to fabrication limitations. Some examples are the microstrip [37] and quasi-Yagi-Uda antennas [38]. The designs of these antennas are basically printed onto a substrate. However, although this results in lower profiles, the proximity of the antenna to the substrate introduces parasitic components such as surface waves.

These carry power away from antenna, stealing from the radiation power. They can also affect the radiation pattern of the antenna by interfering with the radiated signal.

Research into these issues has shown that with a substrate height of around $1/4\lambda$ (where λ is the wavelength of the signal) and a substrate permittivity of 4.5 or smaller, radiation efficiency better than 50% can be achieved. This ratio is more favourable as the permittivity decreases. Since the permittivity of air is 1.0005, this implies that if the antenna is elevated, performance should be better. Attempts at bringing the antenna out of plane by [22] and [23] have given favourable results. The conclusion by these two groups suggest that it is beneficial to raise the antenna out of plane, making the use of 3D microassembly in this area applicable.

Once again due to time limitations stemming from the fabrication deadline set for the project, in depth antenna design analysis was not possible. Certain antenna designs are well documented and have design rules that can be found in numerous literary sources such as [5, 32]. Taking these factors into consideration, a popular antenna, the Yagi-Uda, was chosen as the potential device. The design of this antenna is fairly straightforward and there is potential that it will benefit from 3D assembly. The reason only a semi-Yagi-Uda antenna was achievable through printed circuit technology is because the driven dipole (the section being fed with an electrical source) is sided by a reflector and director(s) as seen in figure 2.2. Once the feed is printed and connected to the driven dipole, printing a reflector after it is difficult. This is shown in figure 2.3. By elevating the elements of the antenna, the feed line can be on a lower level with respect to it. Hence this allows for the addition of a reflector element, similar to the Yagi-Uda antennas in the macro world. For example, the feed line will run up the support structure that is holding up the driven element.

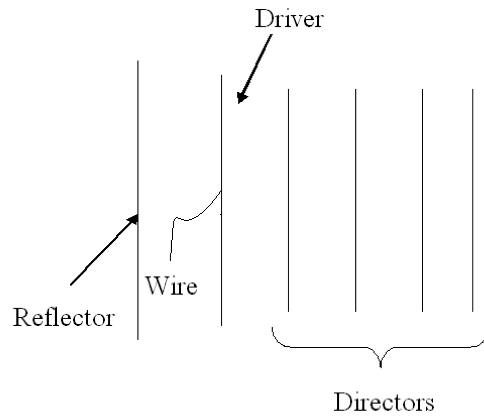

Figure 2.1: Components of a typical Yagi-Uda antenna.

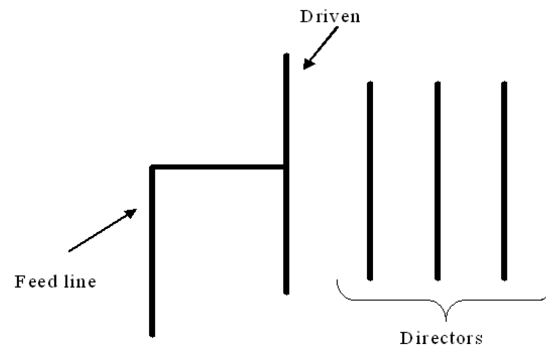

Figure 2.2: Printed Yagi-Uda antenna with the reflector missing due to the positioning of the feedline.

Chapter 3

Design

3.1 Comments

Two main sections need to be designed for fabrication, the grippers and the corresponding parts making up the Yagi-Uda antenna. The main focus of the gripper designs will be on the actuation methods, while the main focus of the parts designs will be on the interconnection of the parts such that they form a 3D structure. The considerations outlined in chapter 2 are kept in mind during the design process. The following sections outline the designs that were submitted for fabrication.

3.2 Gripper Design

As mentioned in chapter 2, the actuation method of choice is the passive approach. Typically passive grippers have compliant parts that allow for flexible movement when they interact with their interfaces. When the gripper is pushed towards the interface, certain parts may bend to accommodate it. Once the gripper is in place within the interface, the part is considered grasped. Ideally a secure grasp will restrict the part from moving in the X-Y-Z directions relative to the gripper. In other words, the part's movement should be restricted, preventing if from falling off or drastically shifting with respect to the gripper, when it is moved.

To assemble a 3D structure a pick and place approach is taken, where each part is picked up, reoriented and placed into its final position. The following steps are applied to each part.

1. Grasp the part with the gripper.
2. Break any restraints that were holding the part down.
3. Lift the part and rotate and/or translate such that it is ready for insertion at the desired site.
4. Insert the part.
5. Release the part from the gripper.

These steps have an impact on the design of the gripper since it must be capable of doing all these things. The first step is rather obvious in that the main point of the gripper is to securely grasp the part. The second step concerns the structural strength of the gripper. It must be strong enough to be able to break the restraints that are holding down the part. The third step is dependent on equipment setup and its ability to rotate and translate on the micron-scale. The griper itself does not rotate or translate, but rather it is the robotic arm that is attached to it that does so. The equipment setup must be established such that the necessary operations can be achieved. Further details are found in chapter 4. Step four pertains to inserting the part either into the substrate or attaching it with another part. By attaching subsequent parts to each other, the 3D structure can be built up. The final step affects the design of the gripper since the grasping feature must also be reversible. In other words the grasping step is not permanent. The release of the part should not be extremely difficult such that it causes the part to come out of its connection or causes damage to either the part or gripper. All these things must be taken into consideration when designing the components to be fabricated.

Two designs were conceived of and will be referred to as gripper A and gripper B. Gripper A employs cantilever beams as the flexible parts, while gripper B uses a serpentine spring. The following sections describe these two designs in greater detail. Commonalities between the two grippers are limited to only the bonding pads and the tethers used to hold them down. These are described first.

3.3 Bonding Pad

As mentioned in chapter 2, the bonding pad is used to connect to the probe tip. In the case of an active gripper it is also the point where an electrical source is applied.

Also mentioned previously is the use of adhesive as the bonding mechanism between a probe tip and the bonding pad. Since the application of the adhesive is to be done manually, the size of the bonding pad is based on the previous experience of other researchers. In [24] it was determined that a pad size of approximately 300 μm by 300 μm is sufficient to accommodate a drop of liquid adhesive.

The pad consists of a Poly 1, Poly 2 and gold metal layer to increase the structural strength. The metal is not necessary for the passive grippers since no electrical connection is required. Due to the large surface of the pad, etch holes are required to ensure that the oxide underneath it is dissolved for full release. This may be of concern during the bonding phase, where some of the adhesive may leak through to the other side.

Each gripper has a bonding pad attached to it. When the term tip of the gripper is used, it is referring to the portion that grasps objects and not the bonding pad. Other than for the purpose of bonding to the probe tip, the bonding pad does not contribute in any other way.

3.4 Tethers

At the end of the fabrication process, it is necessary to release all the parts from the substrate so that they may be picked up and manipulated. This is done by removing all the silicon oxide layers in between the polysilicon layers. At this point, the chip must still be handled and transported to the lab, during which the loose parts are guaranteed to move around. For that reason, once the parts are released something must keep them in a fixed position, otherwise they will be scattered throughout the chip and may even fall off. The solution to this problem, which has been used in previous work [13] is to tether down the part. A tether is created by having a thin beam of polysilicon with one end connected to the part and the other anchored to the substrate. Figure 3.1 shows an L-Edit image of a tether component with dimensions. L-Edit is a layout editor from Tanner Research, which produces files that can be submitted to CMC Microsystems for fabrication. The square section on the right side of the tether is an anchor to the substrate. The dark square represents an anchor in the L-Edit colour scheme and is the only part of the tether attached to the substrate. The left end of the tether is meant to

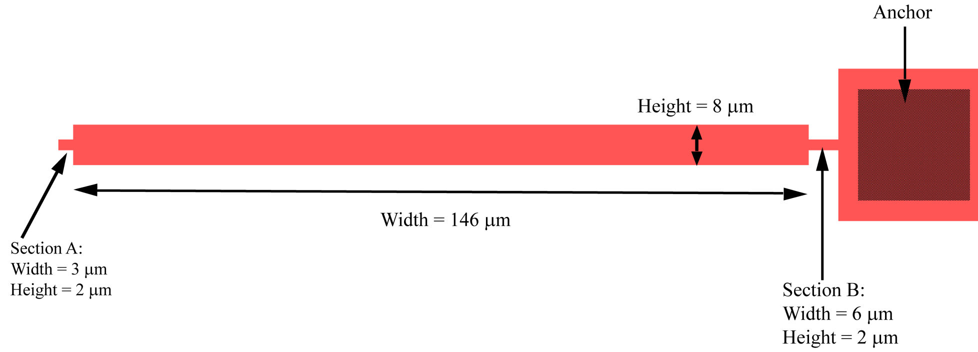

Figure 3.1: Dimensions of the tether design.

attach to a part, therefore tethering it down. Typically, parts will have more than one tether holding them down and will be placed symmetrically about the part to ensure equal restraint. The number of tethers used is dependent on the size of the part and what is necessary to keep it in place.

There are two main sections of interest in terms of the tether design, Section A and Section B. The two are identical in height with Section B being slightly longer. Ideally, the tether should break at Section A, leaving the rest of the tether structure anchored to the substrate. For this reason the height of this portion has the minimum allowed thickness of 2 μm. Section B on the other hand, is meant to provide some elasticity. It is intended to bend when the gripper is grasping a part. This is done in an attempt to promote breakage at Section A since some bending is necessary at that point for a clean break. The flexibility of Section B is the reason why it is longer than Section A. Analysis in [24] shows that the predicted force required to break the first tether is approximately 120 μN.

A reaction force from the tether is necessary during the insertion step otherwise the gripper will just continue to push the part forward, without grasping the part. The tethers were designed to provide a 30 μN reaction force in order to withstand the grasping step of the gripper designed in [24]. This force will change however for different gripper designs since the amount of force required to grasp a part will change. Logically, the reaction force should be less than the force required to break the tethers and remove the part. An approximate reaction force value can be predicted based on the geometry and horizontal force necessary for the gripper to grasp the part. This analysis will be done after the gripper designs have been discussed.

3.5 Gripper A

3.5.1 Functionality

Keeping in mind the goals and restrictions of the gripper design mentioned previously, a lot of potential structures were still possible. It was decided that keeping the structure as simply as possible would most likely reduce areas of failure. Looking at the criteria of structural stability and flexible components such that the gripper locks into the interface when it grasps a part, the simplest approach is to separate the two. Since the flexible parts are expected to bend, they will typically be thinner, making them more susceptible to structural failure. By having a section of the gripper dedicated to the structural support and another dedicated to flexibility allows for separate design of each, making the whole process easier.

This is the basic idea behind gripper A, the scanning electron microscope (SEM) image of which is pictured in Figure 3.2. Here the structural support is embodied by the two exterior rectangular arms. The two interior arms are the flexible components. The interior arms are an identical mirror image of each other and a single arm can be broken down into two sections: the three flexible beams and the semi-octagonal head. Bending is achieved through the flexible beams. The octagonal tip is used to hook onto the interface, explained later on. The rest of the gripper is composed of the bonding pad and 7 tethers spaced evenly around the bonding pad to hold the gripper down. As mentioned earlier, the squares in the bonding pad correspond to etch holes, necessary during the release process for access to the oxide underneath the pad. The exterior arms are composed of Poly 1, whereas the interior arms are made of both Poly 1 for the flexible arms and Poly 2 for the semi-octagonal tip. What cannot be seen in the picture is the higher elevation of the semi-octagonal head. This height difference is achieved by using the Poly1 sacrificial layer (rectangular piece underneath the head). This sacrificial layer is fully released and not tethered down because there is no need for it to stay in place after release. It has served its purpose during fabrication by elevating the semi-octagonal tip. The rectangular Poly 1 part in the bottom right corner of the figure above is a sacrificial part that has moved from its original position.

The dimensions of the flexible arms and exterior arms are given in figures 3.3 and 3.4 respectively. These figures were taken from the L-Edit designs and have

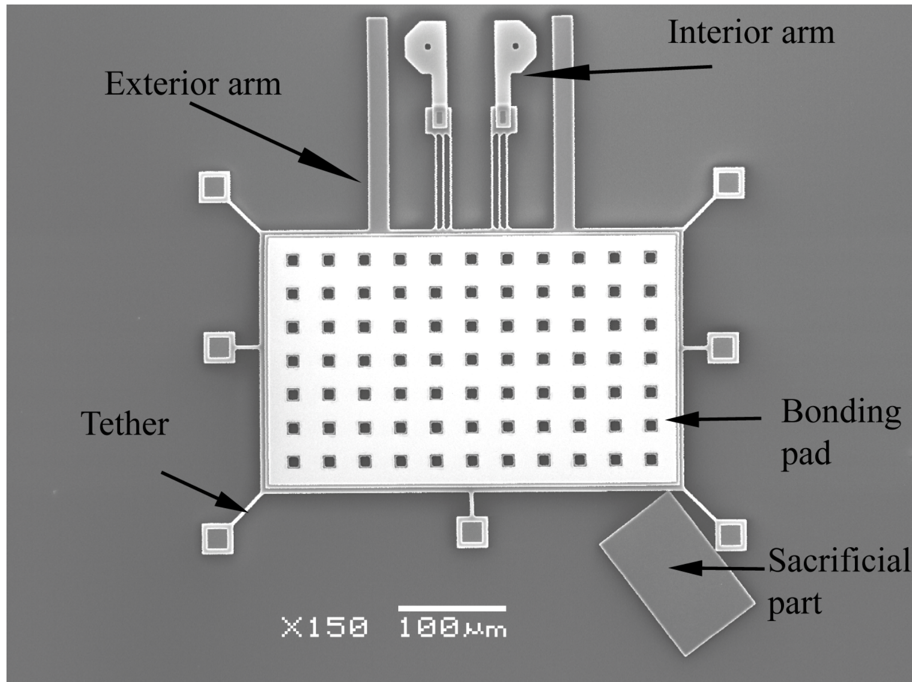

Figure 3.2: SEM image of Gripper A design. A sacrificial part is located in the bottom right hand corner.

colours corresponding to a specific layer in the PolyMUMPS process.

To understand how the gripper works it is useful to refer to the corresponding interface shown in figure 3.5, which is designed to fit it like a puzzle piece. Since the interface is basically a negative of the gripper, once the gripper is designed, it is fairly straightforward to derive the interface design. However, there are some cases where the interface design for a potential gripper is not possible due to design rules dictated by the PolyMUMPs process. Therefore this must also be taken into consideration. Once again Poly 1 sacrificial parts are used to elevate the Poly 2 layer above it. The square portions at either side of the interface (light colour) represent a VIA (hole connecting two layers) between the Poly 1 and Poly 2 layers, meaning they are attached to each other. To be clear the Poly 2 is not attached to the Poly 1 sacrificial parts (section A) since the two are separated by a layer of oxide. When the oxide is removed, the sacrificial parts are free and can be removed using the probe tip. The T-shape design was done such that the probe tip can catch onto one of the edges and pull the part away. Once again the etch holes are present such that the HF solution can reach all oxide layers underneath the part.

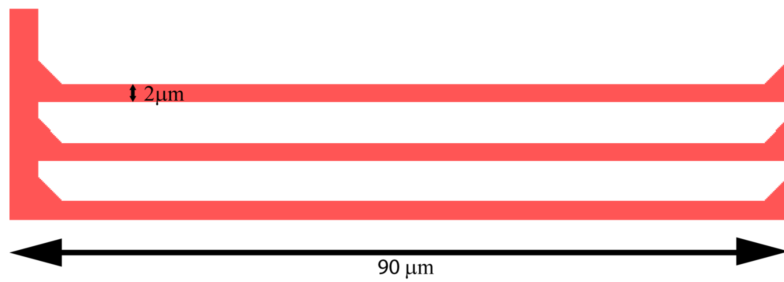

Figure 3.3: Dimensions of the interior arms in μm.

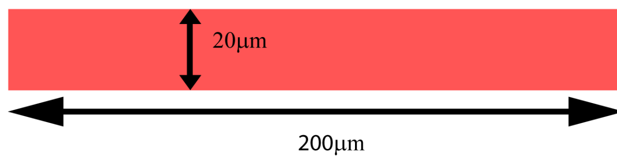

Figure 3.4: Dimensions of the exterior arms in μm.

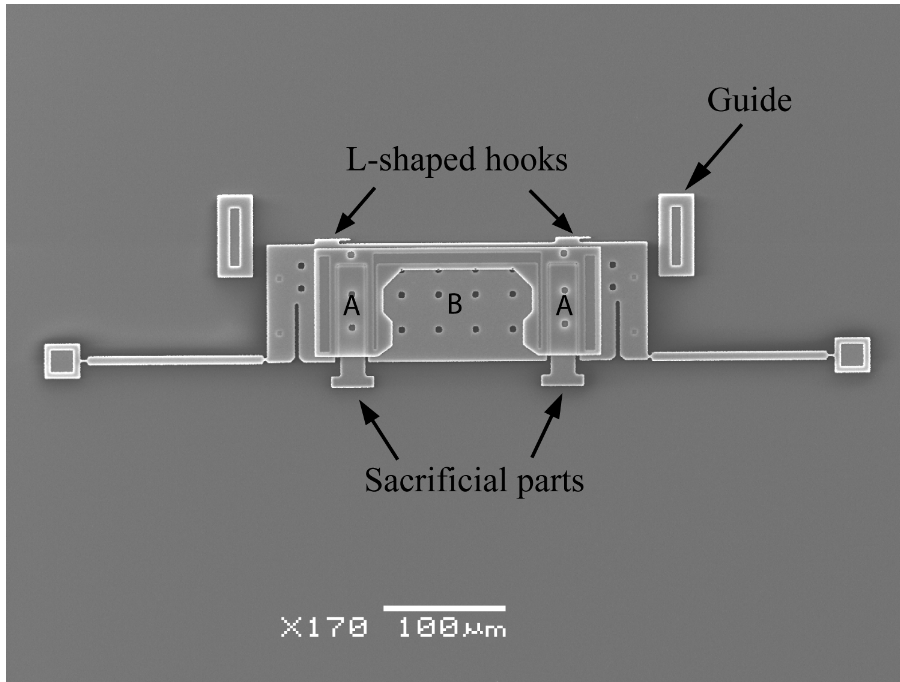

Figure 3.5: SEM image of the interface for Gripper A.

The tethers on either side of the part are used to hold it down once it is released from the substrate. The lettering, A and B, for the different sections will be used for reference later on, when the interaction between the gripper and the interface are explained. To clarify, A refers to the section elevated by the sacrificial part and B is the section of Poly 1 that is surrounded by Poly 2 in the shape of the gripper tip.

Referring to both figures 3.2 and 3.5, it is rather clear that the two parts are meant to fit together. A side view showing the placement of the gripper parts with respect to the interface parts is shown in figure 3.6. The outer Poly 1 exterior arms of the gripper are on a lower level compared to the interior arms and will slide into section A, once the sacrificial parts have been removed. Due to the use of the sacrificial parts, the Poly 2 layer above it is elevated enough to accommodate the exterior arms located underneath. The use of a sacrificial part in the gripper design, to elevate the octagonal tip, means that it can slide over the exposed Poly 1 layer, section B. The neck area of the interface is designed to be slightly narrower than the interior arms when at rest. This is where the flexible arms come into play. As the gripper is slid forward into the interface, the interior arms will encounter

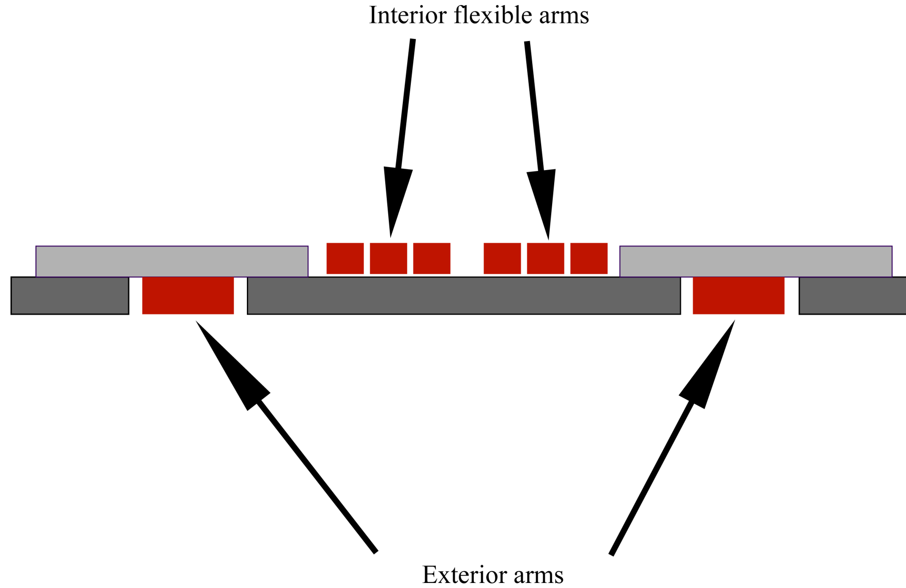

Figure 3.6: Due to height difference, the different layers of Gripper A and its corresponding interface fit together.

the Poly 2 layer that is sitting on top. When it hits the neck area, the interior arms will be forced to bend inwards by a deflection of 7.5 μm each. Once the neck area is cleared, they are allowed to expand outwards, essentially clasping the interface and restricting its movement in the X-Y direction. At this point, the exterior arms are underneath section A and the interior arms are on top of the interface in section B, further restricting its movement in the Z direction. This results in a fully grasped part.

3.5.2 Mathematical Analysis

Analyses for gripper A was done by first breaking it down into its basic structures, then applying boundary conditions and relevant forces as dictated by the operation of the gripper. Grasping, part removal from the tethers, insertion and gripper release of the parts are all steps that can potentially damage the gripper. Therefore it must be confirmed that the gripper structure can withstand the displacements and forces involved in these steps. Both exterior arms are identical and as mentioned previously, the same holds true for the interior arms, meaning analysis is only required on one of each.

The design for gripper A can be broken down into simpler structures and the

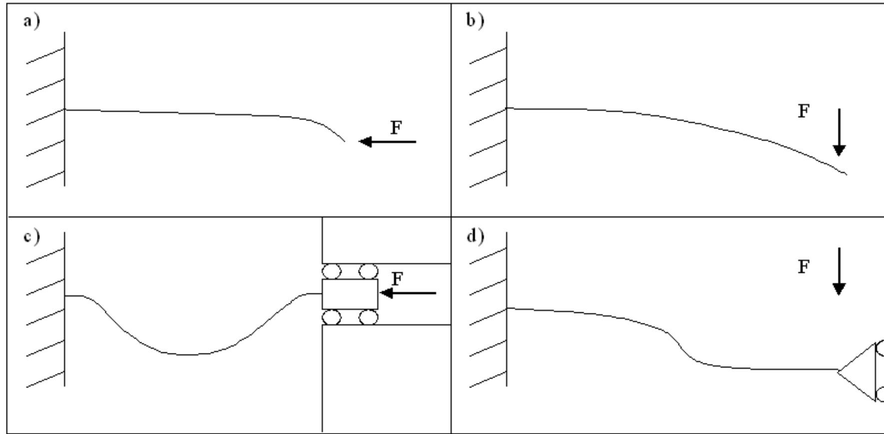

Figure 3.7: a: Bending of a cantilever from a horizontal force, b: bending of a cantilever from a vertical force, c: bending of a fixed-guided beam from a horizontal force, d: bending of a fixed-guided beam from a vertical force.

corresponding forces that act upon them. The major components, the exterior arms and the flexible arms of the interior arms, are all beam structures. They differ in the restrictions at the ends of the beams and the forces that act on them. It is assumed here that connections with the bonding pad act as a fixed connection, meaning the bonding pad does not move. The exterior arms are cantilever beams, fixed at one end by the bonding pad and free at the other end. Each of the flexible arms is fixed-guided, where one end is fixed by the bonding pad and the other is guided by movement of the semi-octagonal tip. The semi-octagonal tip acts as a rigid structure that binds the three flexible arms at one end. Figure 3.7 displays the restrictions on the beam ends and the resulting bending motion when a force is applied in the vertical and horizontal directions. Figures 3.7a and 3.7b show a cantilever beam with a horizontal and vertical force being applied respectively. Figures 3.7c and 3.7d show a fixed-guided beam being subjected to a horizontal and vertical force respectively. Here the restrictions on the fixed-guided beams are more obvious. The effect of the semi-octagonal tip is that it prevents the end of the beam from rotating unlike with the free end of the cantilever beam. This means the angle of the beam tip at the point where it is connected to the semi-octagonal tip is zero with respect to semi-octagonal tip. However because the tip can move around in the horizontal and vertical directions, it results in bending within the flexible arms.

During the part removal a force acts on all the beams as they push against the interface to break the tethers. The direction of this force corresponds to the horizontal force in figure 3.7 above. As a result, this causes the bending of the beams as seen in figures 3.7a and 3.7c. When the interior arms bend to pass through the neck area of the interface, the situation of figure 3.7d occurs. These two situations will be looked at in the following sections.

Some constants that will be used in the analyses are: Young's Modulus of 169 GPa, Poisson's ratio of 0.22. In addition, polysilicon has a reported ultimate strength ranging from 1.3 to 3.2 GPa [25, 26]. The median of this is 2.25 GPa and was used for stress analysis comparison.

When a force acts along the axis of a beam, it will reach a certain point where the beam will buckle. This is the case during the removal of a part, where the removal force acts along the axis of each exterior and flexible beam. As mentioned previously, the tether design was based on the design documented in [13], which estimates the breaking force of the first tether to be 120 μN. Between the interior and exterior arms, there are 8 beams where to break the tether, each one takes on 15 μN of the removal force. Buckling beam analysis falls under column theory, which can be found in most fundamental mechanics books. The critical force where buckling occurs in a beam is given by the following equation [16]:

$$P_{CR} = \frac{n\pi^2 EI}{L^2} \tag{3.1}$$

where E is the Young's Modulus and I is the moment of inertia given by:

$$I = \frac{bt^3}{12} \tag{3.2}$$

where b is the width of the beam and t is the height of the beam, when looking at the cross section of the beam.

The value of n in (3.1) is a constant dependent on the end conditions of the beams. Using the values of the parts outlined in figures 3.3 and 3.4, the results for the cantilever and fixed-guided beams can be found in table 3.1.

Assuming the beam conforms to Hooke's Law, the stiffness of each beam can be found and is used to relate the force applied to the amount of displacement as seen in the following equation.

$$F = kx \tag{3.3}$$

Beam	n	Moment of Inertia (μm^4)	$P_{CR}(\mu$N)
Cantilever	1/4	13.33	138.99
Fixed-guided	4	1.33	1098.25

Table 3.1: Buckling point for different end conditions.

where F is the force applied, K is the spring constant and x is the displacement. The total spring constants for beams in series and parallel are given as follows

$$Series : \frac{1}{K_{total}} = \frac{1}{K_1} + \frac{1}{K_2} + ... \tag{3.4}$$

$$Parallel : K_{total} = K_1 + K_2 + ... \tag{3.5}$$

These relationships will be used once the spring constant is found.

A basic relationship between the deflection of a beam to the mechanical properties of the beam material can be found by applying a geometric analysis to the bent beam. This relationship can then be used as the starting point in finding the relationship between applied force and the resulting deflection. The problem is well-documented and a step-by-step analysis can be found in [16] as well as other numerous books.

An alternative approach is to use an energy method. The strain energy of a beam based on a variable bending moment can be found using [27].

$$U = \int_0^L \frac{M^2 dx}{2EI} \tag{3.6}$$

$$U = \int_0^L \frac{EI}{2} (\frac{d^2y}{dx^2})^2 dx \tag{3.7}$$

where M is the bending moment, E is the Young's Modulus and I is the moment of inertia, x is the distance along the beam where the force is being applied and y is the resulting displacement of that point.

Equation 3.7 clearly shows the relationship between the strain energy and the bending displacement, y. To find the displacement based on the amount of strain energy, Castigliano's theorem can be used, which essentially states that a partial derivative of the strain energy of a structure with respect to any load is equal to the displacement caused by that load [28]. This is mathematically represented by:

$$\delta_i = \frac{\partial U}{\partial P_i} \tag{3.8}$$

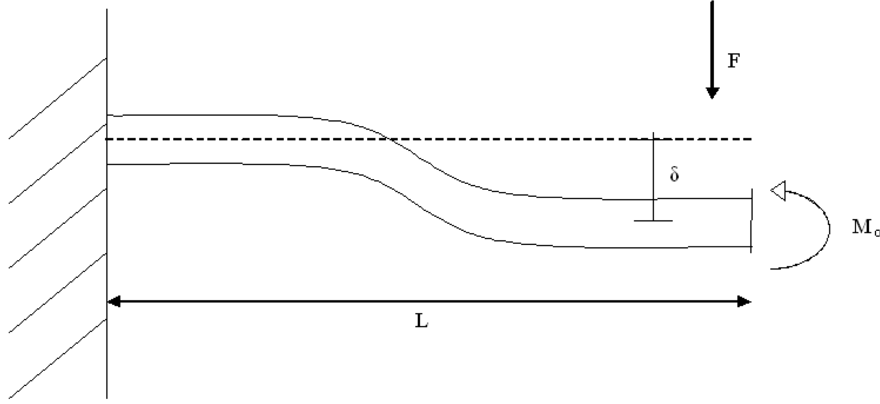

Figure 3.8: Free diagram of fixed guided beam.

where δ_i is the displacement of the bent beam in the direction of the force and P_i is the force being applied. Similarly this can be applied to moments (M_i) and corresponding angles of bending (Θ_i) as follows:

$$\Theta_i = \frac{\partial U}{\partial M_i} \tag{3.9}$$

To find the displacement of a beam as a result of an applied force, an equation for the bending moment must first be found. This is dependent on the end conditions of the beam. Since the bending moment in (3.6) is squared, this can lead to long and tedious equations. A modified version of Castigliano's theorem can help simplify the analysis and is given by:

$$\delta_i = \frac{\partial}{\partial P_i}\int_0^L \frac{M^2 dx}{2EI} = \int_0^L (\frac{M}{EI})(\frac{\partial M}{\partial P_i})dx \tag{3.10}$$

The partial derivative of the bending moment with respect to the force applied should result in a simpler equation. Equations (3.10) and a similar variation on equation (3.9) will be used for beam analysis for gripper A and gripper B.

Taking the fixed-guided beam for example, the forces and moments acting on it are shown in figure 3.8. The moment M_O prevents the end of the beam from rotating and making the angle Θ at the end of the beam zero, as required by a fixed-guided beam. As mentioned previously, this moment is applied through the connection of the flexible beams to the semi-octagonal tip. The beam has height, h, and width, w, with a length, L. The location along the beam axis is represented by x, which varies from 0 to L. Mathematical analysis was done to determine the

relationship between the applied force, F, and the displacement, δ, and is as follows:

$$M = M_O - Fx \tag{3.11}$$

Solving for M_O using the end condition of $\Theta = 0$,

$$\Theta = 0 = \frac{\partial U}{\partial M} = \int_0^L (\frac{M}{EI})(\frac{\partial M}{\partial M_O})dx \tag{3.12}$$

$$= \frac{1}{EI}\int_0^L (M_O - Fx)(1)dx \tag{3.13}$$

$$= \frac{1}{EI}(M_O x - \frac{Fx^2}{2})_0^L \tag{3.14}$$

Setting this to 0 and solving for M_O,

$$0 = M_O L - \frac{FL^2}{2} \rightarrow M_O = \frac{FL}{2} \tag{3.15}$$

Plugging this into the displacement equation,

$$\delta = \frac{1}{EI}\int_0^L (M)(\frac{\partial M}{\partial F})dx \tag{3.16}$$

$$= \frac{1}{EI}\int_0^L (\frac{FL}{2} - Fx)(-x)dx \tag{3.17}$$

$$= \frac{1}{EI}(\frac{-FL^3}{4} + \frac{FL^3}{3}) \tag{3.18}$$

$$= \frac{FL^3}{12EI} \tag{3.19}$$

Given that the spring constant (K) is force applied divided by the displacement, K is defined as:

$$K = \frac{12EI}{L^3} \tag{3.20}$$

A similar approach is taken for a cantilever beam using the energy method. The only difference would be the equation for the bending moment which is dependent on the end conditions. Table 3.2 summarizes the spring constant for cantilever and fixed-guided beams for applied forces in the transverse directions for each beam type. These constants are for point forces acting at one end of the beam [29].

Looking at the structure of the interior arms which comprise of three flexible arms each, it can be seen that this is equivalent to three fixed-guided beams in parallel. Applying equation (3.5), the total spring constant for the interior arm is:

$$K_T = \frac{36EI}{L^3} \tag{3.21}$$

Beam Type	Tranverse Force
Cantilever	$K=\frac{3EI}{L^3}$
Fixed Guided	$K=\frac{12EI}{L^3}$

Table 3.2: Tranverse force equations for cantilever and fixed guided beam types.

Using the length of the flexible arm as seen in figure 3.3 and the Young's modulus for polysilicon, the moment of inertia from table 3.1, the resulting spring constant was calculated to be $K_T = 11.13\ \mu N/\mu m$.

3.5.3 Simulation

To simulate the gripper structures, designs made in MEMSPro were imported into ANSYS 8.0. These were then analyzed by applying the appropriate boundary conditions and forces. The purpose of these simulations is to confirm the mathematical analysis and observe the behaviour of the gripper through animation. It will also show the distribution of stress through the gripper structure and overall provide a better understanding of the gripper.

The first simulation comparison concerns the axial forces along the exterior and flexible arms, basically buckling analysis. This analysis is done to determine the critical force P_{CR} that can be applied to the beam before it buckles. Two types of buckling analyses can be conducted, an eigenvalue analysis and a nonlinear analysis. The former provides a theoretical P_{CR}, which is larger than the actual value since it does not take non-ideal behaviour into consideration. It does however provide a starting point for a nonlinear analysis, which provides a more accurate value. That being said, as a simple check, the eigenvalue analysis should always provide a larger result than the nonlinear analysis [30].

The eigenvalue analysis for a single exterior arm and a single flexible arm resulted in values of 138.99 μN and 1098.00 μN respectively. To determine the buckling point for a nonlinear analysis, a plot of displacement versus force applied is made. The point where a sharp change in displacement occurs is the buckling point. Figures 3.9 and 3.10 show the plots for an exterior and flexible arm, respectively, and it is quite obvious where buckling occurs for each. Figures 3.11 and 3.12 show the bending shape of each beam. It is clear that the bending shape is drastically

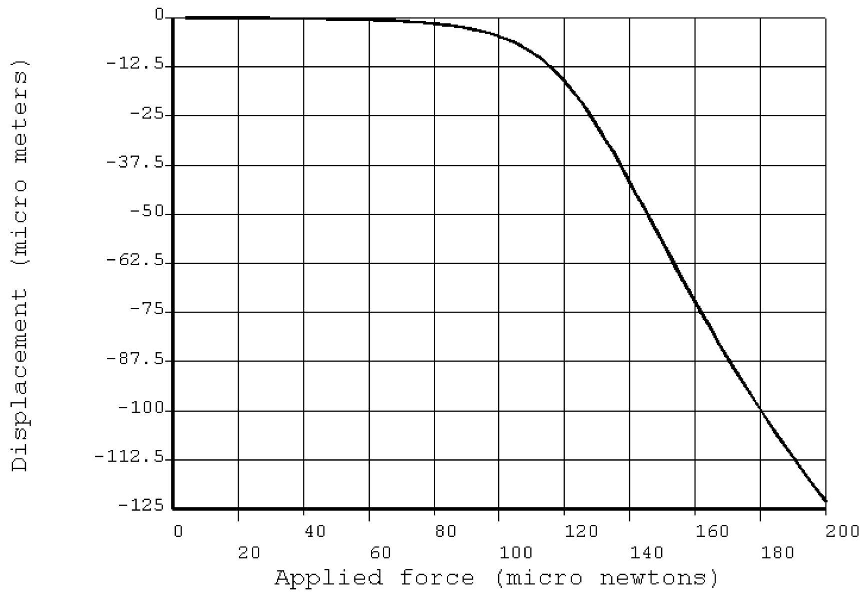

Figure 3.9: The buckling point of the exterior arm can be seen to be at approximately 120μN.

different depending on the type of end conditions. This is also reflected in the difference in P_{CR} values despite the fact that the flexible arms are significantly smaller than the exterior arms; due to the end conditions, they have a much larger P_{CR} value. From the above figures, it can be seen that the simulated buckling for the exterior and interior arms are approximately 120 μN and 1000 μN, respectively.

The second simulation is to determine the required force and the stress that results when the three flexible arms are displaced the necessary amount for them to fit within the interface. Since the interior arms are symmetrical, analysis was only conducted on one of the arms. A meshing size of 1 μm was used with a solid 92 element. The Young's modulus and Poisson ratio values used were the same as those stated previously. Each flexible arm was restricted according to a fixed-guide beam with the end connected to the bonding pad restricted in the X, Y and Z directions and the other end connected to the octagonal tip free to move in only the X direction. Based on the spring constant analysis done previously, a force of 90 μN was applied to the center of the right face of the octagonal tip. This resulted in a maximum displacement of 7.599, which can be seen in figure 3.13. This results in a spring constant value of 11.84. The corresponding Von Misses stress values

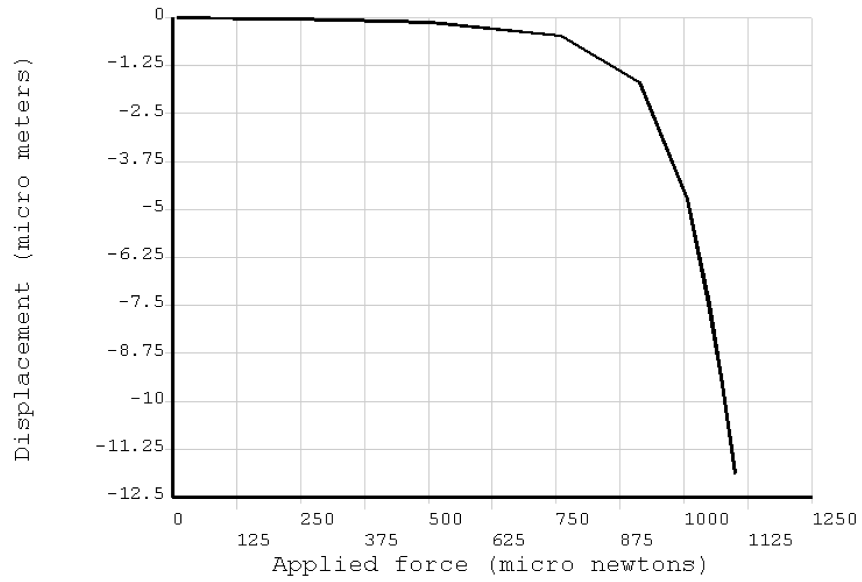

Figure 3.10: The buckling point of the interior arm can be seen to be at approximately 1000μN.

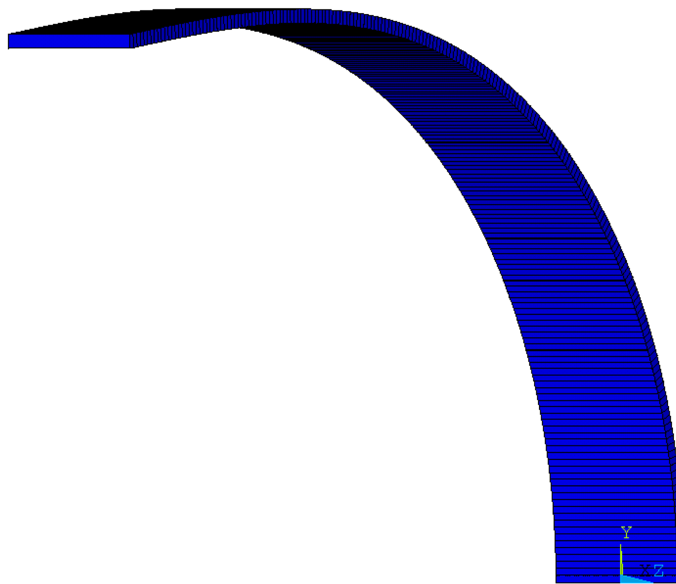

Figure 3.11: Bending shape of the exterior arm.

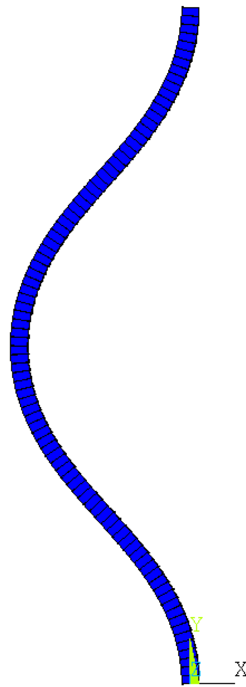

Figure 3.12: Bending shape of the interior arm.

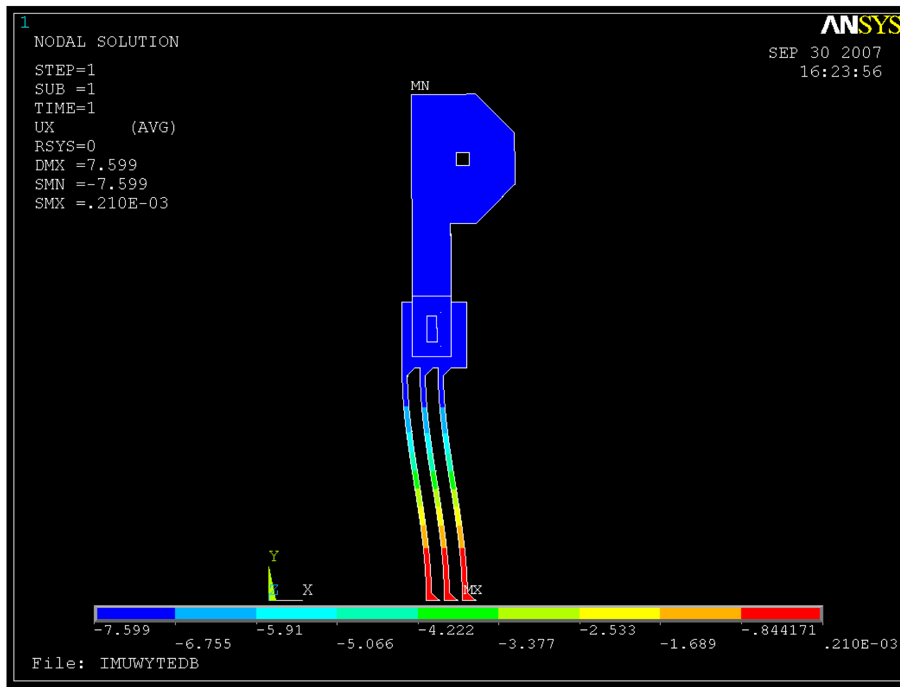

Figure 3.13: ANSYS simulation of the interior arm shows a displacement of 7.599μm with an applied force of 90μN.

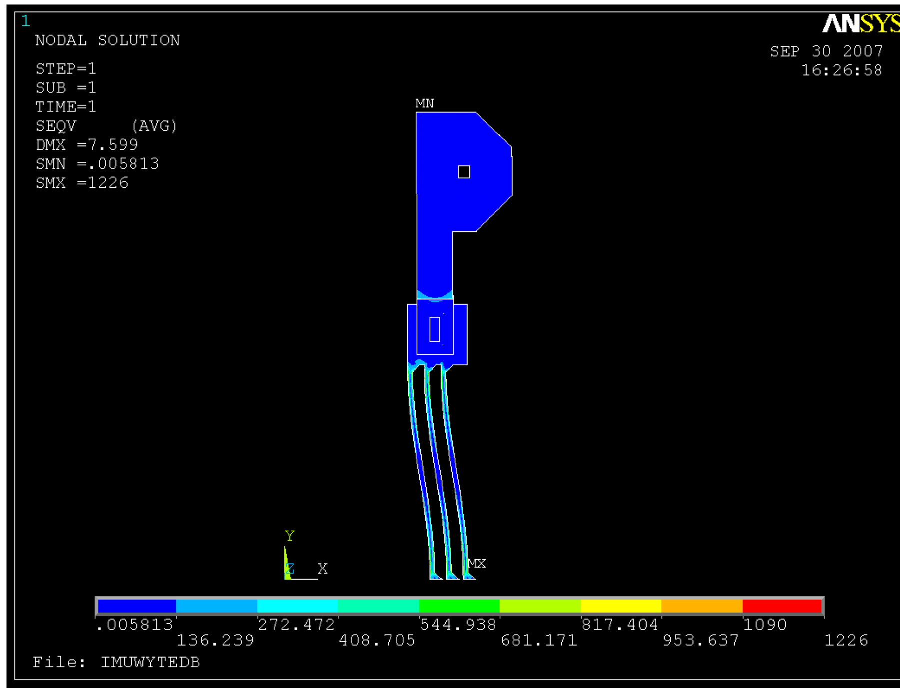

Figure 3.14: ANSYS simulation of the interior arm shows a Von Misses stress value of 1.226GPa with a displacement of 7.599μm.

can be seen in figure 3.14.

A summary of the calculated and simulated values with the corresponding percentage error can be found in table 3.3. The buckling percentage error can also be attributed to the reading of the graph, since it is difficult to determine the exact point at which the buckling occurs.

3.6 Gripper B

3.6.1 Functionality

Whereas gripper A attempts to simplify the design approach by separating the structural needs from the flexibility ones, gripper B attempts to combine them into one main structure. An SEM image of gripper B is seen in figure 3.15.

As with gripper A, a bonding pad with tethers to hold down the gripper once it is released is attached to the functional tip. The tip itself is made up of two main parts, the serpentine spring in the middle and the two-level side arms that

	Calculated	Simulation	%
Buckling			
Exterior arm	138.99μN	120μN	15.8 (error)
Single flexible arm	1098.00μN	1000.00μN	9.8 (error)
Traverse bending			
Interior arm - spring constant	11.13μN	11.84μN	6.0 (error)
Interior arm - stress	2.25GPa	1.226GPa	54.49 (of ultimate strength of polysilicon)

Table 3.3: Summary of mathematical and simulation results for gripper A.

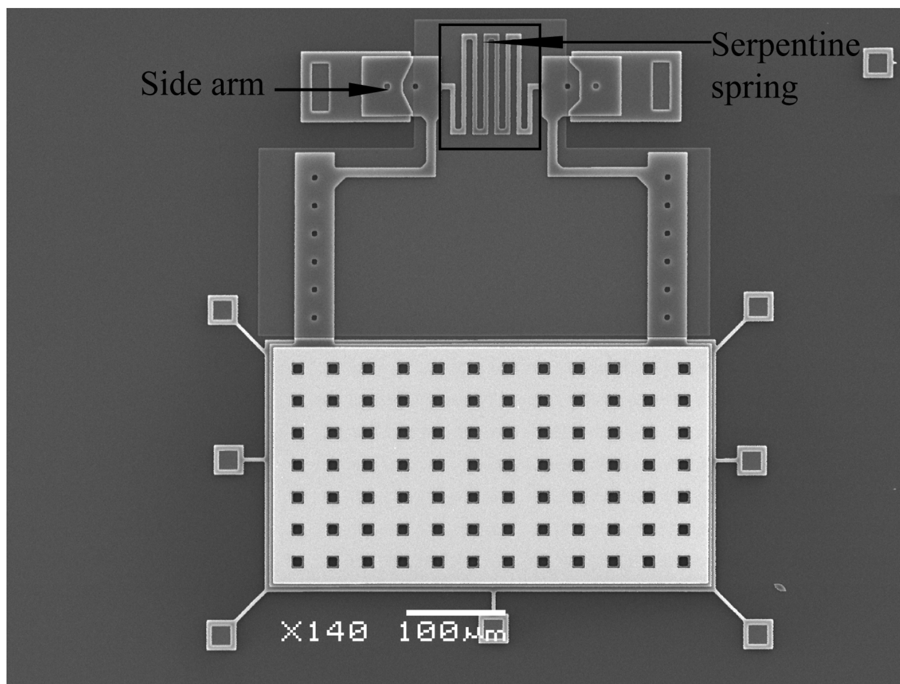

Figure 3.15: SEM image of Gripper B design. Sacrificial parts are located on either side of the gripper.

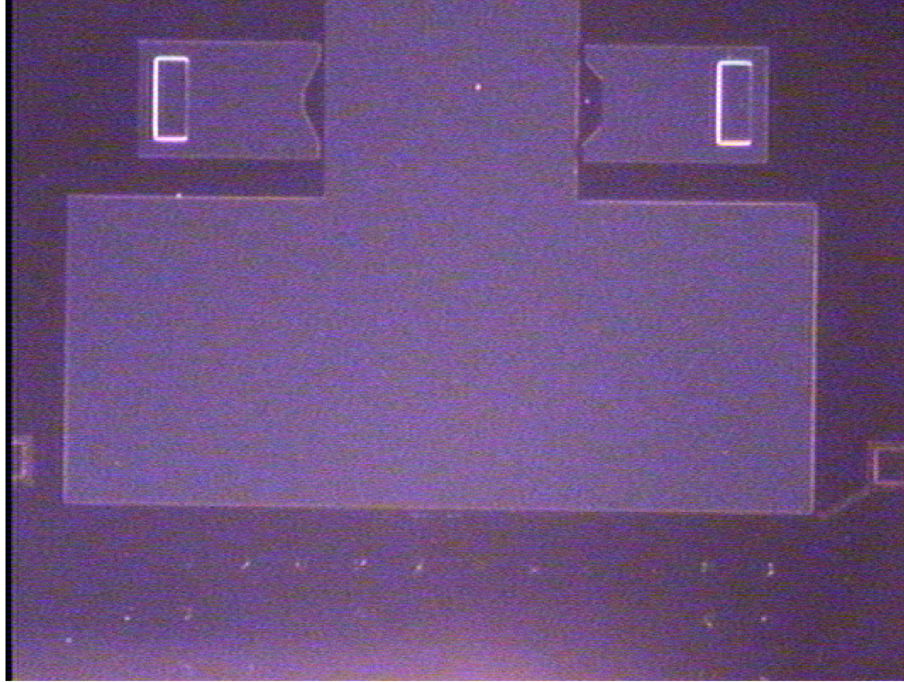

Figure 3.16: Image of sacrificial part left behind after removal of Gripper B from the substrate.

are attached to it, which are both composed entirely of Poly 2. The two levels are created by sacrificial parts made of Poly 1, which are anchored into the substrate. It is difficult in this picture to distinguish between the gripper and the sacrificial parts. Seeing the two together using the following images, figure 3.16 and 3.17, taken with the lab cameras, will help show this. The two anchored side structures in figure 3.16, are composed of Poly 1 and the larger upside down T portion is composed of Poly 0. The Poly 0 has no oxide separating it from the substrate and hence requires no anchor. The reason two different layers are used as sacrificial parts is because due to their thicknesses and the oxide layers that separate them, they can achieve different heights. Here the Poly 0 sacrificial layer is underneath the majority of the tip structure, this is done so that the tip will fit more snuggly into the interface. Figure 3.17 shows the gripper after it has been lifted off the substrate. The dimensions of the serpentine spring are shown in figure 3.18.

Since the Poly 1 is thicker and has a first oxide layer separating it from the substrate, the anchored side sacrificial layers create a higher elevation for the Poly 2 layer of the gripper that is deposited over it. A closer look at the two-level side arm, pictured in figure 3.19 of the gripper will explain this better. This figure was

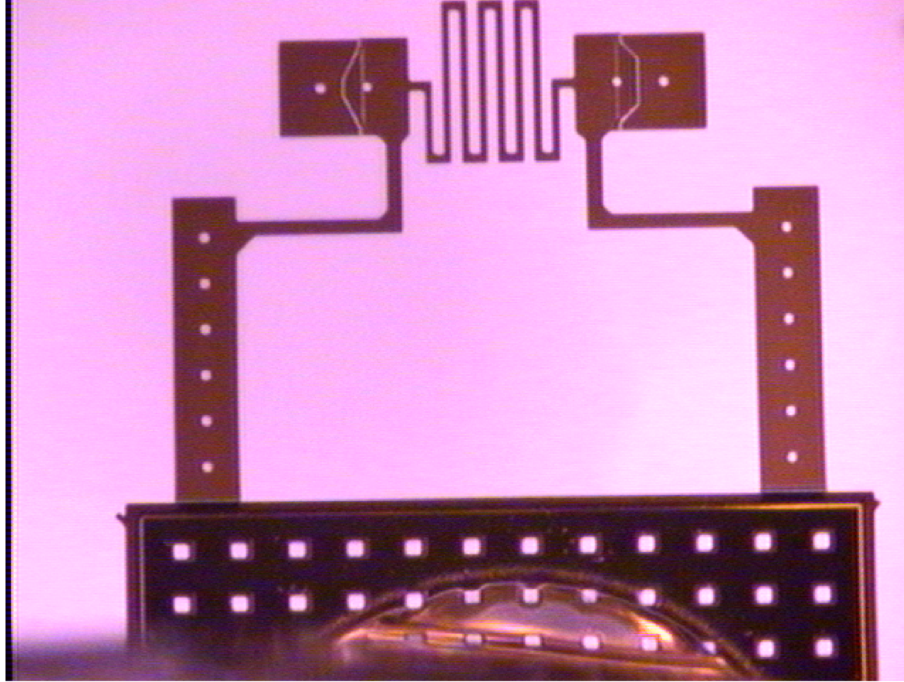

Figure 3.17: Gripper B connected to the probe tip using adhesive.

taken from the L-Edit design. Here the colours correspond to different PolyMUMPS layers and are labeled to clearly indicate what they are. It is important to remember that between each polysilicon layer there is an oxide layer (not shown here) which was removed at the end of fabrication. The Poly 2 layer of the side arm overlaps three areas, the sacrificial Poly 0 and Poly 1 areas and a small portion which does not have any polysilicon underneath it. Two etch holes are present, once again for oxide removal. As mentioned before, the Poly 1 sacrificial structure is more elevated than the Poly 0 layer due to their differences in thickness and the oxide layer that separates them. This puts the section of the gripper that is overlapping the Poly 1 higher than the rest of the gripper. To illustrate the height difference, figure 3.20 shows the different layers and the resulting gripper structure. The resulting Poly 2 layer conforms to the shape of the layers that have been laid down before it. Hence in the section where there is no sacrificial polysilicon underneath it, there will be a dip in the Poly 2 structure. This is the lowest part, with the area over the Poly 0 sacrifice next in height and finally the area over the Poly 1 being the highest. The gap between the Poly 0 and Poly 1 are a result of PolyMUMPS rules, which states that different layers must be placed a minimum distance away from each other. The resulting dip, although not ideal, does not pose a problem since it does not hinder

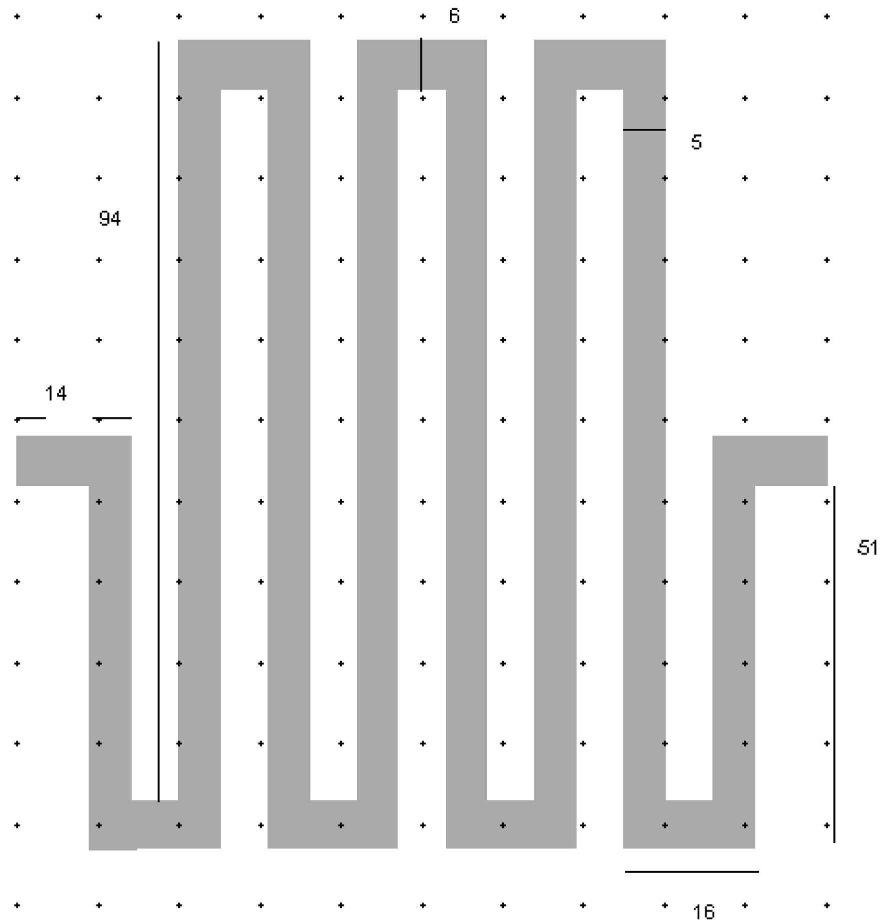

Figure 3.18: Dimensions of the serpenting spring in μm.

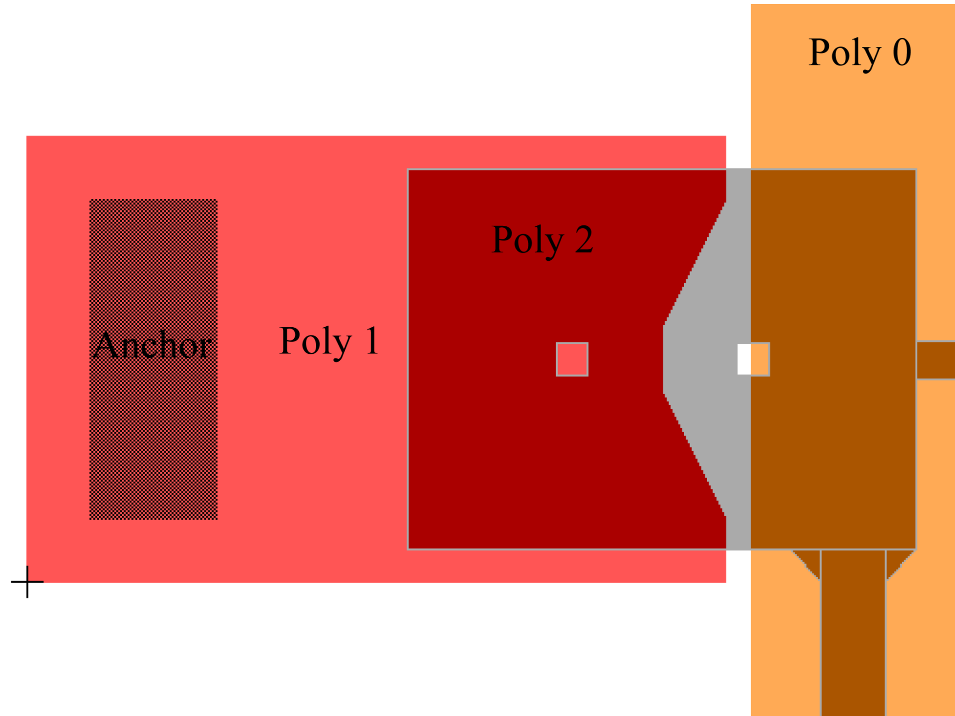

Figure 3.19: The different colours reflect different layers. It can clearly be seen where the layers overlap each other.

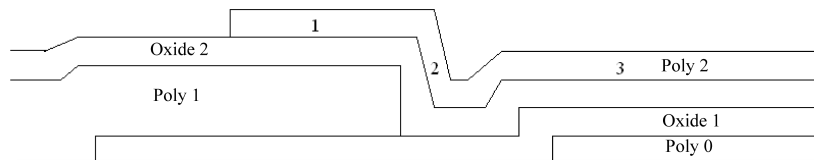

Figure 3.20: The difference in height created by the overlapping layers can be seen.

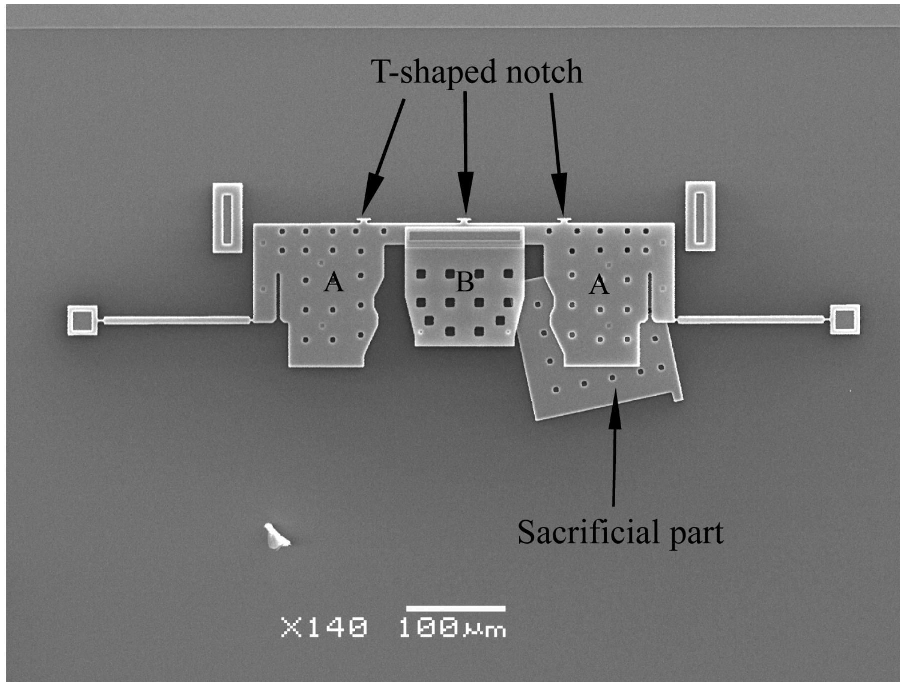

(b)

Figure 3.21: The interface for Gripper B done in MEMSPro.

the operation of the gripper. The important feature to note is the wall created as a result of the height difference between the Poly 1 and Poly 0 layers. The numbers will be used to refer to different sections of the gripper when the interaction with the interface is being explained. To be clear, section 1 refers to the higher elevated plane of the gripper, section 2 the wall between sections 1 and 3 and finally section 3 represents the lower plane of the gripper.

As with the interface for gripper A, the interface for gripper B was designed to be the puzzle piece that fits it. Figure 3.21 shows the finite element method (FEM) image of the interface. Once again a sacrificial part is used to elevate the middle section. The lack of anchors and tethers indicate that once the oxide is removed, the sacrificial part will be free to move around, which is the case in the figure. This part will be removed by the probe tip before an attempt at grasping is made. By using the sacrificial part, it makes the center portion of the interface more elevated than the side portions. This is the exact opposite use of the sacrificial parts in the gripper design. The interface is composed of Poly 1 and Poly 2 layers, attached to each other using the VIA represented by the rectangular area at the top of the section labelled B. The white squares are once again etch holes and the darker

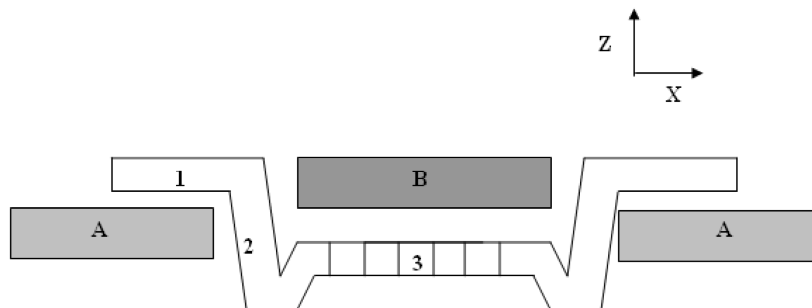

Figure 3.22: The parts of the gripper and part are elevated in certain sections that they are able to interact as seen in the above picture.

squares are dimples.

The pattern along the side arms is done to help guild the gripper into position. The neck area is narrower than the gripper when at rest (i.e. when the serpentine spring is uncompressed). Therefore when the gripper is pushed into the interface, it will reach the neck and bend inwards (the serpentine spring compresses). Once it is past this section, it will reach a wider area and return to the rest position. The letters indicate areas that will be referred to when describing how the gripper is used to grasp the interface. Section A refers to the two side sections and section B the Poly 2 center that is elevated. For purposes of clarity and readability, the numbered parts from figure 3.20 and the lettered parts from figure 3.21 will from now on be referred to by their respective number and letter.

As a reminder the sacrificial part will be removed before a grasping attempt. When the gripper is pushed into the interface by movement in the Y direction, it will first encounter resistance when 2 meets the side walls of A. Due to the height differences, 1 will slide overtop of A and 3 (serpentine spring) will slide underneath B. As mentioned before, as 2 follows the side walls of A, it will hit the neck area and bend inwards. This bending is facilitated by the serpentine spring structure in the middle of the gripper compressing inwards. Figure 3.22 is a side view of how the layers of the gripper and interface interact with each other.

Clearly, by having the gripper restricted by sections A and B below and above respectively, movement in the Z direction is restricted. When the gripper passes the neck portion of the interface and comes to rest, it will take some force for it to

come back out past the neck once again. This requires that the part is attached to something, to supply a necessary resistance to the removal force such that the part does not just move with the gripper. After being released from the tethers, this only occurs when the part has been inserted. As a result, for the time that the part is broken from the tethers and not yet inserted, its movement in the X and Y directions are restricted by the gripper.

3.6.2 Mathematical Analysis

When the gripper grasps the interface, the serpentine spring compresses as the two-level side arms are bent inwards by 4μm each in order for the gripper to fit into the interface. Therefore, the serpentine spring is an integral part of the gripper actuation, making the design of it crucial. The serpentine spring should be designed such that it can provide the necessary actuation without permanent damage to the spring structure.

To determine if a design is appropriate, the spring constant can be found using energy analysis methods, in particular Castigliano's theorem as defined by equation (3.10). An analysis using the unit-load method was done in [31] for the serpentine spring structure shown in figure 3.23.

Analysis of the above serpentine spring structure results in the following equation for an even number of n (where n is the number of beams with a length of "'a"'):

$$K_x = \frac{12EI_Z[(a'+b)n^2 - 3bn + 2b]}{b^2[(3a'^2 + 4a'b + b^2)n^3 - 2b(5a'+2b)n^2 + (5b^2 + 6a'b - 9a'^2)n - 2b^2]} \quad (3.22)$$

where $a' = \frac{I_Z a}{I_Z}$

Referring to figure 3.23, 'a' is the length of the short connecting arm, 'b' is the length of the long arms, 'F' is the force applied to the free end of the spring, 'E' is the Young's Modulus and 'I$'_Z isthemomentofinertia.ThisequationassumesthatmovementintheYandZdir$
$thefirstsectioncorrespondingtoaserpentinespringstructurethatcanbeclassifiedaccordingtothatoffi$

Figure 3.24 shows the two separate structures that the serpentine spring can be broken down into.

The spring constant of the crab leg can be found in [31] and is given as:

$$K_X = \frac{Etw_b^3(4L_b + \alpha L_a)}{4L_b^3(L_b + \alpha L_a)} \quad (3.23)$$

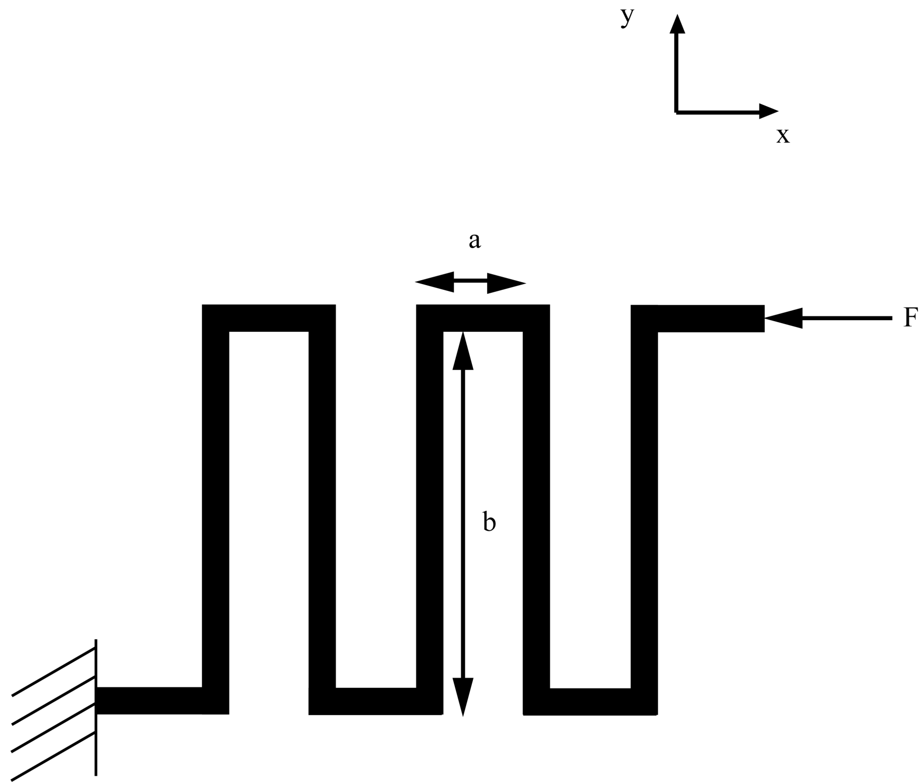

Figure 3.23: A typical view of a serpentine spring where the one end is fixed and a force is applied at the other end.

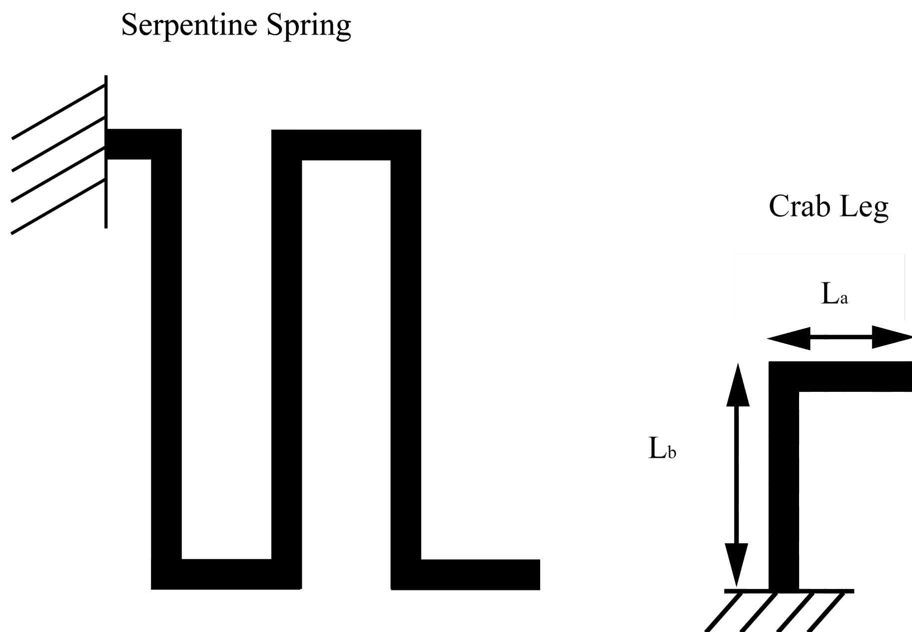

Figure 3.24: The serpentine spring of gripper B is broken down into two parts.

where $\alpha = (w_b/w_a)^3$ and w_a and w_b are the widths of the beams with lengths L_a and L_b, respectively.

During operation of the serpentine spring, it is assumed that two equal and opposite forces act on either side of the spring as it compresses to fit within the interface. Consequently, it is assumed that the symmetrical center of the spring has a net displacement of zero, since the displacements resulting from the applied forces are assumed to be of equal and opposite magnitude. The combination of the results of equations 3.22 and 3.23 using equation 3.4 was done to calculate the spring constant of only one half of the serpentine spring. The result of 3.22 using the dimensions of the serpentine spring was 13.4239μN/μm and the result of 3.23 was 285.7588μN/μm, making the total spring constant 12.8216μN/μm.

3.6.3 Simulation

Simulation of the entire serpentine spring was done using ANSYS once again. As stated above in the mathematical model, the ends at which the forces are applied are assumed to have no displacement in the Y and Z directions. The model was meshed using 1 μm elements and a solid 92 element type. The values for Young's modulus and Poisson's ratio are the same as those used previously.

Based on the results of the mathematical analysis and the subsequent calculation of the spring constant, a force of 52μN in the positive X direction and a force of -52μN in the negative X direction were applied to each end of the serpentine spring. Figure 3.25 shows the resulting displacement of the serpentine spring. Table 3.4 summarizes the displacement of each end and the percentage error with the calculated value.

As can be seen the simulation and mathematical results are very close with each other.

The resulting von Mises stresses due to the above applied forces can be seen in figure 3.25. The maximum stress is 789.869 MPa, this corresponds to 35% of the ultimate strength of polysilicon, which is a reasonable value.

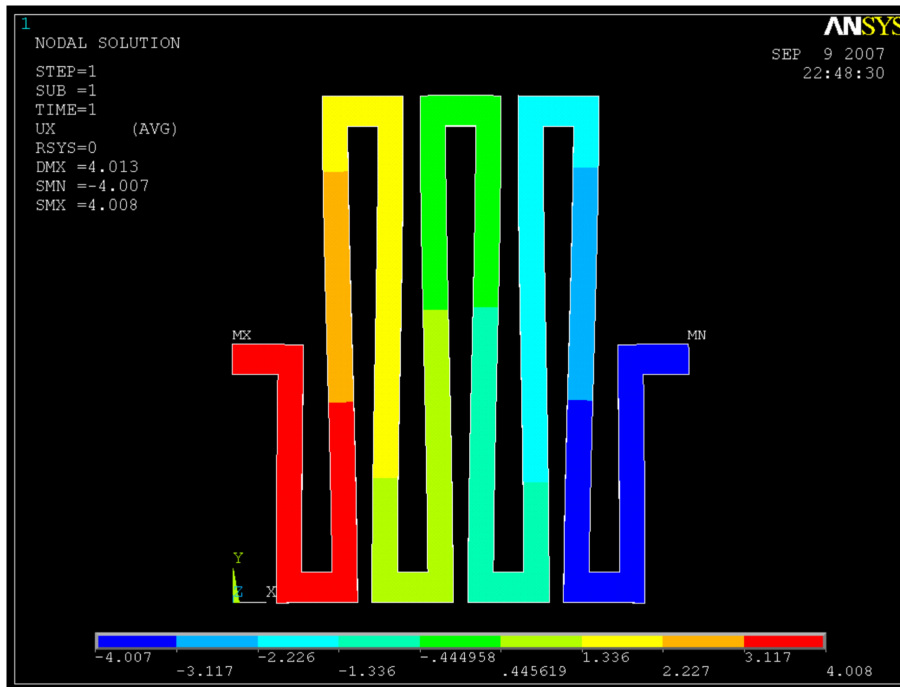

Figure 3.25: The resulting displacement of the serpentine spring after application of 52 μN forces.

	Left end	Right end
Displacement(μm)	4.009	-4.007
Force applied(μN)	52	-52
Spring constant	12.97	12.98
Calculated spring constant	12.82	12.82
%Error	1.15	1.23

Table 3.4: Summary of displacements and spring constants.

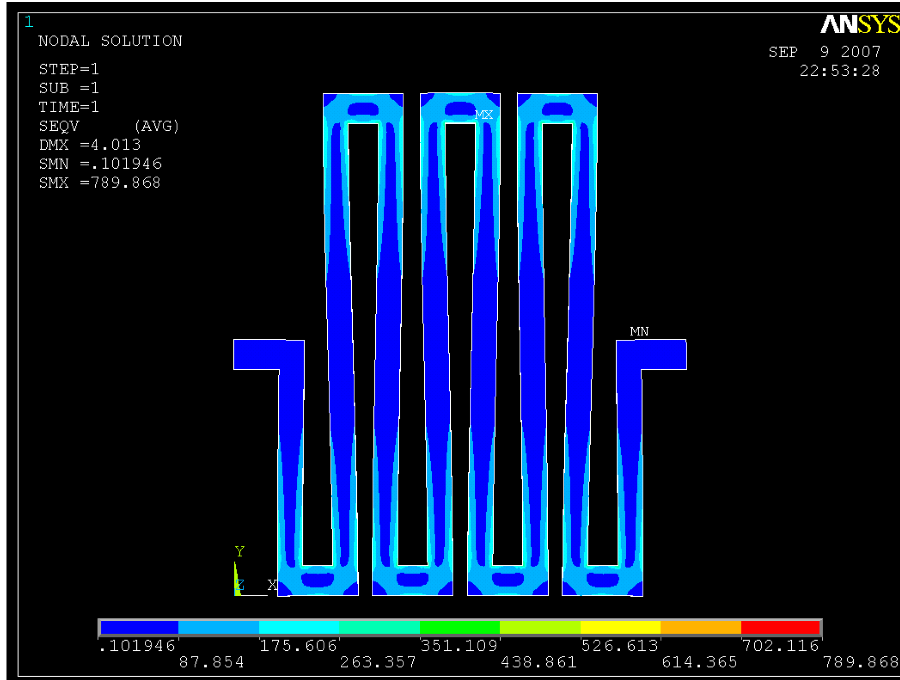

Figure 3.26: The resulting Von Mises stress from a displacement of the serpentine spring after application of 52 μN forces.

3.7 Antenna design

As mentioned previously, the first goal of the project is to establish a working 3D microassembly system. This includes working equipment and setup and working gripper designs. It was expected that at least two design iterations were required to have efficiently working gripper designs. However, since it was necessary to have parts for the gripper to interact with, it was decided to have them form a potentially useful structure. It was decided to form a 3D Yagi-Uda antenna, the design of which is fairly straight forward and well-documented in the macro world.

Since the various parts of the Yagi-Uda antenna are directly related to the wavelength of a signal and consequently the intended working frequency of the antenna, it was necessary to determine feasible working frequencies. The allowed fabrication space for all the parts and grippers is $10mm^2$. Clearly, it is necessary to have antenna parts smaller than this and at the same time there must be enough room left for the other parts. Due to this size restriction, the working frequency must be in at least the gigahertz (GHz) range, which results in wavelengths in the millimeter range. Looking at available equipment and taking the previous points

into consideration, it was decided that a working frequency of 94 GHz would be used to design the antenna.

Once the working frequency was determined, the following equations based on macro world designs were used to determine the dimensions of the different elements of the Yagi-Uda antenna (see figure 2.1) [32]:

$$\alpha = \frac{c}{f} \rightarrow \frac{3 \times 10^8}{94 \times 10^9} = 3191.489\mu m \tag{3.24}$$

Calculations for lengths of the different elements.

$$Director: \ \tfrac{2l_1}{\lambda} \ = 0.450 \tag{3.25}$$

$$Driven: \ \tfrac{2l_2}{\lambda} \ = 0.475 \tag{3.26}$$

$$Reflector: \ \tfrac{2l_3}{\lambda} \ = 0.500 \tag{3.27}$$

Calculations for width of each element:

$$\frac{a}{\lambda} = 0.0032 \rightarrow a = 10.213 \tag{3.28}$$

$$a = \frac{1}{4}(w + t) \rightarrow w = 4a - t \rightarrow w = 40.351\mu m \tag{3.29}$$

Here, 'α' represents the wavelength at 94 GHz, 'c' is the speed of light, 'λ is the frequency and 'a' is the width of each element. The ratios used to calculate the lengths of each element varies slightly between different references but for the most part is approximately on the scale of half of the wavelength. Due to space limitations on the chip, it was decided to only have one director, driven element and reflector as opposed to multiple directors, which are common in a typical design.

Figure 3.27 shows the driven element with the interface of one of the grippers installed at a location at approximately the middle of the element. For extra mechanical support, the monopole section is composed of a Poly1, Poly 2 and metal layer. Etch holes are present in order to allow release of the part. It is not sure if the etch holes will affect the electromagnetic properties of the element. The interface attached to the monopole is the same as described previously. There is also an additional section separating the monopole and the interface. This section contains a slot which will be used to place the entire section on a column part described next.

As mentioned previously, it was beneficial to bring the antenna out of plane in order to reduce parasitic effects such as surface waves. Therefore each of the above

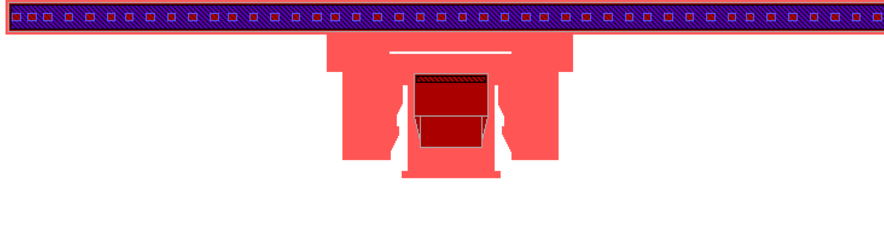

Figure 3.27: Driven element connected to the interface for gripper B.

elements is further raised off the substrate by using the following part shown in figure 3.28. The column has an expanding section at the top where the element of the antenna is inserted using the slot. As the element is initially placed over this section and lowered, the increasing size of the section causes it to catch onto the column. The gripper then releases the element and it remains resting on the protruding edge. The height from the intended resting place of the element form the substrate is half the wavelength at 94 GHz. This is also a typical design feature of Yagi-Uda antennas. There are two insertion slots at the bottom of the part which are used to place the column onto two base parts described below. The insertion slots have an array of deformable parts near the top, the design of which are based on that disclosed in [24]. Essentially, the array of arms is designed to be long enough to intrude into the slot space, such that when the column is inserted onto the base parts, the arms deform applying a reaction force keeping the part in place.

For each column, two base parts will be inserted to provide a more stable support. The reason for this extra step is to provide extra support for the column, which will become clearer as the design of the base parts and the interfaces that they are inserted into are described. Figure 3.29 shows one example of the base part. This base part is dominated by the interface designed to interact with the gripper B design. There are several extra parts added onto the interface that facilitate the extra functions of the base part. In particular, there is an insertion mechanism on the edge of each base part. This insertion mechanism is used to insert the base part into an interface on the substrate. Two insertion mechanisms were used; the first is a T-notch design disclosed in [24], and the second is a modification of the array

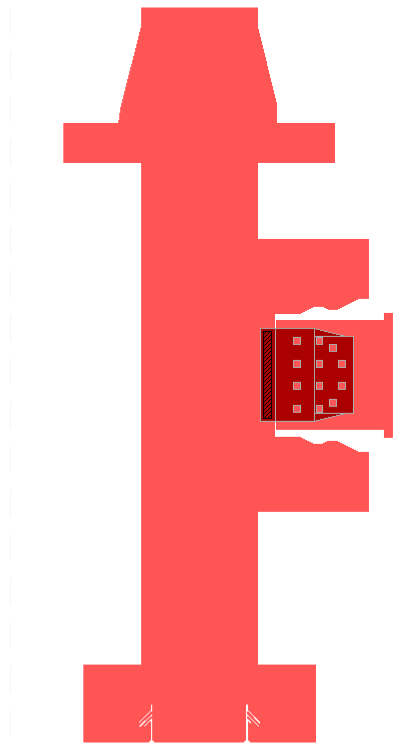

Figure 3.28: Column used to lift the antenna off the substrate.

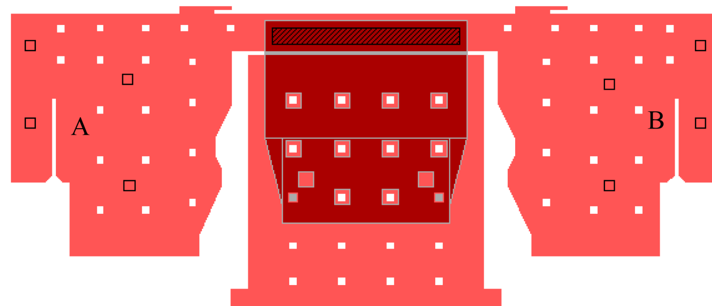

Figure 3.29: The base part of the antenna used to insert the column into and attach to the substrate.

Figure 3.30: The T-notch attached to the base part for insertion into the substrate.

Figure 3.31: Overhead view of the T-notch interface. This part is permanently attached to the substrate

of deformable arms used in the slot for the column called the L-hook design.

Figures 3.30 and 3.31 show the T-notch design, both the part that is attached to the base part and a top view of the interface on the substrate, respectively. The interface is composed of Poly 2 and anchored to the substrate. The Poly 2 layer is elevated by 2.25μm, created by the removed oxide layers. Therefore, there is a gap between the Poly 2 layer and the substrate which the wider part of the T-notch can slide under. To insert the T-notch, it is first inserted in the wider section of the interface. It is then slide forward towards the narrower section of the interface such that the wide section of the T-notch slides underneath the Poly 2 layer; once this configuration is achieved, the part is considered inserted and the gripper is pulled

Figure 3.32: The L-hook attached to the base part for insertion into the substrate.

Figure 3.33: Overhead view of the L-hook interface. This part is permanently attached to the substrate

out.

Figures 3.32 and 3.33 show the L-hook part attached to the base part and the corresponding interface on the substrate. Similar to the T-notch interface, the L-hook interface is composed of Poly 2, and anchored to the substrate such that there is a 2.25μm gap between the substrate and the Poly 2 layer. The array of deformable arms is similar in design as described previously for the insertion slot of the column. Initially, the part is inserted by lowering the L-hooks into the widest part of the interface. Once this is done, the part is slid right towards the array. As the part slides in, the arms deform and apply a reaction force, keeping the part in place. The L-hooks are located under the Poly 2 layer preventing the part from coming out.

Going back to the base part, either of the two slots, A and B, at the side of the interface can be used to have the column part inserted into. For example, two of the base parts will be inserted parallel to each other on the substrate using either of the T-notch or L-hook mechanisms. One insertion slot of the column will be inserted into an A slot on both of the base parts or a B slot on both of the base parts. Therefore, the base parts are attached to the substrate via the interfaces

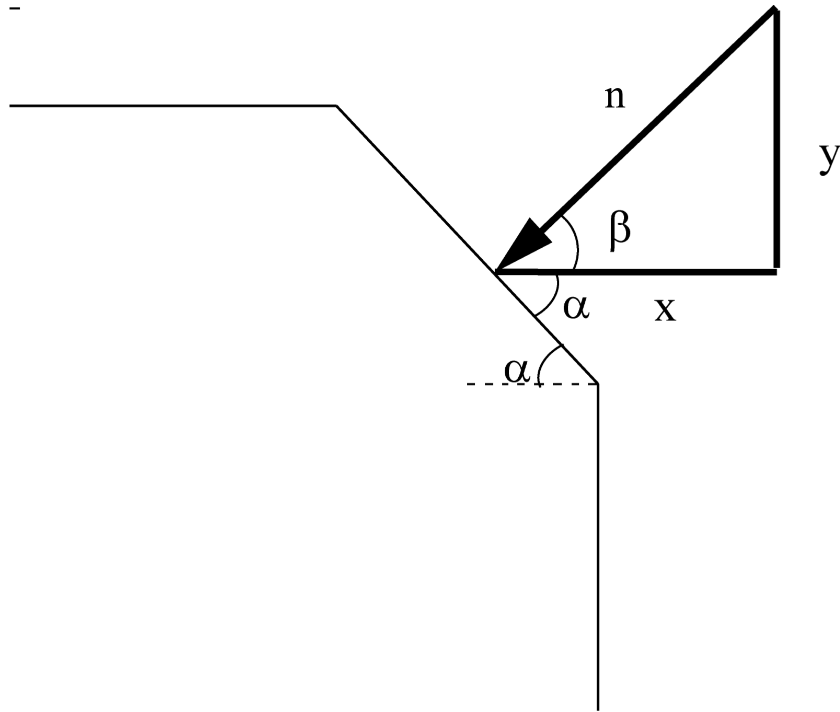

Figure 3.34: The reaction force applied to the slanted face of both grippers.

and the column is attached to two base parts. The final step would be to insert the antenna element onto the column.

3.8 Tether adjustment

Previously it was mentioned that the tethers were designed for breaking at a force of approximately 120μN. After analyzing the necessary force to compress gripper A and gripper B in order to insert them into their respective interfaces, it is possible to determine the theoretical force that will be applied to the tethers and which may contribute to premature breaking of the tethers. Looking at figures 3.2 and 3.15 of the grippers, it can be seen that during insertion, each of the grippers applies a force normal to a slanted face located on the tip. A generic diagram of the forces is seen in figure 3.34. By knowing the angle and the necessary horizontal force to compress the gripper, the normal force and the vertical force can by found according to the

	$\alpha(\beta)$	X force (μN)	n (μN)	y (μN)
Gripper A	45(45)	90.00	63.64	90
Gripper B	45(45)	52.00	36.77	52

Table 3.5: Theoretical forces applied to tethers during grasping.

following equations.

$$\beta = 90^\circ - \alpha \tag{3.30}$$

$$n = x \cos \beta \tag{3.31}$$

$$y = x \tan \beta \tag{3.32}$$

Here y is the vertical force that is applied during insertion of the part. A summary of the geometric values for gripper A and B and the resulting forces are seen in table 3.5. It should be noted that friction was not taken into consideration.

Previously it was stated that a force of 120μN was required to break the first tether. Based on the y values of table 3.5, it appears that the present design is sufficient for the gripper A and B designs.

Chapter 4

Equipment Setup

4.1 Comments

To complete the task of picking and placing a part, both hardware and software are used. Since the gripper only picks up the part and itself is not capable of rotation or translation, these necessary movements must be done by the setup equipment. The chip is placed on a stage capable of 4-degrees-of-freedom (4 DOF) movement. In addition, the gripper is attached to a micromanipulator, which in itself is also capable of 4 DOF movements. To accomplish the required steps of bringing the gripper to the part or bringing the grasped part to a location of insertion, the stage, the micromanipulator or both can be moved.

An operator is intended to manually control both the stage and micromanipulator. Feedback to the operator is necessary such that he or she knows what is happening to the parts and gripper. This is done through the use of 3 cameras, placed to provide a side view, an overhead view and an angled view of approximately 45° from the horizontal. The cameras provide a real time view of what is happening, which can also be recorded for later review.

All of these devices are connected to a computer and control of them is done through a single LabVIEW program. The interface of this program has 3 windows allowing for simultaneous viewing of each camera. Separate coordinate input boxes are provided for the stage and micromanipulator, although the latter can also be controlled through an accompanying controller. An initiation program for the stage is also written in LabVIEW and sets the stage at a known home position when

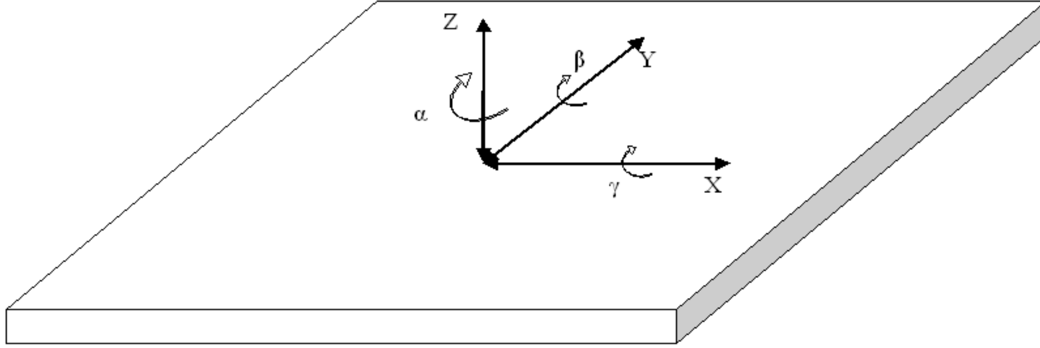

Figure 4.1: The microcomponents can be translated and rotated, resulting in 6 DOF movement.

executed. Together, all these form the microassembly system used to construct the 3D MEMS. The following sections will go into greater detail about each setup component and any issues relating to them.

4.2 Required Movements

Before it can be determined if a piece of equipment is sufficient to meet the experimentation requirements, the requirements themselves must first be defined. This is dictated in part by the orientation of the parts and the movement required to pick them up and then translate and rotate them accordingly to have them inserted. The orientation of the gripper relative to the micromanipulator is also important to determine, since the gripper can only grasp in one direction, but bonding to the gripper can be done in more than one position. Figure 4.1 shows all the potential movements that can be done on a part lying on the substrate.

Potentially a part can have 6 DOF corresponding to translation in the X, Y and Z directions and rotation about the X, Y and Z axes. For a single step of grasping and inserting a part, typically only 4 DOF are required, translation in the X, Y and Z directions and rotation about one of the axes. For example, if part removal is done by translation in the Y direction to break the tethers, then further translations in the X, Y or Z directions are done to bring the part to the necessary insertion site. At that point, only a rotation about the X axis, for example, by 90° is required to bring the part out of the XY plane and ready for insertion. The insertion step itself only requires more translation in the X, Y or Z directions. This

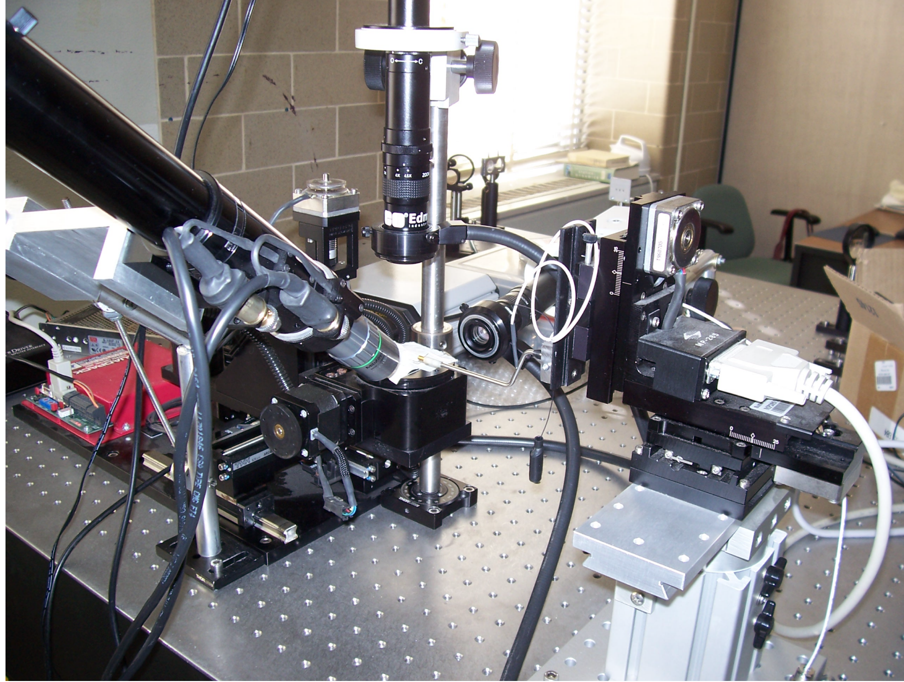

Figure 4.2: View of the 4 DOF stage, cameras, and micromanipulator.

simplifies the equipment requirement assuming that only rotation about the same axis each time is required. This however is not true as the construction of the structure progresses. For example, once a first part is inserted, a second part may be inserted at an orientation perpendicular to the first one. This then requires further rotation about the Z axis, which is easily achieved by rotating the chip using the stage. Rotation about the X and Y axes are similar and are done to bring the part out of plane. Through careful planning, only 1 rotation about either the X or Y axis is necessary.

4.3 Stage

The stage provides movement in the X, Y, Z directions and rotation about the Z axis. Hence 4 DOF movements can be achieved. A picture of the setup is shown in figure 4.2. Referring back to figure 4.1 rotation is about the Z axis, meaning that if the chip is placed on the stage, its surface is in the XY plane. Hence rotation using the stage will move the whole chip about the Z axis.

The resolution of movement for the stage is 0.25μm for translations and 0.01°

Direction	Range
Horizontal	204 mm (length of cantilever)
Vertical	73 mm (169-242 mm - bottom to top)
Rotational	360

Table 4.1: Summary of ranges for MT-75S stands.

for rotations. For the translational movement, 3 sliders and 3 motors are used, one pairing of slider and motor for each axis. The length of each slider arm is approximately 15 cm, however this does not mean that the arm can move that distance. The motors have no feedback as to whether they have reached the physical end of the arm and so when they hit it, they continue to turn resulting in grinding. To prevent damage to the system, this should be avoided. Hence, movement restriction is set in software to a range of 12.5cm. This is more than enough to traverse the distance of the chip on which the microcomponents will be lying which is approximately 1cm^2.

4.4 Micromanipulator

There are two robotic micromanipulators available for the microassembly system. They are the MP-285 micromanipulators from Sutter Instrument. These arms are each placed on top the MT-75S series stands and are controlled using the MPC 200 controller, all from Sutter Instrument. Both the stand and the arms can provide different placements in 3-D space.

4.4.1 MT-75S Stands

The MT-75S stands are heavy stands made of mainly stainless steel and aluminum [33]. They provide adjustment of the micromanipulator position in the vertical and horizontal directions as well as 360° rotation. The position of the manipulator must be set manually by the user. A schematic drawing of the stand is shown in figure 4.3 and the range of movement is summarized in table 4.1. The horizontal range listed is that of the cantilever length. It should be noted however that the base of the manipulator takes up approximately 1/3 of that space. Hence there is really

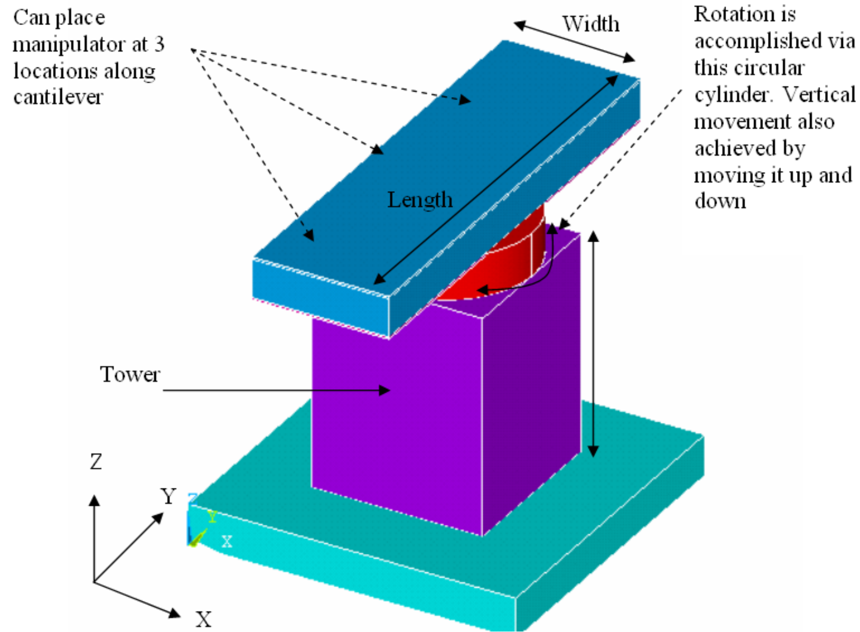

Figure 4.3: The stands are used to place the mircomanipulators on top of.

only 3 positions available, each spaced by $204/3 = 68$ mm. The base of the arm is screwed into the cantilever and is placed such that it is awkward and difficult to remove. However, the cantilever itself can slide in the Y direction, moving the micromanipulator with it. Hence, when the range of the micromanipulator is not sufficient, it is possible to move the cantilever to different positions. This is only suitable for inaccurate movements, since this is done manually and there is no system of measurement on the stand to determine how far along the horizontal axis the cantilever has been moved. Fine adjustments using the micromanipulator can be made after moving the cantilever.

The vertical position along the Z axis and rotational position are easily modified by loosening two screws at the side of the tower. Once again, the only problem with this type of adjustment is that it's hard to accurately determine the movement and rotation. In comparison to the other components which can be moved using software, adjustments to the stand are comparatively cumbersome [33].

4.4.2 MPC 200 Controller

Both micromanipulators are attached to one controller unit, the MPC 200 which is not capable of controlling them simultaneously and instead allows the user the

Feature	Value
Travel Distance	25 mm (all axes)
Resolution	Low: $0.2 \mu m/step$ High: $0.04 \mu m/step$
Maximum Speed	5 mm/sec
Drift	$< 1 \mu m/hour$

Table 4.2: Summary of ranges for the MP-285

capability of toggling between them. Connected to the MPC 200 and acting as an interface between human and micromanipulator is the rotary optical encoder (ROE) 200. This unit contains all the buttons and knobs necessary to input desired actions. Three turning knobs are present, one for each axis, X, Y and Z as well as a display panel which shows the location of the manipulator in 1 micron steps. Communication between a computer and the system is done through a USB connection with the ROE 200. Due to this connection, control of the micromanipulator is possible either through software or the ROE 200. The former requires inputting numerical values for the location of the micromanipulator and is time consuming since an affirmation button must then be pressed to send the command. On the other hand control through the ROE allows for smooth, continuous movement by using the rotating knobs [33].

4.4.3 MP-285 Micromanipulator

The MP-285 micromanipulator utilizes three stepper motors to provide movement in the X, Y and Z directions. As mentioned before, this unit is placed on top of the MT-75S stands. Figure 4.4 shows the setup of the manipulator with its 3 motors.

The capabilities of the MP-285 are summarized in table 4.2. As can be seen in the first entry, the range for each axis is from 0 to 25000μm. The firmware installed on the MPC 200 controller stops movement when the manipulator reaches one of these extremes.

The manipulator is capable of different speeds and different step sizes. This is controlled by the different modes, which range from 0 to 9. As the MODE increases, the movement becomes slower and finer. For this reason MODE 0 is referred to as acceleration mode and is generally used for wide movements. In addition to

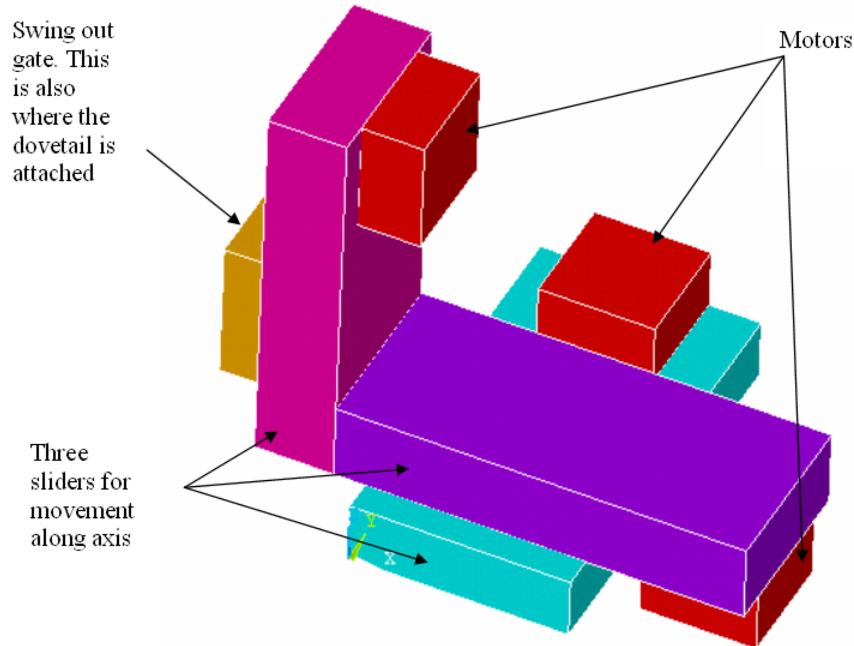

Figure 4.4: Three motors are used for movement in the X, Y and Z directions. Manual rotation can be done as well.

setting the MODE, movement control is also achieved through how fast the knobs are turned. This behaviour corresponds to what is intuitively expected, the slower you turn, the slower the movement.

The microprobe will be attached to a dovetail which in turn is attached to a swing gate of the MP-285 which allows for manual rotation. This is done by loosening a hex screw and adjusting the angle of the dovetail, which is essentially a rectangular plastic plate. For each of the arms, a 4 inch long dovetail is used and has an additional plastic plate attached to it. The rotation is done manually and also introduces a potential source of error since accurate rotation is difficult to achieve [33]. However, an interface between the two is necessary since the dovetail has no mechanism for directly attaching a probe to. Subsequently, some sort of attachment has to be designed. This part from hereon will be referred to as the micromanipulator arm extension (MAE) and its concept can be seen in figure 4.5. As mentioned, rotation can be done manually at the head of the dovetail, resulting in a displacement as seen in figure 4.6. Rotation using the dovetail results in an undesirable translation of the probe tip, which must be corrected afterwards. Ideally it would be best to rotate along the axis that the probe tip lies along, but

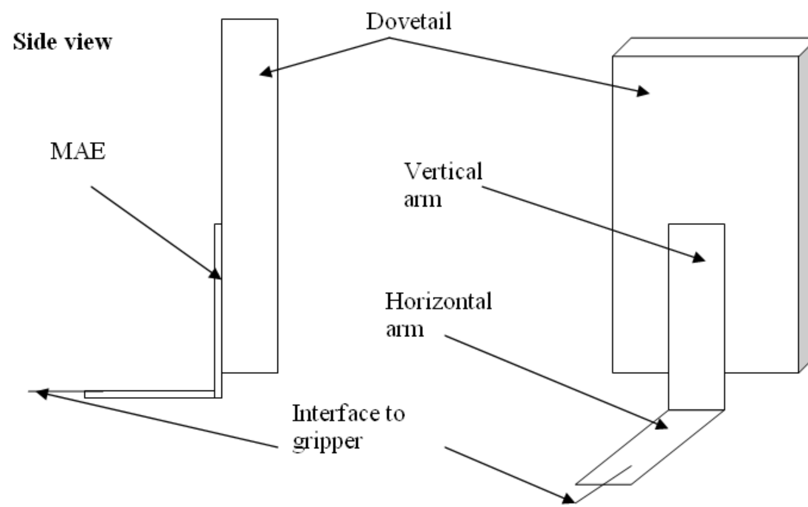

Figure 4.5: Different parts of the dovetail.

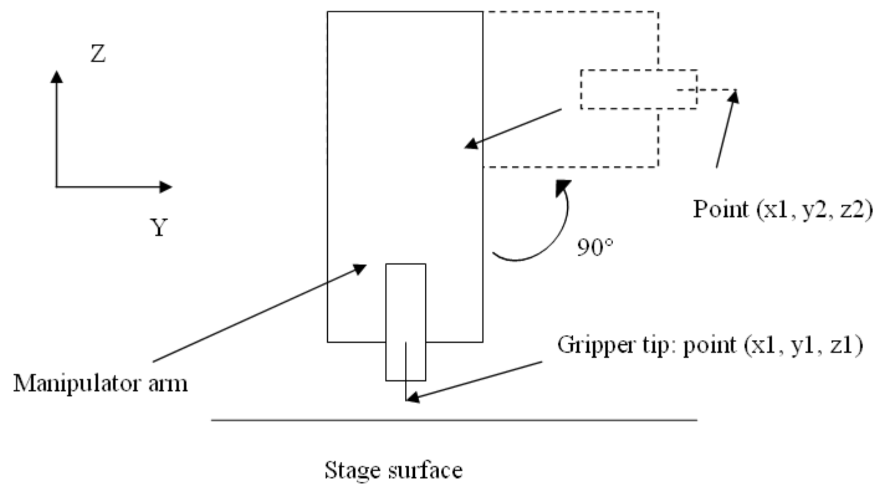

Figure 4.6: Possible rotation of the dovetail.

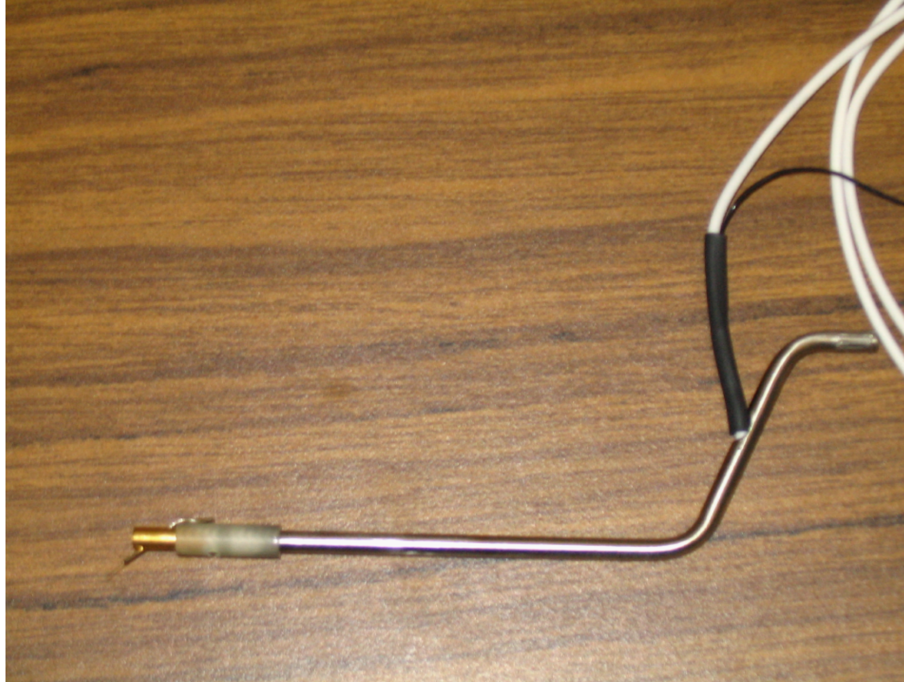

Figure 4.7: The probe holder with a probe in the tip.

this is unlikely to happen, since it requires a more complicated setup to rotate the probe as opposed to rotating a larger part belonging to the MAE. In other words, rotating the probe itself may result in damage to the delicate gripper and any part attached to it.

Typically, commercially available probes also come with probe holders, which are specifically designed to hold the probe and may even provide an electrical feed to the probe. It was decided to purchase the probes and a corresponding probe holder from the Micromanipulator Company, Inc. to ensure that both are compatible with each other. A probe holder with an electrical connection was purchased for potential future uses. The probes themselves have microscale tips, with a larger body that can easily be handled. Information on the parts can be found at [7].

A component was designed in the machine shop at the university to act as the interface between the probe holder and the flat face of the dovetail. The combination of the interface and the probe holder form the bridge between the macro and micro worlds. Figure 4.7 shows an image of the probe holder with a probe inserted at the end. Combined, the designed component and the probe holder form the MAE.

Taking the overall setup of having the probe connected to the probe holder and the probe holder then connected to the dovetail of the micromanipulator, it can be seen that another point of rotation is at the interface of the probe holder and the dovetail. As mentioned previously, since rotation at the probe tip is difficult and can potentially damage the micro parts, the next closest location for rotation is at the interface between the probe holder and the dovetail. To attach the tip of the probe to the bonding pad of the gripper, an adhesive, Loctite 401 was used. A data sheet for this can be found at [8].

4.5 Cameras

During experimentation, different camera views were required to properly see what was happening during different pick and place steps. For example, bonding the probe tip to the gripper required an overhead view to align the probe tip with the gripper bonding pad. A side view also assisted in determining when the probe tip is lowered enough to form a contact with the bonding pad. However this view is not necessary, since contact with the bonding pad can be determined from the overhead view by observing changes in the adhesive around the probe tip.

For the most part, an overhead view and side view are sufficient, with the exception of the insertion step. The insertion step requires aligning the part with the receiving interface, whether it is another part or an interface fabricated onto the substrate. In addition, it must be determined how far to lower the part to ensure that damage does not result to the part, the gripper or the receiving interface, as a result of lowering the part too much. When the gripper is rotated, the overhead view is distorted due to the probe tip and the adhesive bond between it and the bonding pad of the gripper. This makes it impossible to align the grasped part with the receiving interface. As a result of this, an angled view is required that will allow for a partial overhead view combined with a partial side view.

The usage of a single camera is possible if a rotating camera holder is used. However, this was not available and instead 3 separate holders were used, one for each view of the overhead, side and angled view.

The main microscope used for the system is a Navitar microscope, attached to a PULNIX camera. The vision system is crucial for manual operation because it

lets the user see the work area for feedback and the planning of future moves. If in the future, automation is achieved this vision system may be less important but nice to have regardless. In the current setup, the microscope is positioned normal to the plane of the stage platform, such that it provides an overhead view of the workspace. This setup allows for side access to the chip on the stage. As mentioned previously, two other cameras are used to provide a side view and an angled view.

For the microscope to be of any use in this system, one must consider the following characteristics:

1. Resolution: the size of the smallest feature that can be discerned.
2. Depth of focus: this is the distance along the z axis (perpendicular to the surface of the chip) that is in focus when looking at a scene.
3. Working Distance: this is defined by how close the microscope has to be to the chip for focused images. If this is too small to allow for interaction with the chip surface, then no work can be done.
4. Field of view: the area that the camera can see.

The objective lens is a Mitutoyo M Plan Apo, with a magnification of 20x. A table outlining the above characteristics for the Navitar microscope can be found at [34]. With a working distance of 20mm, there should be enough space to interact with the chip, although it will be tight.

The camera used to capture the images is a Pulnix $\frac{1}{2}$" charged coupled device (CCD) camera. This camera is connected to a frame grabber in a PC so that capturing images is made easy through the use of software. Having this setup makes controlling the vision system easier since the microscope can be controlled and the resulting images can be viewed all from the same PC. The one downside to the camera is that it is in colour. Colour images are not necessary for successful operation of the system and it also takes away from the resolution of the images. Hence, a black and white camera would be more preferable.

Chapter 5

Experiments and Results

5.1 Comments

The experimental process can be broken down into four stages listed as follows:

1. Bond the probe to the gripper and remove the gripper from the substrate
2. Grasp a part using the gripper
3. Reorient the part
4. Insert the part into the substrate and remove the gripper

These steps are a more condensed version of those outlined in section 3.2 for the pick and place approach and are derived based on the step by step goals of experimentation. The rest of the chapter will outline the results for each step.

5.2 Gripper Bonding and Removal

As mentioned in previous chapters, an adhesive, Loctite 401 was decided on as the bonding mechanism between the probe and bonding pad of the grippers. Since the adhesive had a lower viscosity than necessary for application it was exposed at room temperature for approximately 45 minutes to allow for thickening. Once this was done, a small amount was applied to the end of the probe tip. Due to

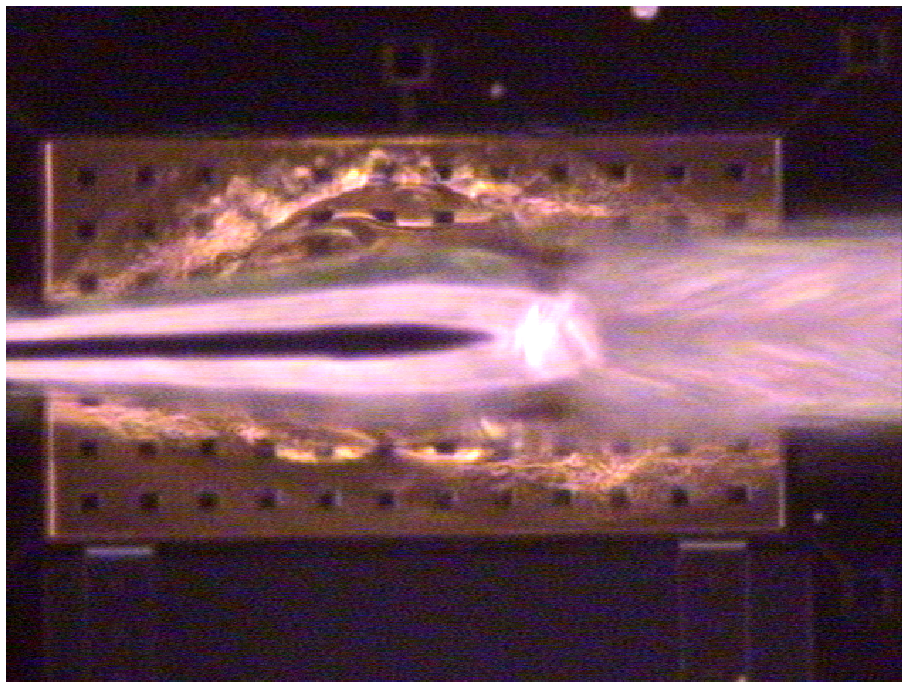

Figure 5.1: The adhesive bond between the probe tip and bonding pad can be clearly seen.

the downward angling of the probe, the adhesive typically gathered near the tip or slightly off of it. At this point, the probe was lowered onto the bonding pad and left to dry. An overhead view of a probe bonded to the gripper can be seen in figure 5.1.

Once the adhesive has dried, the gripper is removed from the substrate, either by moving the probe up using the micromanipulator or by raising the stage. Neither method appeared to be superior to the other. Ideally, the gripper will be lifted off, breaking the tethers that were holding it down. Figure 5.2 shows a cleanly removed gripper. Here the background is white because the chip laying on the stage has been lowered and the gripper is being lifted via its bond with the probe tip.

Certain difficulties arose during this step, with consequences ranging from a failed bond to gripper damage. A failed bond typically resulted from two scenarios: not enough adhesive or the probe tip was not placed close enough to the bonding pad for contact. In the first case, applying too much adhesive can cause some to overflow over the edges, resulting in bondage between the bonding pad and substrate. Hence it was better to err on the safe side and apply as little adhesive as possible. Since the application of the adhesive was done manually, it took some

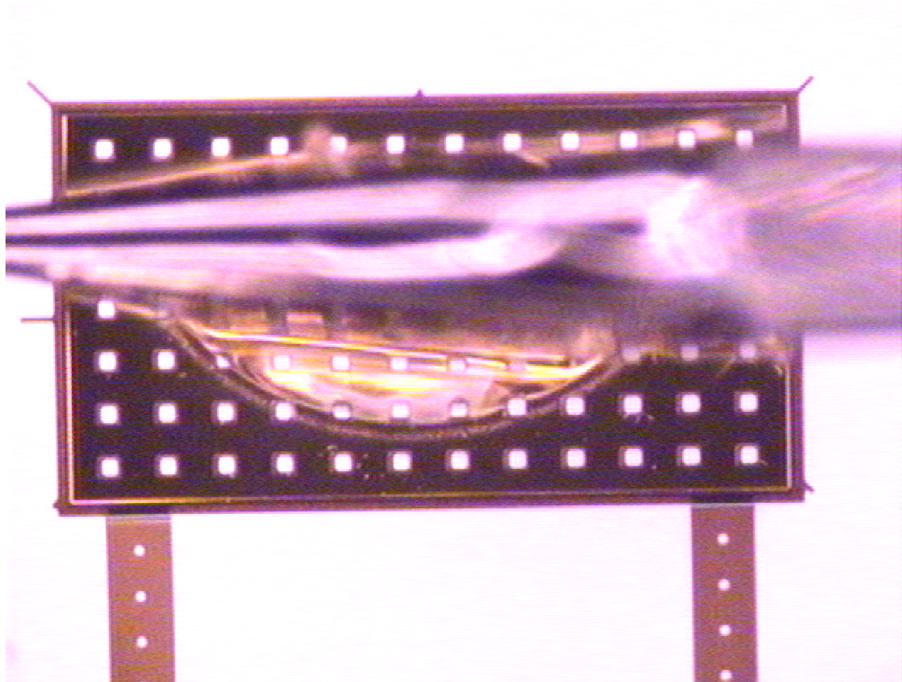

Figure 5.2: The white background is a result of lowering the stage. At this point the gripper is held in the air only by the bond with the probe.

time to recognize the right amount required. The second case was also a result of overflow avoidance. In same cases pressing the probe down too much would cause the adhesive to spill over the bonding pad edges. For this reason in some cases the probe was not lowered enough to come in contact with the pad. It was observed that as the adhesive dried, it would also contract. This meant that although there was initially adhesive contact between the probe and bonding pad, by the time it dried this contact was extremely thin or broken. Typically, any fragile contact leftover would be broken during the attempt to remove the gripper. Failed bonds did not result in damage to the gripper and at most resulted in some left over adhesive on the bonding pad. In most cases it was possible to reattempt another bond with the same gripper.

Damage to the gripper during removal has been attributed to an uneven removal force. This conclusion came about from several observations made during experimentation. Sometimes during boding, while there was no leakage of adhesive over the edges of the bonding pad, there was evidence that some would seep through the etch holes. This can be seen in figure 5.3. Consequently this resulted in a bond between the bonding pad and the substrate.

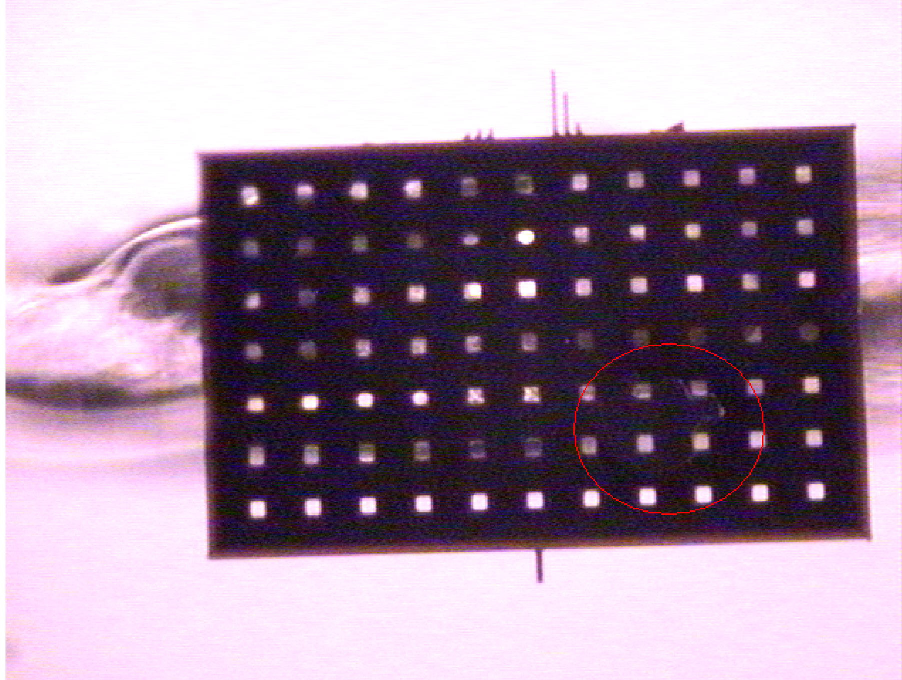

Figure 5.3: Some white parts under the bonding pad appear to be adhesive, which would explain some of the difficulty in removing the grippers.

As stated previously, the substrate was laid upon the stage and the probe holder is attached to the micromanipulator at one end, with the other attached to the gripper. The effect of this is that when movement is produced via the micromanipulator, the force in the direction of movement acts on the end of the probe holder attached to it. In this case, the probe tip is in turn bonded to the gripper resulting in a support that is not as strong as a fixed support, but more inline with a pinned support. As the manipulator moves up in the Z direction, rotation about the probe tip occurs. In one case the bond between the probe and the bonding pad fails and the gripper remains attached to the substrate. The other case is when the bond between the bonding pad and substrate fails, leaving the pad attached to the probe. Looking at the moment where this occurs in figure 5.4, one can see an uneven removal force, where the side of the bonding pad closest to the manipulator breaks away first.

This predicts that damage to the gripper will most likely occur on the side furthest away from the manipulator, which is consistent with the experimental results.

Between gripper designs A and B, A turned out to be more susceptible to

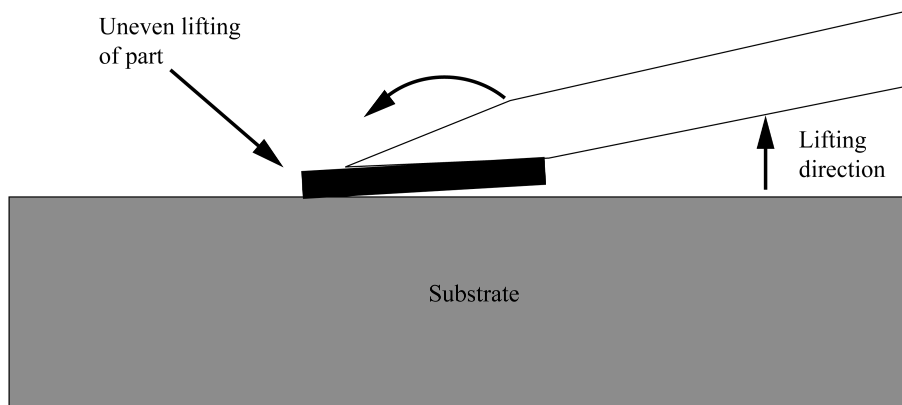

Figure 5.4: An uneven removal force results from the bond between the probe and the part.

damage during gripper removal. Typically damage occurred to the more fragile interior arms and rarely to the thicker exterior arms. Comparing the two designs, clearly design B is the sturdier of the two. In addition, design B was experimented on second and most likely benefited from the knowledge gained from working with design A. Certainly, quite a few grippers were damaged during the initial attempts at removal. Experience in this case played a large role in the success rate.

5.3 Grasping a Part

Once a gripper is successfully removed from the substrate without any serious, substantial damage, it was used to grasp a part. Due to the drastic differences in designs between gripper A and B, it's not surprising that their ease in grasping a part varies. Figure 5.5 shows a grasped part by gripper A.

It was determined for gripper A, that part manipulation could be achieved without the whole gripper intact. In fact one of the interior arms could be missing and the gripper could still work. There were rare cases where grasping with a missing exterior arm would work, but typically issues came up when the part was lifted off the substrate. Since the lifting force is supplied by the two exterior arms, missing one resulted in an uneven lifting force, which in turn caused the part to rotate and fall off the gripper. Figure 5.6 shows the side view of a grasped part rotated 90°, such that it is now perpendicular to the substrate. Obviously this situation is not ideal as it results in a less restrictive grasp. This means that it will

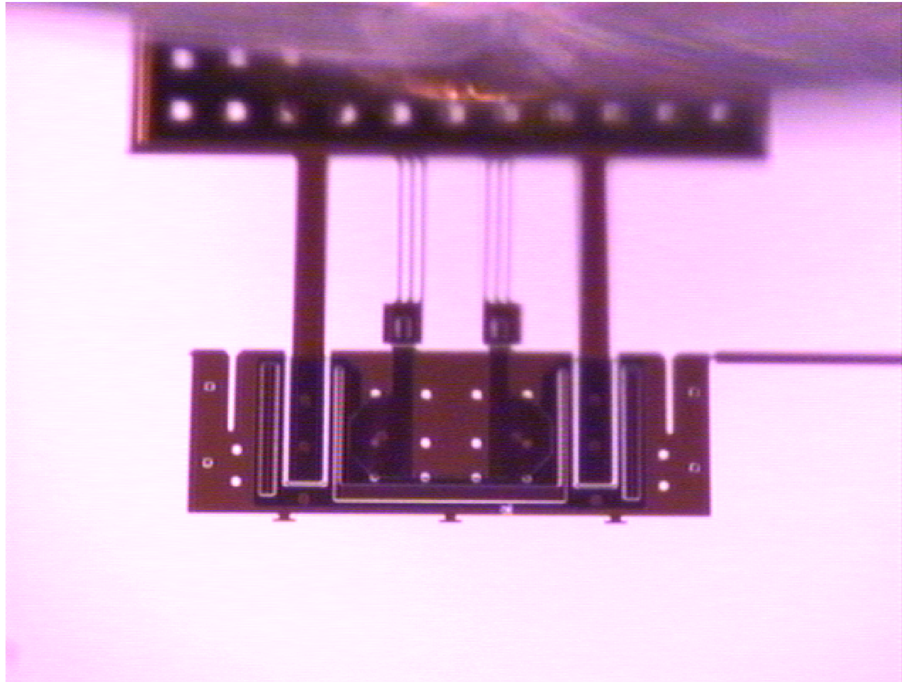

Figure 5.5: A part is grasped and lifted off the substrate using the gripper A design.

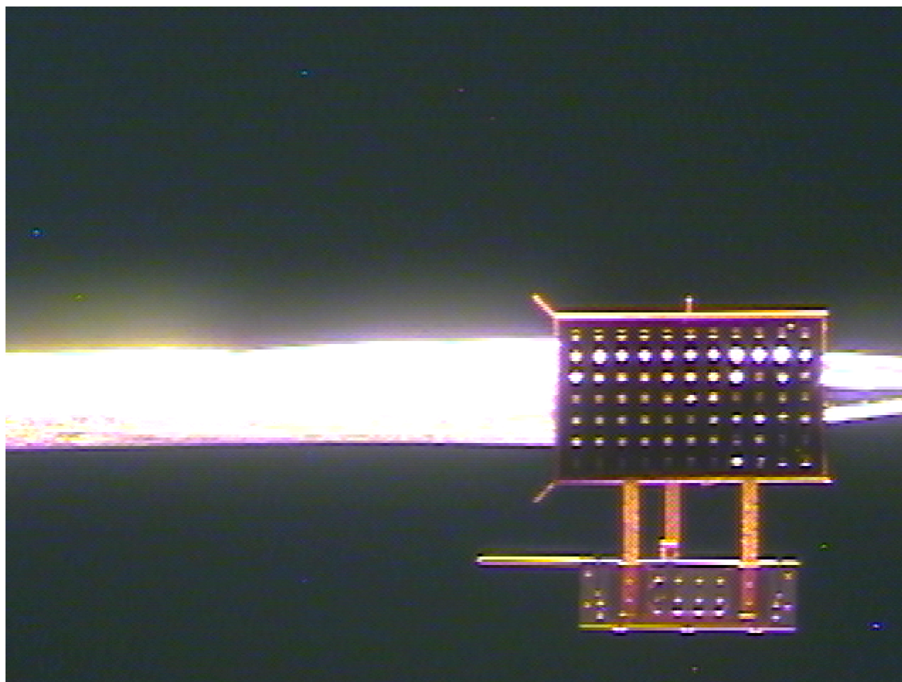

Figure 5.6: After rotating the grasped part, the damage to the gripper can be seen.

be easier to dislodge the part as compared to a full grasp.

Before the part can be grasped however, the released sacrificial parts used to elevate certain portions of the interface must be removed. This step can sometimes result in damage to the part, ranging from broken parts to broken tethers. At the time of part design, the method that would be used to remove the sacrificial parts was unknown. The general idea of having a probe tip sliding the parts out was conceived of, but the type of probe and consequently the size of probe tip itself were not decided upon. For this reason, the design of the T-section of the sacrificial parts, where the probe tip is suppose to hook onto the part, was on the small side when it came time to remove the parts. Had they been larger, it would have been easier to hook onto the sacrificial part and remove it.

Another design error was the lack of dimples in the sacrificial parts. These were left out due to the affect they would have on the layers deposited over top the sacrificial parts. Dimples in the lower layer would have also resulted in indentations in subsequent layers. The sacrificial parts themselves were not large enough to require etch holes. Hence, they were composed of solid Poly 1, which were then completely released during the removal of the oxide. In some rare cases, the sacrificial parts were already removed either during the final wash or during transportation and handling. The majority of the parts however remained in place or only moved slightly but not enough to be clear of the part. For these situations, the probe tip was used to initially remove them before an attempt at grasping with the gripper was made. As explained before, this was done to avoid damage to the gripper.

In some cases it appeared that the parts and sacrificial parts were still stuck together. This would generally result in the whole structure coming off the tethers. At this point it was practically impossible to remove the sacrificial parts and extremely difficult to grasp the parts. Other cases, the sacrificial parts were stuck to the substrate and because of this more force was applied by the probe tip to try and remove them. When the parts did finally move, it typically resulted in a violent moment affecting the tethered parts. Four situations can arise from this:

1. No broken tethers: the ideal case, the sacrificial part is now loose and can be pulled away from the tethered part.

2. One broken tether: it is still possible to grasp a part with only one tether attached, although more difficult than if both were attached. Once again the

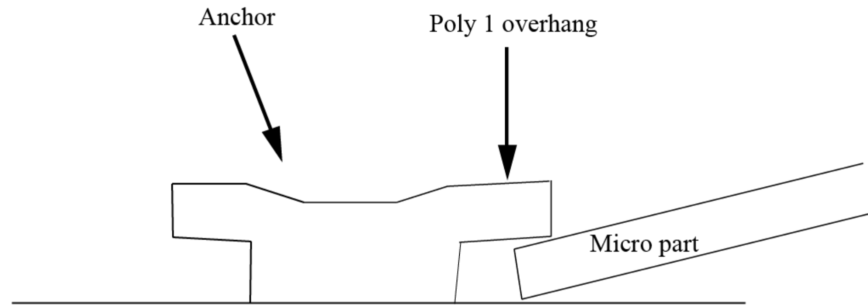

Figure 5.7: An overhang can be seen, a result of the design rules of the PolyMUMPS fabrication.

part is now loose and can be pulled away.

3. Two broken tethers: the part is still intact and usable but not tethered. It is nearly impossible to grasp a part that doesn't have a support to supply a reaction force against the movement of the gripper. For this reason the part is repositioned such that it has an anchored guide as the support providing the reaction force. The part can now be grasped by the gripper pushing the part against the guide.

4. Damaged parts: in some cases, the part is damaged when the sacrificial part becomes unstuck. These parts are not salvageable.

Situations 1 to 3 resulted in parts that could still be used. An interesting result came about from situation 3 however. Due to the PolyMUMPS design rules, the anchors can only be placed 4.0 μm from the edge of the Poly 1 layer, resulting in the following structure, seen in figure 5.7. In situation 3, when the parts are pushed against an anchor for support, sometimes the edges will hook on the overhanging Poly 1. In some instances the gripper may be attempting to grasp a part at a downward angle, meaning the gripper tip may be unintentionally angled downwards towards the substrate. This in turn may angle the part in the Z-direction, tilting the edge that pushes into the anchor. Since an overhead view is the active view used for grasping a part, this is extremely difficult to see. From the operator's perspective, the part will simple fly off upon further application of force. Since this

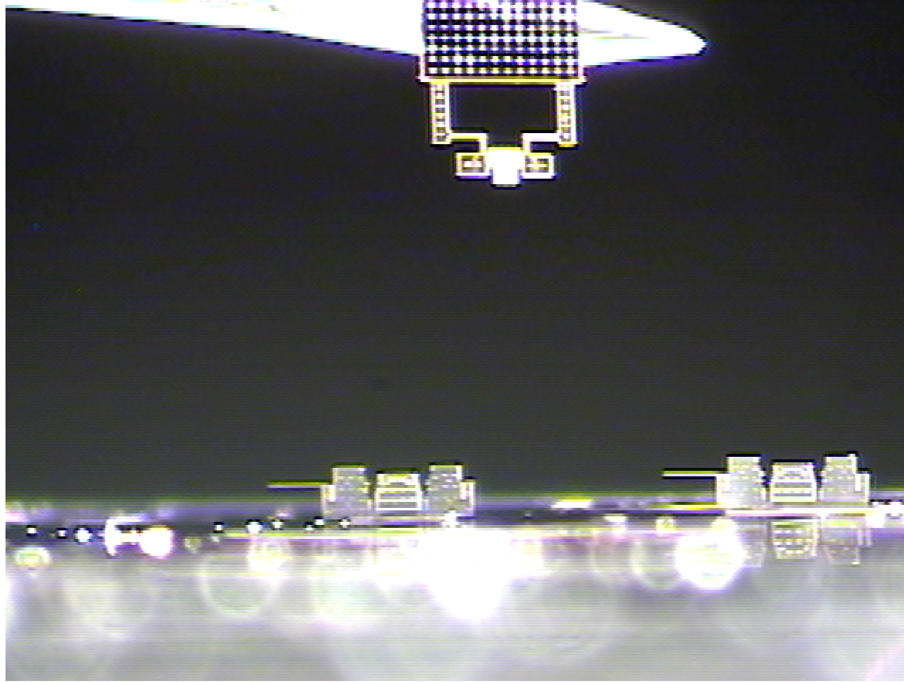

Figure 5.8: A rotated gripper after insertion of parts that were rotated with the gripper.

only occurred when an anchor part was being used, it is fairly reasonable to assume that the edge of the part was getting caught on something.

5.4 Reorienting Part

The reorientation of the part was done through the equipment setup and required no direct manipulation of the gripper and grasped part itself. When the part is grasped, both the gripper and part are laying parallel to the substrate. To insert the part, it must be rotated by 90° making it perpendicular to the substrate as can be seen in figure 5.8, which shows the rotated gripper after insertion of the part. A translation is also required to move the part to the appropriate location for insertion. As explained in chapter 4, the equipment setup is capable of making the necessary movements. There were a few instances where the grasped parts dislodged during rotation and translation. However, these were attributed to excessive force, for example accidentally hitting the probe holder during handling. Otherwise, with gentle handling, this step did not pose much of a problem during experimentation.

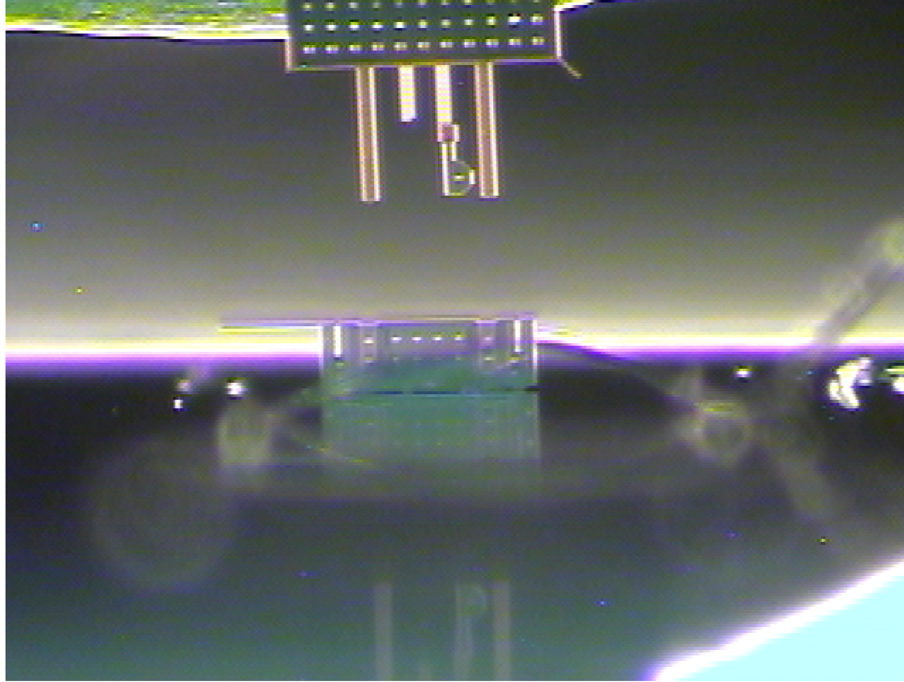

Figure 5.9: The inserted part is standing on its own. The view is obscured by a piece of debris on the substrate.

5.5 Insertion

Inserting the part requires aligning it with the receiving part or interface and moving it accordingly to lock it into position. The conducted experiments were only able to progress to the point where the base parts were inserted into the interfaces on the substrate. Further mention of insertion from hereon will refer to this step. Initial insertion steps failed due to inexperience in working with the view provided by the 45° camera angle. This is explained in greater detail later on. After the first few attempts it was possible to review the video taken and get an understanding of what was being seen. Subsequently, the following insertion attempts were successful. Initial insertion testing was done using gripper A. For this reason, this design also suffered the bulk of the failed attempts resulting from inexperience with the equipment setup. Despite this, there were successful insertions for parts designed for both interfaces. Unfortunately, the inserted parts for the gripper A design did not survive the attempts for SEM images and only images taken with the lab cameras are available. One can be seen figure 5.9. Here, the gripper has been damaged during the insertion step. The insertion method cannot be seen here, but

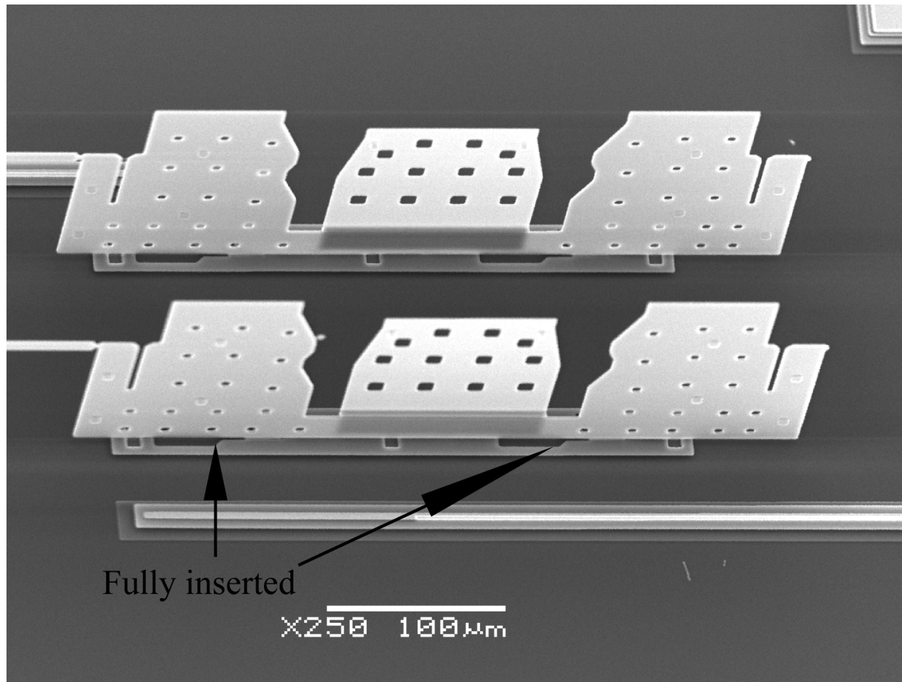

Figure 5.10: SEM image of inserted part using gripper B, L-hook interface.

it is the L-hook design. Details to note are the tether attached to the part that broke at the wrong end and a piece of debris that is obscuring the view. The tether does not affect the insertion process.

Insertion using gripper B was more successful, partly a result of the experience gained from insertion using gripper A and partly due to a better design for this step. Once again it was possible to insert parts corresponding to both interfaces. SEM images were obtained for these insertions and are shown in figure 5.10 and 5.11. Figure 5.12 shows a larger view of the inserted parts.

Several factors make the insertion step difficult. The first, as explained in the equipment section, is the need for an angled view. The top view is distorted by the probe, making it impossible to align the part with the interface. Also it is difficult to tell if the part has been lowered enough to touch the substrate. The side view can tell when this occurs, but does not help with aligning the part. Because of this, a view angled at approximately 45° is required. This provides the operator with a view of the substrate and gives him or her an idea of how far the part is from the substrate. The only difficultly is in determining how to interpret the images since it is angled. Figure 5.13 shows an example of what the operator sees. In this picture,

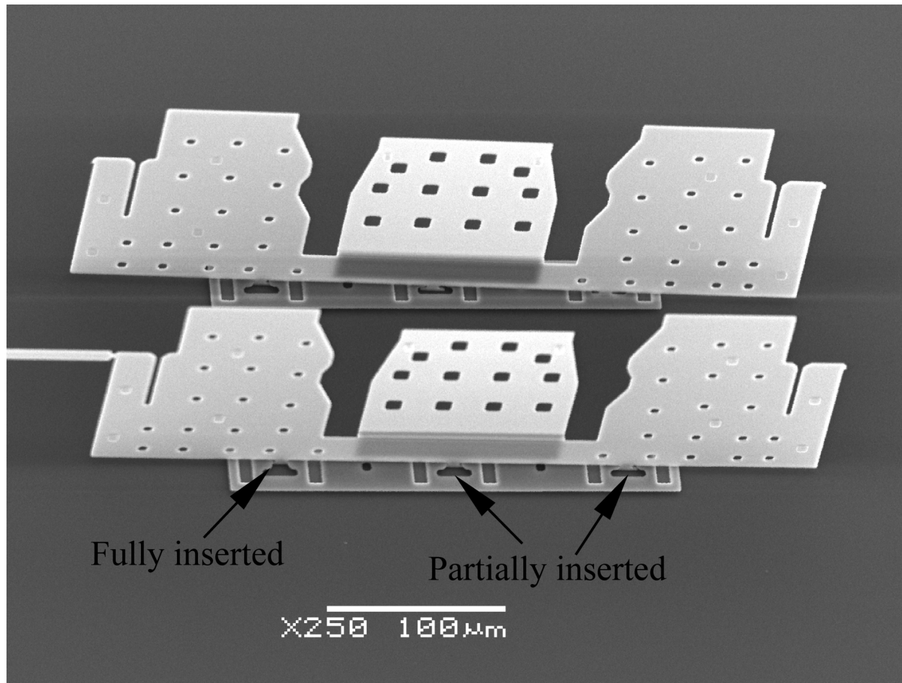

Figure 5.11: SEM image of inserted part using gripper B, T-notch interface.

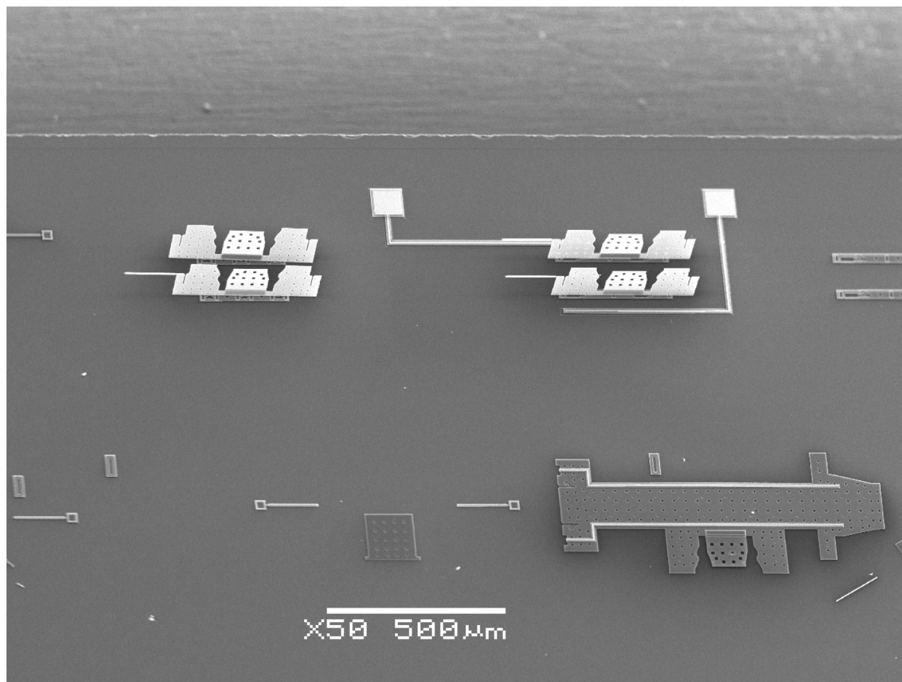

Figure 5.12: A wide view of the inserted parts shows their orientation with respect to each other.

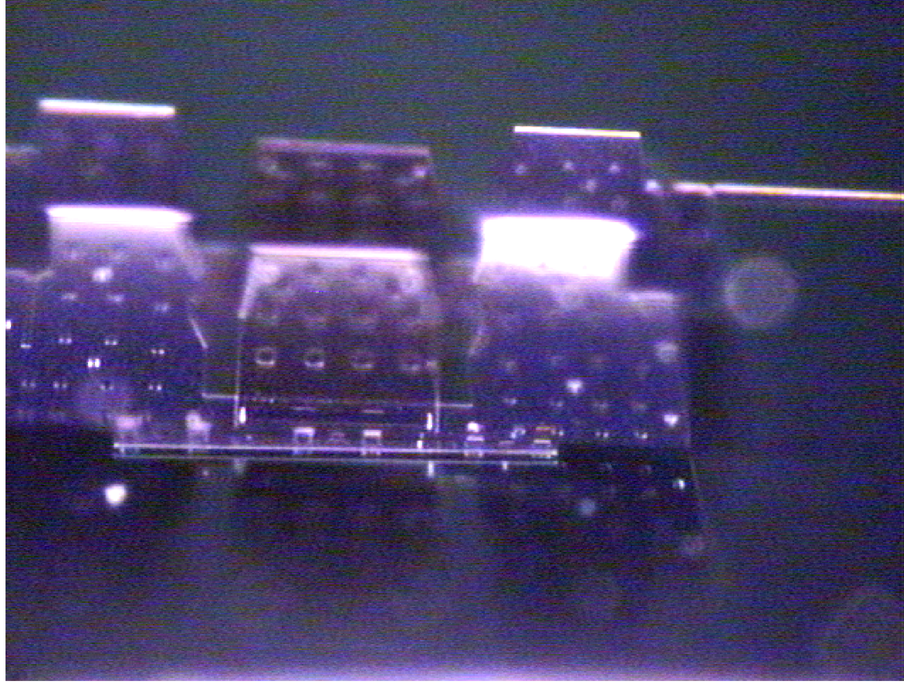

Figure 5.13: The angle is enough to see where the part will connect with the interface.

the interface and part about to be inserted can be seen. Due to the polishing of the chip surface, a reflection of the part can be seen. As the part is lowered, it comes closer to the reflection, such that the point where they meet indicates that the part has now touched the substrate. By aligning this point with the interface, it was easier to insert the part.

Based on the previous figure, another obvious issue arises and that is the alignment of the part with the interface. The part must align with the interface both in the plane in which the interface lays, in this case the substrate, and the plane perpendicular to it. Alignment with respect to the plane perpendicular to the substrate is dependent on the accurateness of the 90° rotation. Since this step is done manually, it is difficult to ensure that this is accurately achieved. To a certain extent, the side view can be used to see if there are any extreme over or under rotations, but slight differences are too difficult to see. Looking at the interfaces, both have larger areas where the part is initially inserted before it is slid into its final lock position. Since this opening is larger than the corresponding key structures on the part, there is room for error in terms of alignment. In addition, although sufficiently restrictive, the grasp supplied by the gripper allows for some movement.

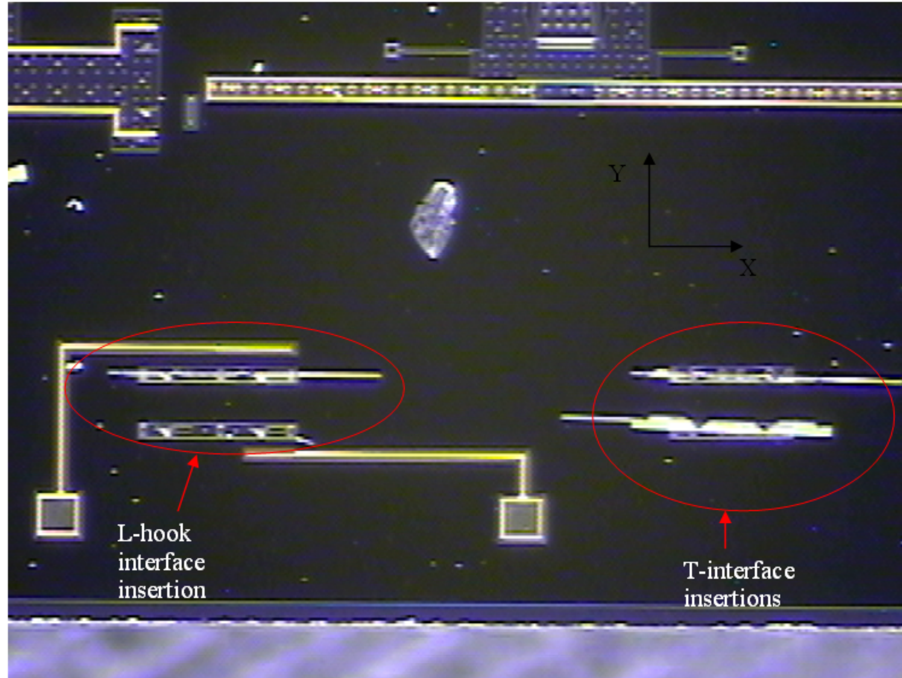

Figure 5.14: It can be seen which parts are straighter in terms of insertion.

Hence when the part is inserted and pushed into the lock position, it essentially self corrects the misalignment as it conforms to the lock. For this reason, there were no significant issues during experimentation regarding the alignment of the rotated part with the plane perpendicular to the substrate.

Looking at figures 5.10 and 5.11 it's clear that the L-hook interface insertions provides better aligned parts as compared to the T- shaped interface ones. In figure 5.11 the left key of the part is inserted completely, whereas the right key is still in the wider portion of the interface and the middle key is somewhere in-between the two. During insertion, the gripper is pushed forward and the part is fully inserted into the lock position. However during the release portion, if the gripper is not exactly aligned such that it is perpendicular to the substrate, it will pull the part out of the locked position as is the case here. The L-hook interface potentially suffers from this problem as well, but instead of coming unlocked, it will just have a tendency to lean to one side. There is also a possibility that the part self corrects itself once the gripper is free and there is no longer any force being applied to it. Overhead views of inserted parts (a different attempt, not relating to the previous pictures) appear to support this theory as they are seen as only straight lines. For example, figure 5.14 shows an overhead view of inserted parts. One of the T-notch

insertions is leaning to the side and hence has a wider overhead view as compared to the thin line of the L-hook interface insertion. The L-hook interface is locked by movement in the -X position. Locking the part into the T-notch is done by moving it in the -Y position. If at the time of insertion, the part is aligned with the plane perpendicular to the interface such that it is leaning in the +Y direction, when the gripper is removed after insertion it will have a tendency to pull the part in that direction. This appears to be the case with the lower T-notch inserted part. This is also a result of the removal process, which pulls the part out of its locked position.

Aligning the part with respect to the plane of the substrate is rather straightforward since the stage is capable of rotations in that plane. As the part is lowered and it begins to converge with its reflection, the line where the two meet can be compared with the interface. If the two are inline then the part is ready for insertion. On the other hand if they are not, a rotation of the stage generally only a few degrees can be done to bring them into alignment.

Another issue that arose during experimentation was the placement of the part into its lock position. The designs of the grippers and their respective interfaces were ideal for movement in one direction, namely the direction required to remove the part from its tethers. When the parts are inserted, depending on the interface, movement is required in directions other than this one. For gripper B, few issues were encountered since the gripper provides an enclosing grasp on the center portion of the interface. It is impossible to have the gripper release the part in a direction other than the one intended without damaging the gripper.

In some cases, this is not the case for gripper A. Once again due to the lack of restriction for bending out of plane, it is possible that during movement in a non ideal direction, the gripper may slide out of its grasped position. As the gripper is pushed in a direction that along the surface of the part (i.e. pushing the part to the side to insert it into the L-hook interface), there are instances where the interior and exterior arms move out of the plane the part lies in and begins to slide over the part. This can be corrected by pushing the gripper back in the opposite direction and having it re-grasp the part by sliding back into position.

Chapter 6

Conclusions

6.1 Design

6.1.1 Gripper Design

After considering the results and taking into consideration the initial errors due to operator inexperience, it would appear that Gripper B is the better design. This conclusion was the result of two major observations: (i) Gripper B typically sustained less damage during removal, grasping and insertion of a part and (ii) Gripper B resulted in a more secure grasp of the part.

Regarding (i), it is rather evident just by looking at the designs that Gripper A is more fragile than Gripper B. Since it is necessary for the interior arms of Gripper A to bend inwards, each flexible arm is slim and long. At the same time this also reduces their structural strength. In comparison the exterior arms did not prove to be a weak point of the design. Figure 6.1 shows a damged Gripper A with typical damage to the interior arm. In this figure, it can be seen that one of the arms is missing.

In contrast, Gripper B sustained almost no damage during the necessary steps to insert a part. There were instances where damage to the serpentine spring occured. This was only observed during the grasping of a part, where the break could be seen when the spring compresses. This however was rare and the gripper was still able to grasp the part whereas in most cases a damaged Gripper A could not.

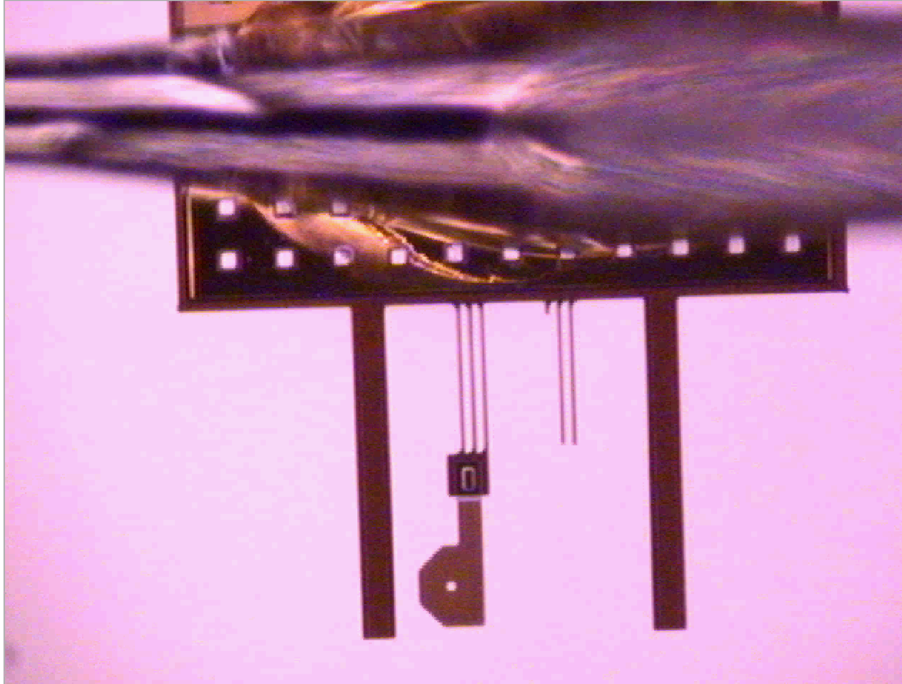

Figure 6.1: Typical damage to the interior arm of Gripper A can be seen.

Regarding (ii), although no parts were dislodged from either Gripper A or Gripper B during rotational and translational movement, the difference in the grasps was seen during the insertion step for the L-hook design. This is because to insert the part, it was necessary for the grippers to move sideways, perpendicular to the direction of insertion. Since there is nothing to stop the part from sliding between the interior and exterior arms of Gripper A, there were instances where the grasp was broken and the part slid inbetween. In contrast, the two side arms of Gripper B are connected to the ends of the serpentine spring. Therefore, when pushing the gripper sideways to insert the part, it is impossible for the grasp to break.

For the above reasons, it is concluded that Gripper B is the better design over Gripper A.

6.1.2 Insertion Interfaces

Two different interface designs were used for part insertion into the substrate: the T-notch and L-hook. Overall it is concluded that the L-hook design was easier to insert and provided a better insertion connection with the interface on the substrate.

Regarding the ease of insertion, since the L-hook design only has two hooks

to insert into the corresponding interface, it is easier to align. Additionally, since the corresponding interface has a wider area for initially inserting the hooks, it is more forgiivng in terms of misalignment (see figure 3.33). In contrast, the T-notch design has three notches that must first be aligned before sliding the part forward (see figure 3.31).

As seen in figures 5.10 and 5.11, the L-hook results in better inserted parts. Additionally, due to the direction of insertion for the L-hooks, the parts do not become loose during part release.

Consequently, it is concluded that the L-hook design results in easier to insert parts.

6.2 Equipment Setup

Although the experiments produced some success, they also shed light on areas for improvement. In terms of the stage and micromanipulator which allowed for accurate movment in the X, Y and Z directions and easy control through software, there was no clear need for improvement. However, the equipment setup displayed weakness in terms of rotational movement in the areas of vision setup and micro-probe movement. Additionaly, other areas for improvement were also noticed and will be described in the following sections.

6.2.1 Camera Setup

The vision setup required three cameras to produce a side view, an overhead view and an angled view. By placing a single camera on a rotational arm that rotates about an axis that goes through the stage, the view can be adjusted as required. This can be seen in figure 6.2.

Position wise, it is advantageous to have the rotational arm behind the Z axis motor of the stage, since this allows for access to the chip on the opposite side for the micromanipulator. Additionaly, by controlling the rotational motor that the camera is attached to using software, movement of the camera will be made easier resulting in less potential damage to the microchip.

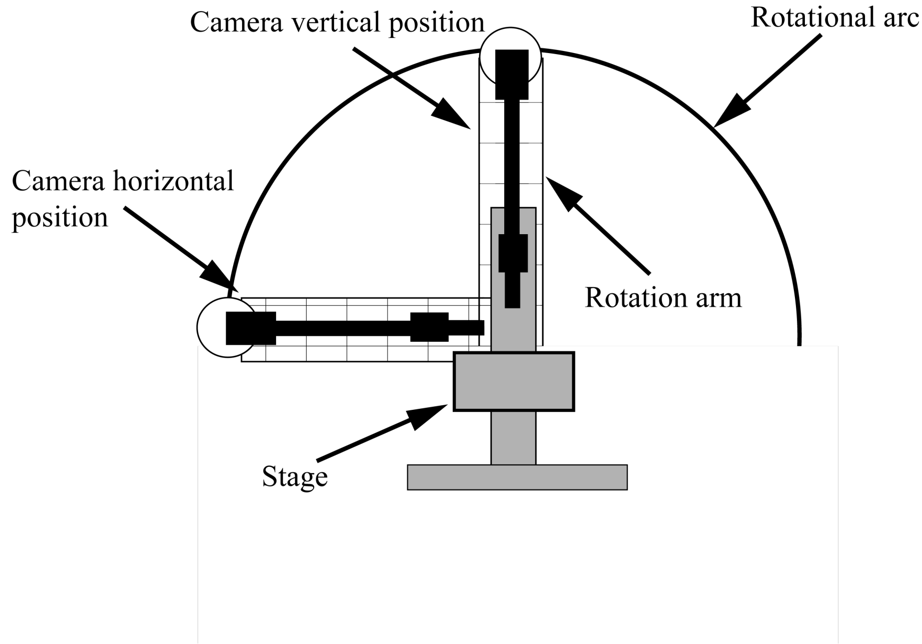

Figure 6.2: Different views can be achieved by attaching the camera to a rotational arm.

A second improvement to the vision system is to replace the coloured camera with a black and white one, since colour is not necessary for experimentation. This improves the resolution of the pictures and results in clearer images which may be beneficial to any future image processing software that may be applied.

6.2.2 Probe Setup

In order to insert the parts into their final resting position, it is necessary to rotate them to bring them out of plane from the initial position they are in. As mentioned previously, the rotational mechanism of the micromanipulator is only capable of manual rotation, which results in potential error, since it is difficult to accurately rotate the probe. Although not a major issue during experimentation, future designs requiring angled rotation may require more accuracy.

One potential option is to integrate a manual rotation unit that allows for more accurate rotation. Such a unit would be less bulky and less costly due to the abscense of a motor. An example is the 07 TRT 507 rotation stage provided by Melles Griot, which is a lower cost option at approximately $202 USD [?]. This stage provides a manual rotation via a screw and a precision which can be read

up to 1 degree. Due to the size of the unit, it should be fairly straightforward to integrate with the existing system. In particular, it can be screwed onto the dovetail and the probe can then be attached.

A more expensive option at approximately \$2, 600, but also conveniently compact is the ART 100 from Aerotech. This unit can have either a integral stepping (8.7 μrad resolution) or brushless servomotor (17.5 μrad resolution) drive system. The compact size will make it possible to easily integrate into the existing micromanipulator system [39].

Appendix A

A.1 Future Applications

A Yagi-Uda antenna was used due to its simple structure and design calculations. Although the current experiments did not completely build the structure due to time constraints, it is difficult not to consider other potential antenna designs for building on the microscale. Another design that was looked at is that of the double ridged guide horn antenna (DRGH), pictured in figure 6.2.

The design for the macro ridged horn design is based on a few equations presented by Walton and Sundberg [1], Whinnery [2] and Hopfer [3]. They are summarized in the paper by Botello-Perez et al and used in their own design [4]. These papers will be used as the basis for the calculations to follow.

The design of the final horn structures can be broken down into three steps:

1. Design of the DRGH.
2. Design of the ridge flared section.
3. Simulation to refine the values and observe antenna behaviour.

The cross section of the DRGH is shown in figure 6.3, with all dimension variables.

As stated in [1], due to the set up of having the signal source in the center of the waveguide and using a straight section to launch the wave, the TE_{20} mode is not excited. The maximum usable bandwidth (MUB) is then described as follows:

$$\frac{\lambda_C^{10}}{\lambda_C^{30}} \tag{A.1}$$

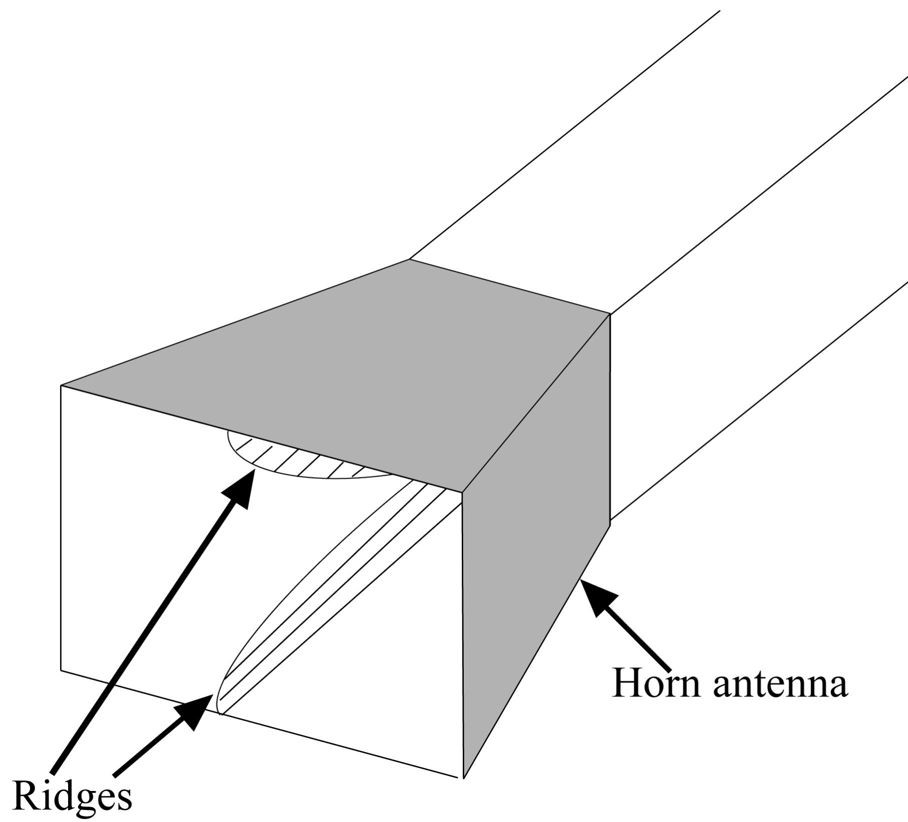

Figure A.1: An example of a double ridged guide horn antenna, which is essentially a horn antenna with two ridges inside.

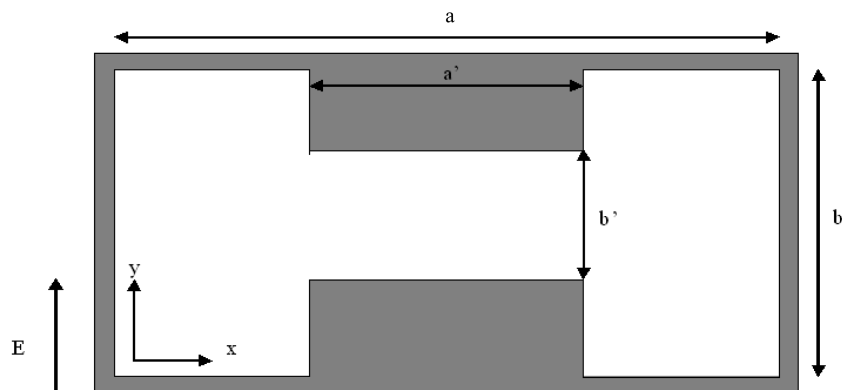

Figure A.2: A cross section of the DRGH showing all the dimensional values.

The cutoff wavelengths for the odd modes are found using:

$$\frac{Y_{02}}{Y_{01}} \tan \frac{\pi}{\lambda_C} a' + \frac{B}{Y_{01}} - \cot \frac{\pi}{\lambda_C}(a - a') = 0 \tag{A.2}$$

where:

$$Y_{01} = \sqrt{\frac{\epsilon}{\mu}} \frac{1}{b} \tag{A.3}$$

$$Y_{02} = \sqrt{\frac{\epsilon}{\mu}} \frac{1}{b'} \tag{A.4}$$

ϵ and μ are the permittivity and permeability of air respectively [4]. The ratio B/Y_{01} is given in [2] as:

$$\frac{B}{Y_{01}} = \frac{2b}{\lambda_C}\left(\frac{\alpha^2 + 1}{\alpha} \cosh^{-1} \frac{1 + \alpha^2}{1 - \alpha^2} - 2 \ln \frac{4\alpha}{1 - \alpha^2}\right) \tag{A.5}$$

where:

$$\alpha = \frac{b'}{b} \tag{A.6}$$

The characteristic impedance for the TE_{10} at infinite frequency is given as:

$$\mathrm{Z}_{0\infty} = \frac{1}{\sqrt{\frac{\epsilon}{\mu}} \frac{\lambda_C}{\pi b'}\left(\left(\frac{2b'}{\lambda_C}\right) \cos^2\left(\frac{\pi a}{\lambda_C}\right) \ln \csc\left(\frac{\pi b'}{2b}\right) + \frac{\pi a'}{2\lambda_C} + \frac{1}{4} \sin\left(\frac{2\pi a'}{\lambda_C}\right) + \frac{b'}{b} \frac{\cos^2\left(\frac{\pi a'}{\lambda C}\right)}{\sin\left(\frac{\pi}{\lambda_C}(a - a')\right)}\left[\frac{\pi(a-a')}{2\lambda_C} - \frac{1}{4} \sin\left(\frac{2\pi}{\lambda_C}(a - a')\right)\right]\right)} \tag{A.7}$$

Newton's method is used to find the ratio of λ_C/a for varying values of b/a, b'/b and a'/a. Both [1] and [4] provide their design values, which are different. [1], being the earlier paper published on this topic, provides detailed graphs showing the relationship between the output and inputs. The final ratios used in each paper are outlined in table 6.1.

Given the inconsistencies of the values found in [4], it was decided to use the ratios of [1] as a starting point.

	Walton & Sundberg [1]	Botello-Perez et al [4]
b/a	0.7	0.7694
b'/b	0.045	0.0191
a'/a	0.375	1
λ_C for TE_{10}	0.3297m	0.7157m
λ_C for TE_{30}	0.0259m	0.07597m
$Z_{0\infty}$(ohms)	26.00	37.27

Table A.1: Comparison of design values taken from different sources.

Poly 1	2.0 microns
Poly 2	1.5 microns
Metal	0.5 microns
Total	4.0 microns

Table A.2: Summary of layers used in the design of the DRGH.

A.1.1 Calculations

The design of the DRGH is done with the PolyMUMPS process in mind. This is because it introduces restrictions on the values of the dimensions, the most obvious of which is on a'. The 3D assembly will be done by constructing a 3D structure out of planar parts. That being said, it follows that the ridge will be fabricated as a planar component and has a thickness determined by the layers in the MUMPS process. For mechanical stability, all three available layers will be used:

Using the ratios from [1], the dimensions in microns are calculated as follows:

$$\frac{a'}{a} = 0.375 \rightarrow a = 10.67 \quad (A.8)$$

$$\frac{b}{a} = 0.7 \rightarrow b = 7.47 \quad (A.9)$$

$$\frac{b'}{b} = 0.045 \rightarrow b' = 0.3361 \quad (A.10)$$

The value for b' is quite small especially considering it is on the scale of microns. However, in figure 6 of [1], it can be seen that the higher the value of b'/b the higher the value of $Z_{0\infty}$. This was confirmed by using a value of b' = 2 microns giving

b'/b = 0.2677 and obtaining a resulting $Z_{0\infty}$ of 146.55. This value is approximately the same as the one predicted in figure 6. Assuming a standard input impedance of 50 ohms, this is undesirable as there is considerable mismatch.

To find λ_C , Newton's method was applied to equation (6.2) with the dimensions as input. This was done in MATLAB. An initial prediction of λ_C is required as input. It is essential that this value is close to the desired zero or it may not converge. To choose an initial estimate of λ_C , figure 6 from [1] was once again used. This figure gives the value of λ_C /a for different ratios of dimensions. For a b'/b of 0.045:

$$\frac{\lambda_C}{a} = 8 \rightarrow \lambda_C = 85.36 \mu m for TE_{10} \quad (A.11)$$

$$\frac{\lambda_C}{a} = 0.8 \rightarrow \lambda_C = 8.536 \mu m for TE_{30} \quad (A.12)$$

When these values were inserted into the MATLAB code, the resulting values were obtained:

$$\lambda_C = 0.0194 \rightarrow 15.464 GHz for TE_{10} \quad (A.13)$$

$$\lambda_C = 0.0134 \rightarrow 22.388 GHz for TE_{30} \quad (A.14)$$

Plugging in the value of $\lambda_C forthe$TE$_{10}$ mode into equation (6.4) results in an impedance value of 27.724 ohms. Not surprisingly this is very close to the value obtained in [1], which has the same dimension ratios $Z_{0\infty}$ is essentially the input impedance into the antenna. The next section will look at the design of the horn antenna.

A.1.2 Horn Antenna

The following design was based on equations found in [5]. The horn type is a pyramidal horn. The following are the desired properties of the horn:

1. Operating frequency: 2.75 THz (middle of 0.5 and 5 THz)
2. Gain of 20dB

The following design is for an optimum horn, where maximum gain is achieved. First figure 6.4 to shows what values are being calculated.

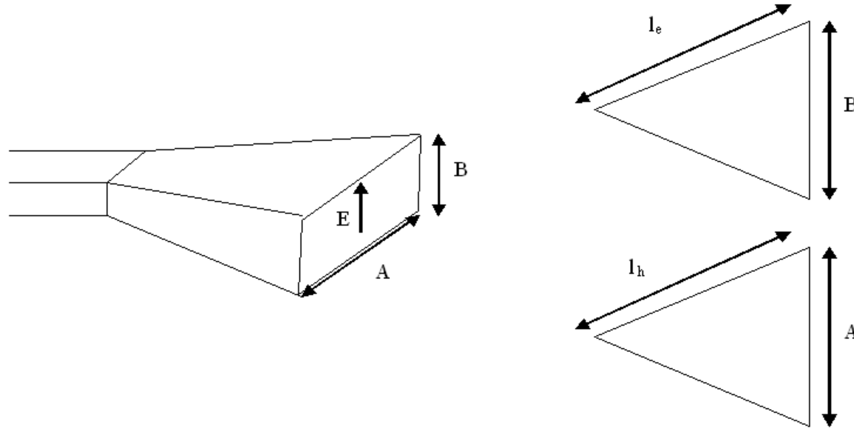

Figure A.3: Different dimensional components for the horn antenna.

If the parameters of the aperture, A and B, are already given then the gain is given as:

$$G = 10(1.008 + \log(\frac{a}{\lambda}\frac{b}{\lambda}) - (L_e + L_h))[dB] \quad (A.15)$$

The values of L_e and L_h are obtained from a graph based on the ratios of A/λ and B/λ. If the dimensions are not given, then A and B are given as:

$$A = \sqrt{3l_h\lambda} \quad (A.16)$$

$$B = \sqrt{2l_e\lambda} \quad (A.17)$$

Clearly, the first step is to choose l_h and l_e. Typically, the waveguide feeding the horn and the desired gain are chosen. This was done in part one and the gain was stated previously. Once this is done the following equation must be satisfied:

$$(\frac{\sqrt{2l_e}}{\lambda} - \frac{b_o}{\lambda})^2(\frac{2l_e}{\lambda}) = (\sqrt{\frac{3K\lambda}{l_e}} - \frac{a_0}{\lambda})^2(\frac{4K\lambda}{3l_e} - 1) \quad (A.18)$$

$$K = (\frac{G}{15.7497})^2 \quad (A.19)$$

Here G is the numerical gain. a_0 and b_0 are the dimensions of the feeding waveguide. An initial guess for l_e was given as:

$$l_e = \lambda\sqrt{K} \quad (A.20)$$

It was decided to use Newton's method once again. The following are the input values:

a_0 = a = 10.67 microns

b_0 = b = 7.47 microns

G = 20 dB = 100

λ = 109.1 microns (2.75 THz)

K = 40.314

l_e initial = 692.712 microns

Plugging this into the Newton's method and solving for l_e a value of 480.5μm was obtained. Next, A, B and l_h are given by:

$$l_h = \frac{K\lambda^2}{l_e} = 998.65\mu m \quad (A.21)$$

$$A = 571.714\mu m \quad (A.22)$$

$$B = 323.798\mu m \quad (A.23)$$

These values should give the desired gain of 20 dB based on equation (6.15) and a quick check confirms this. However, they do not produce a pyramid that has matching adjacent walls. In other words the side walls are too long. To fix this, the values of A, B and l_e are kept and l_h is calculated as 533.438μm. This now forms a side that fits the other. Plugging these values back into (6.15), it can be seen that a gain of approximately 18 dB is obtained. This is acceptable and now the ridge flare can be determined.

A.1.3 Ridge Flare

The ridge will have a length of l_e = 480.5 microns and will be exponential. After some calculations, the ridge equation was found to be as follows:

$$y = 0.1680075exp(0.014529631x)0 \leq x \leq l_e \quad (A.24)$$

Here, x is in microns. A plot of the ridge was made in MATLAB and can be seen in figure 6.4:

The impedance taper is given by:

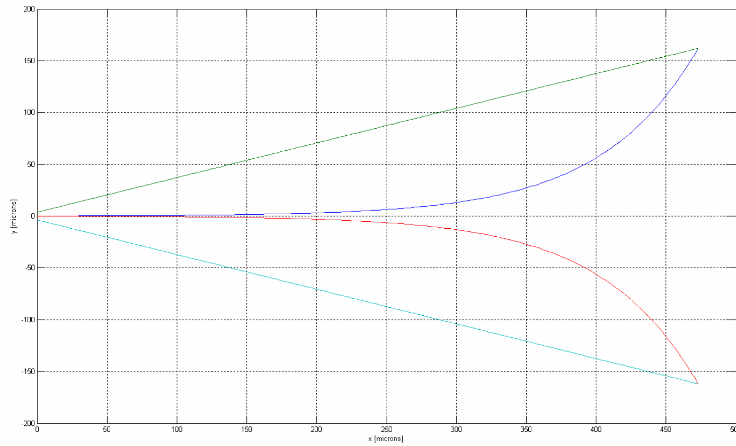

Figure A.4: MATLAB diagram of the antenna ridge.

$$Z = Z_{0\infty} exp(kx) 0 \leq x \leq \frac{l}{2} \tag{A.25}$$

$$Z = 377 + Z0\infty(1 - exp(k(l - x)))\frac{l}{2} \leq x \leq l \tag{A.26}$$

The 'l' in this case is not the same as the l_e value but rather the length along the x-axis and is calculated to be 472.88μm. The constant k is easily found by using the fact that the impedance the midpoint is the average between that of the input impedance and free space. k is then found to be 8.4076×10^{-3} with x in microns. Plotting this in MATLAB results in figure 6.6:

As an intial step, a model was created in HFSS, unfortunately there was not time to complete the simulations. The following are images of the 3D model.

The following is a description of each labeled part:

-Air: This is placed over the opening of the horn antenna where the radiated signal will be coming out of. It has radiating boundaries on all faces except the one that the horn feeds into, which has a conducting boundary.

-Ridge: The design of the ridge was based on the previous equations in the report. The outline was drawn using the draw equation based curve option and then a surface was created using the cover surface option. The last step approximated

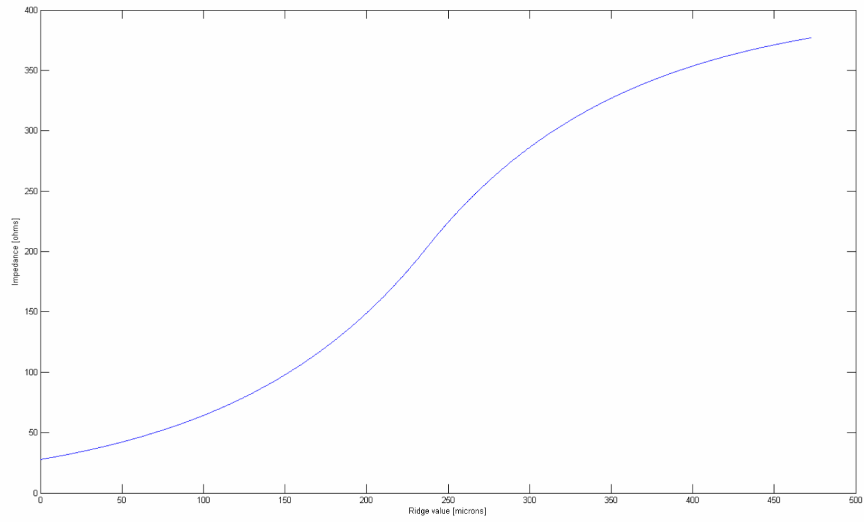

Figure A.5: MATLAB diagram of the impedance taper.

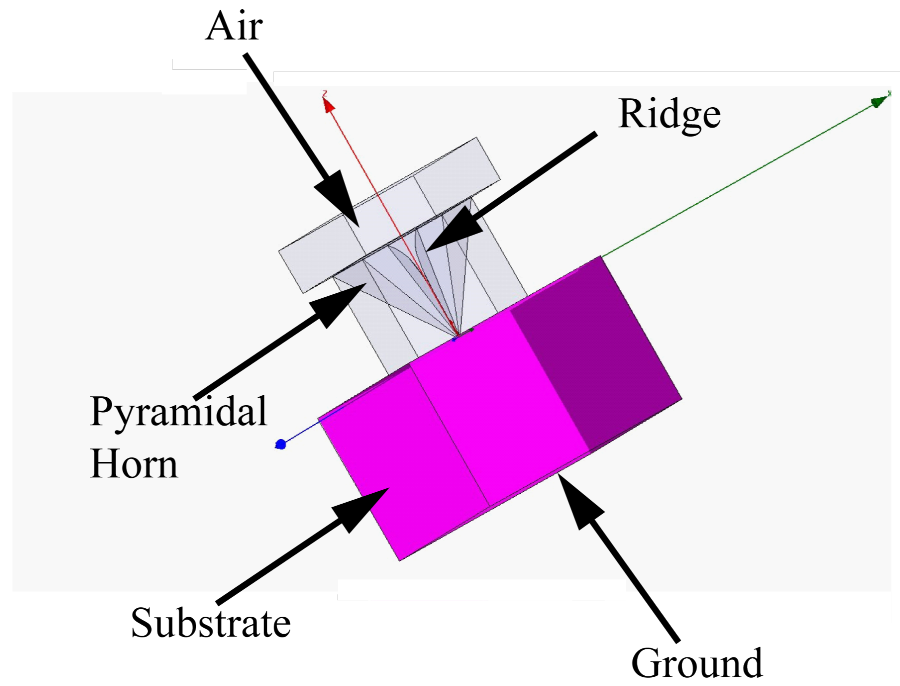

Figure A.6: The designed horn antenna in HFSS.

the curve and did not follow the equation curve exactly. This structure is initially made out of gold of 0.5 micron thickness. Future simulations should take into consideration the 3.5 micron poly-silicon thickness.

-Pyramidal Horn: This was designed using the values outlined previously, with the correction to lh. The way it is designed, makes it a solid mass with the horn shape carved out of it. Hence the corners are smooth transitions. The 3D assembly will be like this as the four walls will be assembled together and may be misaligned or have spaces between them. A future attempt at separately creating the wall piece and then constructing the horn such that there are some spaces between the piece may be something to look at.

-Substrate: The substrate is silicon and has a thickness of 675 microns as dictated by the MUMPS process. Only a small section of the substrate was used instead of the full size to reduce the complexity of the problem.

Unfortunately, there was no time to complete the simulation stage at the time this thesis was written, however the work done so far provides a starting point for researchers who might continue the project.

References

[1] R. Dixon and J. Bouchaud. Prospects for MEMS in the Automotive Industry. `http://www.memsinvestorjournal.com/2007/08/prospects-for-m.html`. 1

[2] Stephen D. Senturia. *Microsystem Design*. Kluwer Academic Publishers, New York, NY, 2001. 1

[3] G. Kovacs, N. Maluf, and P. Kurt. Bulk micromachining of silicon. *Proceedings of the IEEE*, 86(8), Aug 1998. 2

[4] J-B Yoon, C-H Han, E. Yoon, and C-K Kim. Novel and high-yield fabrication of electroplated 3d micro-coils for mems and microelectronics. *SPIE Conference on Micromachining and Microfabrication Process Technology IV*, 3511, 1998. 2

[5] T. Sasayama, S. Seikoo, S. Tsuchitani, A. Koide, M. Suzuki, T. Nakazawa, and N. Ichikawa. Highly reliable silicon micro-machined physical sensors in mass production. *The 8th International Converence on Solid-State Sensors and Actuators*, 1995. 3

[6] K. Pister, M. W. Judy, S. R. Burgett, and R. S. Fearing. Microfabricated hinges. *Sensors and Actuators A.*, 33, 1992. 3, 5

[7] J. C. Langer, J. Zou, C. Liu, and J. T. Bernhard. Micromachined reconfigurable out-ofplane microstrip patch antenna using plastic deformation magnetic actuation. *IEEE Microwave and Wireless Components Letters*, 2003. 3

[8] N. Dechev, W. L. Cleghorn, and J. K. Mills. Microassembly of 3-d microstructures using a compliant, passive microgripper. *Journal of Microelectromechanical Systems*, 13(2), 2004. 5, 18, 26

[9] Michael B. Cohn, Karl F. Bohringer, Mark J. Noworolski, Angad Singh, Chris G. Keller, Ken Y. Goldberg, and Roger T. Howe. Microassembly technologies for mems). Technical report, University of California at Berkeley and University of Washington. 6

[10] C-J Kim et al. Polysilicon microgripper. *Sensors Acturators A*, 33, 1992. 7, 13

[11] J. K. Luo et al. Comparison of microtweezers based on three lateral thermal actuator configurations. *J. Micromech. Microeng.*, 15, 2005. 7

[12] P. Boggild et al. Customizable nanotweezers for manipulation of free-standing nanostructures. *IEEE-NANO 2001*, 2001. 7, 13

[13] Fumihito Arai and Toshio Fukuda. A new pick up release method by heating for micromanipulation. *The Tenth Annual International Workshop on Micro Electro Mechanical Systems*, 1997. 8

[14] J. A. Thompson and R. S. Fearing. Automating microassembly with ortho-tweezers and force sensing. *International Conference on Intelligent Robots and Systems, 2001 Proceedings*, 2001. 8

[15] David Koester, Allen Cowen, Ramaswamy Mahadevan, Mark Stonefield, and Busbee Hardy. *PolyMUMPs Design Handbook*. MEMSCAP, 10 edition, 2003. 10

[16] N. Dechev. *Microassembly of 3D Microstructures and Micro-Electromechanical Systems (MEMS)*. PhD thesis, University of Toronto, 2004. 11, 18, 19, 48

[17] D. M. Pozar. Microstrip antennas. *Proceedings of the IEEE*, 1992. 13

[18] Y. Qian, W.R. Deal, N. Kaneda, and T. Itoh. Microstrip-fed quasi-yagi antenna with broadband characteristics. *Electronics Letters*, 1998. 13

[19] J. C. Langer, J. Zou, and J. T. Bernhard. Micromachined reconfigurable out-of-plane. *IEEE Microwave and Wireless Components Letters*, 2003. 14

[20] K. Jeong-Geun et al. 60-ghz cpw-fed post-supported patch antenna. *IEEE Microwave and Wireless Components Letters*, 2005. 14

[21] William Jakes. *Antenna Engineering Handbook*. McGraw-Hill, 1961. 14, 89

[22] University of Waterloo. *ECE 675 course notes*. 14, 47

[23] W.N. Sharpe Jr., J. Bagdahn, K. Jackson, and G. Coles. Tensile testing of mems materials-recent progress. *Journal of Materials Science*, 38. 26

[24] W.N. Sharpe Jr., B. Yuan, R. Vaidyanathan, and R. L. Edwards. Measurements of young's modulus, poisson's ratio and tensile strength of polysilicon. *Proc. 10th IEEE Int. Workshop on Microelectromechanical Systems*, 1997. 26

[25] James Gere. *Mechanics of Materials*. Thomson-Engineering, 2003. 26, 27

[26] S. Timoshenko. *Mechanics of Materials*. D. Van Nostrand Company, 1948. 27

[27] S. Timoshenko and J. N. Goodier. *Theory of Elasticity*. McGraw-Hill, 1951. 27

[28] Raymond J. Roark. *Formulas for stress and strain*. McGraw-Hill, 1954. 29

[29] ANSYS Handbook. *PolyMUMPs Design Handbook*. 30

[30] G. K. Fedder. *Simulation of Microelectromechanical Systems*. PhD thesis, University of California at Berkeley, 1994. 42

[31] Sutter Instrument. Catalog 2008. 57, 58, 59, 60

[32] Micromanipulator. `http://www.micromanipulator.com`. 62

[33] Loctite. `http://www.loctite.com/int_henkel/loctite_uk/index.cfm?pageid=561`. 63

[34] Edmund Optics. Mitutoyo infinity-corrected long working distance objectives. `http://www.edmundoptics.com/onlinecatalog/DisplayProduct.cfm?productid=1942`. 64

[35] Aerotech. `http://www.aerotech.com/products/stages/art50.html`. 84

[36] K. L. Walton and V. C. Sundbery. Broadband ridged horn design. *Microwave Journal*, 1964. 85, 87, 88, 89

[37] J. R. Whinnery and H. W. Jamieson. Equivalent circuits for discontinuities in transmission lines and waveguides. *Proc. IRE*, 1944. 85, 87

[38] S. Hopfe. The design of ridged waveguides. *IRE Trans. Microwave Theory Tech.*, 1955. 85

[39] M. Botello-Perez, H. Jardon-Aguilar, and I. G. Ruiz. Design and simulation of a 1 to 14 ghz broadband electromagnetic compatibility drgh antenna. *Electrical and Electronics Engineering, 2005 2nd International Conference*, 2005. 85, 87, 88